AD-A134 426 LASER-INDUCED MOLECULAR DYNAMICS: RATE PROCESSES IN THE GAS PHASE AND AT.. (U) ROCHESTER UNIV NY DEPT OF CHEMISTRY J LIN ET AL. NOV 83 UROCHESTER/DC/83/TR-42 1/2

UNCLASSIFIED N00014-80-C-0472 F/G 7/4 NL

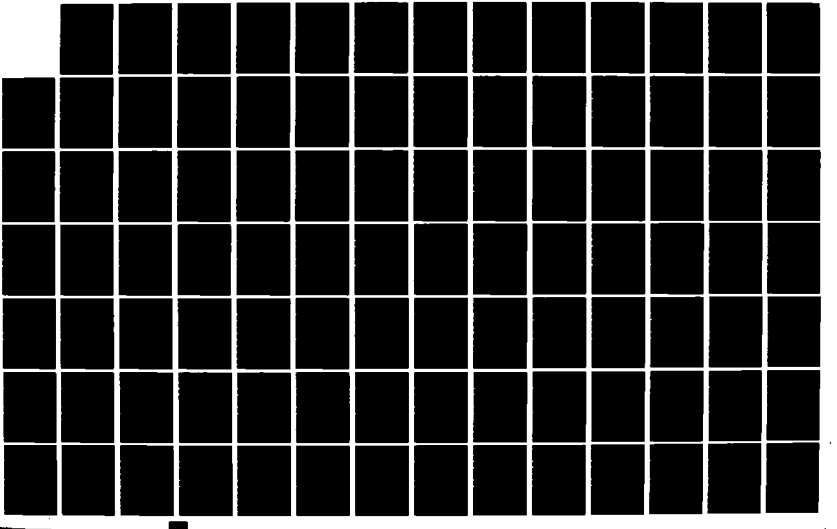

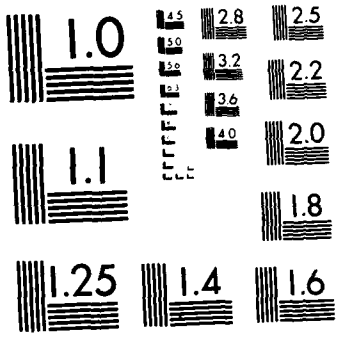

MICROCOPY RESOLUTION TEST CHART
NATIONAL BUREAU OF STANDARDS 1963 A

AD-A134 426

OFFICE OF NAVAL RESEARCH

Contract N00014-80-C-0472

Task No. NR 056-749

TECHNICAL REPORT No. 42

Laser-Induced Molecular Dynamics: Rate Processes in the Gas Phase and at Solid Surfaces

by

Jui-teng Lin, Michael Hutchinson and Thomas F. George

Prepared for Publication

in

Advances in Multi-Photon Processes and Spectroscopy, ed. by S. H. Lin (World Scientific, Singapore)

Department of Chemistry
University of Rochester
Rochester, New York 14627

DTIC FILE COPY

November 1983

DTIC
ELECTE
NOV 0 8 1983
E

Reproduction in whole or in part is permitted for any purpose of the United States Government.

This document has been approved for public release and sale; its distribution is unlimited.

Unclassified

SECURITY CLASSIFICATION OF THIS PAGE (When Data Entered)

REPORT DOCUMENTATION PAGE		READ INSTRUCTIONS BEFORE COMPLETING FORM
1. REPORT NUMBER UROCHESTER/DC/83/TR-42	2. GOVT ACCESSION NO. A134426	3. RECIPIENT'S CATALOG NUMBER
4. TITLE (and Subtitle) Laser-Induced Molecular Dynamics: Rate Processes in the Gas Phase and at Solid Surfaces		5. TYPE OF REPORT & PERIOD COVERED Interim Technical Report 6. PERFORMING ORG. REPORT NUMBER
7. AUTHOR(s) Jui-teng Lin, Michael Hutchinson and Thomas F. George		8. CONTRACT OR GRANT NUMBER(s) N00014-80-C-0472
9. PERFORMING ORGANIZATION NAME AND ADDRESS Department of Chemistry University of Rochester Rochester, New York 14627		10. PROGRAM ELEMENT, PROJECT, TASK AREA & WORK UNIT NUMBERS NR 056-749
11. CONTROLLING OFFICE NAME AND ADDRESS Office of Naval Research Chemistry Program Code 472 Arlington, Virginia 22217		12. REPORT DATE November 1983 13. NUMBER OF PAGES 151
14. MONITORING AGENCY NAME & ADDRESS(if different from Controlling Office)		15. SECURITY CLASS. (of this report) Unclassified 15a. DECLASSIFICATION/DOWNGRADING SCHEDULE

16. DISTRIBUTION STATEMENT (of this Report)

This document has been approved for public release and sale; its distribution is unlimited.

17. DISTRIBUTION STATEMENT (of the abstract entered in Block 20, if different from Report)

18. SUPPLEMENTARY NOTES

Prepared for publication in Advances in Multi-Photon Processes and Spectroscopy, ed. by S. H. Lin (World Scientific, Singapore)

19. KEY WORDS (Continue on reverse side if necessary and identify by block number)

UNIMOLECULAR DYNAMICS
MOLECULAR COLLISIONS
TRANSITION-STATE SPECTROSCOPY
ADSPECIES-SURFACE SYSTEMS
MULTIPHOTON-MULTIPHONON PROCESSES
SELECTIVE EXCITATION AND THERMAL EFFECTS
IOSTOPE EFFECTS
MIGRATION AND DESORPTION
LASER APPLICATIONS TO SURFACE CHEMISTRY

20. ABSTRACT (Continue on reverse side if necessary and identify by block number) Various theoretical approaches to laser-induced molecular dynamics in the context of multiphoton processes are reviewed. The presentation is divided into two general categories: gas-phase processes and surface processes. Within the first category, unimolecular dynamics and molecular collisions are addressed. Within the second category, energy flow in adspecies-surface systems is examined, and laser applications to surface chemistry are discussed.

DD FORM 1 JAN 73 1473

Unclassified

SECURITY CLASSIFICATION OF THIS PAGE (When Data Entered)

To appear in *ADVANCES IN MULTI-PHOTON PROCESSES AND SPECTROSCOPY*, edited by S. H. Lin (World Scientific Publishing Company, Singapore).

LASER-INDUCED MOLECULAR DYNAMICS: RATE PROCESSES IN THE GAS PHASE AND AT SOLID SURFACES

Jui-teng Lin
Laser Physics Branch
Optical Sciences Division
Naval Research Laboratory
Washington, D.C. 20375 USA

and

Michael Hutchinson and Thomas F. George
Department of Chemistry
University of Rochester
Rochester, New York 14627 USA

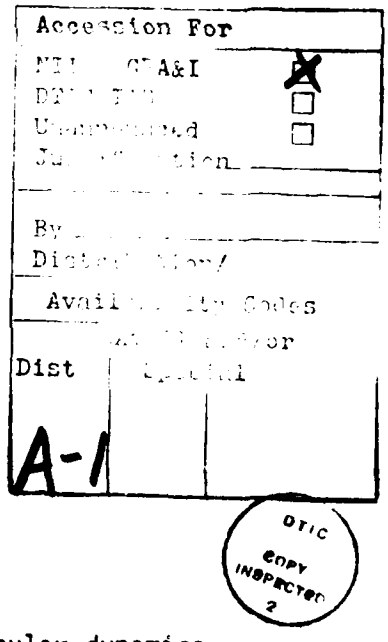

Various theoretical approaches to laser-induced molecular dynamics in the context of multiphoton processes are reviewed. The presentation is divided into two general categories: gas-phase processes and surface processes. Within the first category, unimolecular dynamics and molecular collisions are addressed. Within the second category, energy flow in adspecies-surface systems is examined, and laser applications to surface chemistry are discussed.

CONTENTS

I. Introduction

Theoretical techniques for describing laser-induced molecular dynamics combined with multiphoton processes are reviewed, with emphasis on our own work carried out during the past five years. The presentation is divided according to Sections II and III as Gas-Phase Processes and Surface Processes, respectively. The former section is further divided into two parts, where Part A is Unimolecular Dynamics and Part B is Molecular Collisions. Within Part A we address five topics: 1. heat-bath models (both classical and quantum mechanical); 2. the rate equation approach using a quasi-continuum model; 3. the excitation of intramolecular modes; 4. selectivity in multiphoton processes; and 5. multiple-frequency laser excitation. Within Part B we address two topics: 1. resonance formation, chemical reactions and transition-state spectroscopy; and 2. isotopic selectivity.

Section III is also divided into two parts, where Part A is Energy Flow in Adspecies-Surface Systems, and Part B is Laser Applications to Surface Chemistry. Part A constitutes most of Section III and is further divided into five topics: 1. microscopic treatment of single-phonon and multiphonon processes; 2. selective excitation and thermal effects, including (a) the use of the memory function to describe feedback mechanisms from the substrate to the adspecies, (b) the competition between selective and nonselective processes in a multilevel system, and (c) adbond excitation in the hydrogen/tungsten system; 3. photon energy population; 4. isotope effects; and 5. dynamic effects associated with migration and desorption.

II. Gas-Phase Processes

A. Unimolecular Dynamics

Since the first report of infrared laser dissociation of polyatomic molecules in 1971,[1] the phenomena of multiphoton excitation (MPE) and dissociation (MPD) have been extensively studied and have been shown to be a novel method for vibrational-mode-controlled infrared photochemistry.[2] Most of the major aspects of MPE and MPD are now qualitatively understood by experimental measurements and related theoretical studies. However, the quantitative understanding of multiphoton processes and their applications to selective photochemistry is still in its infancy. The complexity of the aforementioned processes results not only from the coherent properties of the laser radiation but also the states of the excited molecular system. Some of the important questions which have been (or are expected to be) addressed are the following:

(i) For a large molecular system, what is the nature of the excited vibrational state and how does it change with laser parameters, such as intensity, fluence (intensity x time) and frequency?

(ii) What is the magnitude of the absorption cross section?

(iii) What is the interplay between coherent and incoherent processes when the molecular system is excited and makes the transition from discrete states to the so-called quasi-continuum?

(iv) What is the role of intramolecular vibrational relaxation (IVR) in MPE, and what determines the rate of IVR? Is it always fast enough to randomize the energy absorbed by the intramolecular modes, so that a a statistical theory may be used to describe MPD?

(v) How is the degree of isotopic selectivity determined by the IVR rate, the laser pumping rate and the dissociation rate?

(vi) What are the dynamics of the dissociation event?

(vii) How fast is the randomization of intramolecular energy compared to a chemical process such as fragmentation?

Quantitative answers to the above questions will provide us with an understanding of the photophysical (excitation and relaxation) as well as the photochemical (decomposition and reaction of fragments) processes. However, the theory developed so far and the experimental information are not sufficient for us to construct these answers. We therefore note that the discussions in this Part A of Section II only provide either qualitative or semi-quantitative descriptions of the above features of MPE and MPD.

Two distinctly different approaches will be discussed: (i) heat-bath model (HBM) and (ii) quasi-continuum model (QCM). In the first approach, HBM, the active mode of the molecular system is singled out, and the coupling between this mode and the bath modes provides the relaxation mechanism. With a consequent energy leakage from the active to the bath modes, the molecule is heated up and the increase of the mode-mode coupling results in a red shift and smearing out of the absorption spectrum of the pumped mode. The second approach, QCM, is based on a picture in which the polyatomic molecule forms a quasi-continuum (QC) at high energies due to its high density of states. In this approach, all vibrational modes of the system are treated on equal footing, and each individual state of

the QC is generally a superposition of all the modes. To describe the dynamics of MPE based on HBM, we shall start with a simple classical model and a generalized Langevin theory. Then the results of a quantum treatment will be discussed and compared with those of the classical approach. The second approach, QCM, which involves the rate (master) equation for the energy populations, will be used to describe the phenomena of MPD. To demonstrate the dynamics of MPE, a quantum treatment of IVR will be discussed and the rate of IVR for SF_6 molecule will be estimated. Different types of selectivity and the possibility of bond-selective photochemistry will be investigated. Finally, the cooperative effects in MPE via multiple-frequency lasers will be analyzed based on both a quantum treatment and a classical treatment.

1. Heat-Bath Models

Both classical[3-10] and quantum[10-13] treatments have been employed to calculate the photon energy deposited in a damped anharmonic classical/quantum oscillator. The total energy of a laser-excited molecular system may be described either by a classical Lagrangian or a quantum Hamiltonian, while the energy transfer dyanamics is governed by Newton's or Heisenberg's equations of motion. The absorption cross section may be obtained from the classical power absorption (force x velocity) or from the quantum rate of excitation (expectation value of the energy operator). Immediately below, classical and quantum models are shown, and the results will be compared later in Part A.5 of this section, where the absorption cross section of two-laser excitation will be investigated.

a. Classical Models[6-8]

The classical Lagrangian describing a polyatomic molecule subject to infrared radiation may be written in terms of the normal coordinates Q_i as follows:

$$L(Q_1,Q_2,\ldots Q_i) = L_0 - V + f(t)Q_A, \qquad \text{(II.1)}$$

where L_0 is the unperturbed Lagrangian, and V is the interaction potential of the molecular system in which one of the normal modes, Q_A, is infrared active and coupled to the laser driving force f(t). The corresponding Newton's equations of motion are

$$\frac{d}{dt}\left(\frac{\partial L}{\partial \dot{Q}_i}\right) - \frac{\partial L}{\partial Q_i} = 0. \qquad \text{(II.2)}$$

For a given potential energy V, the equation of motion for the pumped mode (normal coordinate) may be derived by Eq. (II.2). However, the solution of that is in general not available due to the set of coupled equations whose dimensionality is proportional to the numbers of normal modes in the system. It is possible that for a simple functional form of V, e.g., linear coupling case involving terms like $\sum_i Q_A Q_i$, the many-body problem of the system may be reduced to a single-body problem in which the ensemble-averaged equation of motion of the active mode coordinate is given by,[8] letting $Q_A \equiv Q$,

$$\langle \ddot{Q} \rangle + \gamma \langle \dot{Q} \rangle + \omega_{eff}^2 \langle Q \rangle = eE \cos(\omega t)/m. \qquad \text{(II.3)}$$

$\langle \ldots \rangle$ denotes the ensemble average over the bath-mode coordinates; γ is a damping factor resulting from the active- and bath-mode interactions; E is the electric field of the IR radiation linearly polarized in the direction of Q_A with a circular frequency ω; m and e are the reduced mass and the effective charge of the active mode which is treated as an anharmonic oscillator with an effective frequency given by[6]

$$\omega_{eff} = \omega_0 - K^* A^2, \qquad \text{(II.4)}$$

where ω_0 is the harmonic frequency of the active oscillator and is red shifted by the anharmonic term proportional to the anharmonicity K* and the steady-state amplitude A.

By ignoring the transient damping part of the solution of Eq. (II.3), the steady-state solution gives us the instantaneous power absorption of the oscillator defined as force times velocity. For near-resonance excitation, the time- and ensemble-averaged power absorption is found to be[8]

$$\left\langle \overline{\frac{dE}{dt}} \right\rangle = \left(\frac{e^2 E^2}{4m} \right) \left[\frac{\gamma}{(\Delta - K^* A^2)^2 + \gamma^2} \right], \tag{II.5}$$

which is a Lorentzian with FWHM = 2γ. The above expression provides us with a classical absorption cross section $\sigma = \langle \overline{dE/dt} \rangle / I$, where I is the laser intensity related to the electric field by $I = E^2 c/8\pi$, c being the speed of light. The steady-state average excitation (numbers of photon absorbed) of the active mode defined by $X = m\omega A^2/2\hbar = \langle \overline{dE/dt} \rangle / (\gamma \hbar \omega)$ corresponds to the roots of the cubic equation

$$aX^3 + bX^2 + cX + d = 0, \tag{II.6a}$$

$$a = (K^*/m\omega_0)^2 = (\overline{K}^*)^2, \tag{II.6b}$$

$$b = -2\Delta \overline{K}^* \tag{II.6c}$$

$$c = (\Delta^2 + \gamma^2)/(\overline{K}^*)^2 \tag{II.6d}$$

$$d = -e^2 E^2/(4m\hbar\omega). \tag{II.6e}$$

[The coefficient "c" in Eq. (II.6d) is obviously not the speed of light.] We note that the above expression shows an asymmetric Lorentzian when $K^* \neq 0$ and there is an optimal detuning $\Delta^* = \overline{K}^* X^*$, where X^* is the maximum value of X given by $(dX/d\Delta) = 0$. Furthermore, for a fixed laser intensity,

the excitation profiles, X vs. Δ, show the "bistability" feature given by the criterion $\bar{K}^{*}>\bar{K}^{**} = \gamma^2/(2d)^{1/2}$.

We have shown that the absorption cross section is governed by a Lorentzian, Eq. (II.5), where a constant damping factor (or the energy relaxation rate), γ, is assumed. For a realistic system, the damping factor could be time dependent, and the phase of the oscillator could also relax due to the incoherent behavior of the excited molecular system. For a more rigorous description of the dynamics of MPE, instead of the simple equation like Eq. (II.3), we consider the generalized Langervin equation (GLE)[7]

$$\ddot{Q} + \int_0^t dt'[K_1(t-t') + \omega_{eff}^2 K_2(t-t')]\dot{Q}(t') = [f(t) + R(t)]/m. \qquad \text{(II.7)}$$

Here we have introduced the energy damping kernel K_1 and the dephasing kernel K_2. $f(t)$ and $R(t)$ are the laser driving force and the bath-induced random force. Considering a Markoff process with $K_1(t) = 2\gamma_1\delta(t)$ and an exponential dephasing kernel $K_2(t) = \exp(-2\gamma_2 t)$, we find, from the Laplace-Fourier transform of the velocity autocorrelation function, the average energy absorption rate to be (assuming that $\langle R(t)\rangle = 0$)

$$\langle\overline{\frac{dE}{dt}}\rangle = (eE)^2 P(T_0)\left[\frac{\gamma_2 C+\omega D}{C^2+D^2}\right], \qquad \text{(II.8a)}$$

$$P(T_0) = (2\hbar\omega)^{-1}(kT_0/m)[1-\exp(-\hbar\omega/kT_0)], \qquad \text{(II.8b)}$$

$$C = \omega_{eff}^2 - \omega^2 + \gamma_1\gamma_2, \qquad \text{(II.8c)}$$

$$D = \omega(\gamma_1 + \gamma_2), \qquad \text{(II.8d)}$$

where T_0 is the initial temperature of the molecule. For the situation of near-resonance, $\omega_{eff}^2 - \omega^2 \simeq 2\omega\Delta$ and $\gamma_1\gamma_2 << \omega^2$, Eq. (II.8) becomes

$$\left\langle \frac{dE}{dt} \right\rangle = \left[\frac{eE}{2}\right]^2 P(T_0) \left[\frac{(\gamma_1+\gamma_2)}{(\Delta-K^*A^2)^2+(\gamma_1+\gamma_2)^2/4}\right] . \qquad \text{(II.9)}$$

Since at steady state the rate of energy deposited in the active mode equals the rate of energy relaxation, the above expression also represents the rate of energy absorbed by the whole system (active plus bath modes). By conservation of energy, we then readily obtain the rate equation for the active mode energy as

$$\frac{d\langle E_A\rangle}{dt} = \sigma I - \gamma_1(\langle E_A\rangle - \langle E_B\rangle), \qquad \text{(II.10)}$$

where $\sigma I = \langle dE/dt\rangle$ given by Eq. (II.9) is the energy absorption rate of the whole molecule with absorption cross section σ and laser intensity I, and $\langle E_A\rangle$ and $\langle E_B\rangle$ are the ensemble-averaged energies of the active mode and the bath modes. We note that in this classical rate equation the net energy transfer rate of the active mode is characterized by the T_1 energy relaxation rate (γ_1), while the total absorption cross section of the molecule, σI, is governed by the total relaxation rate, $\gamma_1 + \gamma_2$. We shall show later that the above derived classical rate equation can also be derived from a microscopic quantum Hamiltonian.

In addition to the above phenomenological models, a classical trajectory calculation of MPE was recently made for SF_6.[9] The results show that the energy transfer and dissociation rate depend

on laser fluence (intensity x time), and the intramolecular energy relaxation rate is estimated to be on the order of a picosecond.

Another classical treatment of MPE and MPD for a system of two nonlinearly coupled oscillators was studied by means of Krylov-Bogoliubov-Mitropolsky theory.[13] The results show two regions of behavior for the exchange of energy between the system and the laser field: (i) the regular region with well-defined frequencies and (ii) the erratic region. Motion in the latter region leads to dissociation of the pumped molecule. For a single oscillator, the motion is always periodic, while for a system with many oscillators, e.g., a polyatomic molecule, the motion of the system becomes ergodic when it is highly excited due to the strong anharmonic coupling among the intramolecular modes.

b. Quantum-Mechanical Models

In the quantum heat-bath treatment, the MPE of a polyatomic molecule may be described by the total Hamiltonian

$$H = H_A + H_B + H_{AF} + H_{AA} + H_{BB} + H_{BF}. \qquad \text{(II.11)}$$

$H_{A,B}$ represent the unperturbed Hamiltonians of the active (A) mode and of the bath (B) modes with the interaction Hamiltonian H_{AB}; H_{AF} represents the A mode and laser field interaction; and the last three terms, which are often neglected in theoretical studies, represent the mode-mode couplings among the active modes (H_{AA}), the bath modes (H_{BB}) and the direct laser excitation of bath modes (H_{BF}). For an isolated

molecule or collisionless process, H_{AA} is negligible. The mode-mode coupling among the bath modes usually is very strong such that the time scale for reaching a thermal equilibrium among these modes is much faster than that of the active-mode excitation and relaxation. Therefore, the rapid dynamics within the bath modes governed by H_{BB} may be absorbed into H_B in which the occupation number of these modes is treated as a constant. Finally, the direct excitation of the bath modes through H_{BF} is not significant when their frequency spectrum is far off-resonant with the laser frequeny. Within the spirit of the heat-bath treatment, we assume that the active mode can always be singled out from the other modes, which serve as an infinite energy sink defined by a constant temperature. However, we may have the situation that the IVR rate is very fast, particularly when the molecule is highly excited, such that the photon energy is rapidly randomized to all the bath modes. For a finite heat bath, we expect to have energy feedback from these thermal bath modes to the active mode. Furthermore, when the active mode is highly excited, its vibrational frequency may be comparable to that of the bath modes, and the total absorption cross section of the molecule reflects both H_{AF} and H_{BF}. In the above described situation, the heat-bath mode model may not be an appropriate treatment of MPE processes. A more relevant treatment based on an "equal footing" of all the modes will be discussed later. In the following discussion, we shall neglect the last three terms in Eq. (II.11) and focus on the excitation of the active mode while treating the bath modes as an infinite sink.

The second quantization expressions of the components of the Hamiltonian of Eq. (II.11) are given by[12,14]

$$H_A = \hbar(\omega_0 - \varepsilon^* a^\dagger a) a^\dagger a, \tag{II.12a}$$

$$H_B = \sum_j \hbar\omega_j b_j^\dagger b_j, \tag{II.12b}$$

$$H_{AB} = \hbar\sum_\nu (G_\nu B_\nu a^\dagger + G_\nu^* B_\nu^\dagger a), \tag{II.12c}$$

$$H_{AF} = \hbar V \cos(\omega t)\,(a^\dagger + a) \tag{II.12d}$$

$$V = (2\hbar m\omega_0)^{-1/2} \mu'(0) E \tag{II.12e}$$

$a^\dagger$,a and $b_j^\dagger$, b_j are the usual harmonic vibrational ladder operators for the active mode and the j-th bath mode with frequencies ω_0 and ω_j, respectively; ε^* is the anharmonicity of the nonlinear quantum oscillator (active mode) with the derivative of the diple moment $\mu'(0)$ evaluated at the equilibrium point; and $B_\nu = \Pi b_j$ represents a multimode operator with an order p defined by $p \simeq \omega_0/\omega_j$.

In the Heisenberg picture, the equations of motion for the operator $\hat{O}$ are given by

$$\frac{d\hat{O}(t)}{dt} = \frac{1}{i\hbar}[\hat{O}(t), H] \tag{II.13}$$

for $\hat{O} = a^\dagger$, a, $B_\nu^\dagger$, B_ν etc. Here $\hat{O}(t) = \exp(iHt/\hbar)\hat{O}\exp(-iHt/\hbar)$ is a time-dependent Heisenberg operator of the Schrödinger operator $\hat{O}$ which is time independent. In general, tractable solutions of the above coupled

equations are not available due to the many-body effects and the nonlinear couplings of the bath modes. However, by employing the so-called Weiskoff-Wigner single-pole approximation or assuming a Markoff process for the bath modes, the many-body effects resulting from H_{AB} may be reduced to a damping factor and a frequency shift for the active mode. The above treatment is similar to the usual phenomenological approach, where a complex frequency of the active mode is assumed, except that the damping factor may be rigorously derived based on the microscopic Hamiltonian. Beyond this heat-bath model, the actual mode-mode coupling should be rigorously treated without assuming a continuum spectrum for the bath modes. This will be investigated later in the intramolecular mode-mode coupling within the SF_6 system.

Within the heat-bath model, we obtain a set of equations of motion for the active mode operator and the average excitation $n \equiv \langle a^\dagger a \rangle$ in the rotating-wave approximation,

$$\frac{d\langle a\rangle}{dt} = -\left[i(\Delta - 2\epsilon^*\langle a^\dagger a\rangle) + (\gamma_1+\gamma_2)/2\right]\langle a\rangle - iV/2, \tag{II.14a}$$

$$\frac{d\langle n\rangle}{dt} = -(iV/2)\langle\langle a^\dagger - a\rangle\rangle - \gamma_1(\langle n\rangle - \bar{N}). \tag{II.14b}$$

$\langle\langle \ldots \rangle\rangle$ represents the ensemble average over the active- and bath-mode coordinates; $\gamma_{1,2}$ are the bath-mode-induced energy and phase relaxation factors; $\bar{N}$ is the multimode occupation number of the bath modes; and all other parameters are as previously defined. In the adiabatic approximation, $|a|(\gamma_1+\gamma_2) >> |\dot{a}|$, we obtain the rate quation for the active-mode excitation,

$$\frac{d\langle n\rangle}{dt} = \frac{\sigma I}{\hbar\omega} - \gamma_1(\langle n\rangle - \bar{N}). \tag{II.15}$$

This is seen to be the quantum version of the classical rate equation (II.10) by noting that $\langle E_A\rangle = \hbar\omega\langle n\rangle$ and $\langle E_B\rangle = \hbar\omega\bar{N}$. The quantum absorption cross section of the molecule is given by

$$\sigma = \frac{A(\gamma_1+\gamma_2)\hbar\omega}{(\Delta-2\varepsilon^*\langle n\rangle)^2+(\gamma_1+\gamma_2)^2/4}\ , \tag{II.16}$$

where $A = 4\pi(V/E)^2/c$.

Using Eq. (II.16), a cubic equation for the steady-state excitation $X = \langle n(t)\rangle_{s.s.}$ is readily found from Eq. (II.15),

$$X = \frac{AI(1+\gamma_2/\gamma_1)}{(\Delta-2\varepsilon^*X)^2+(\gamma_1+\gamma_2)^2/4} + \bar{N}, \tag{II.17}$$

which is identical to the classical results in Eq. (II.6) [or Eq. (II.9) with γ_2 included] if we ignore the initial heat-bath occupation number $\bar{N}$ and make the corresponding relations: $2\varepsilon^* = \bar{K}^*$ and $AI = d$. The above results show the power law for the steady-state excitation vs. laser intensity $X \propto I^p$, with $p = 1$ in the low-excitation harmonic region, $2\varepsilon^*X \ll (\gamma_1+\gamma_2)/2$, and $1/3 \leq p < 1$ in the high-excitation anharmonic region. Furthermore, from the time integral of the total cross section of the molecule, $\sigma I/\hbar\omega$, we obtain the power law for the mean numbers of photons ($\langle N\rangle$) absorbed by the molecule (active mode plus bath modes) vs. laser fluence (ϕ) as

$$\langle N\rangle = \int dt(\sigma I/\hbar\omega) \propto \phi^q, \tag{II.18a}$$

$$\phi = \int dt\, I\ , \tag{II.18b}$$

where the nonlinear power $q<1$ results from the anharmonicity $2\varepsilon^*\langle n\rangle$ of the absorption cross section. The calculated power law may be used to fit the experimental results in which the average excitations are deduced from the direct attenuation of the laser beam propagating through the SF_6 gas cell.[15(a)] In Fig. 1, we see that in the low-excitation region the data are well fitted by Eq. (II.18) with $q = 1$, whereas in the high-excitation region the curve is bent to a power law with $q = 0.65$. An alternative measurement of $\langle N\rangle$ vs. laser intensity, rather than the fluence, is shown in Fig. 2, which indicates the power law of $\langle N\rangle \propto I^q$ with $q<1$.[15(b)]

From the above calculated results based on the heat-bath model, the following features of MPE may be summarized:

(i) The steady-state excitation of the active mode is governed by the laser intensity, rather than the laser fluence, by a power law $\langle n\rangle_{s.s.} \propto I^p$ with $1/3 \leqslant p \leqslant 1$.

(ii) When the excitation of the active mode is saturated, i.e., the pumping rate is balanced by the relaxation rate, the number of photons absorbed by the molecule (active plus bath modes) is characterized by the laser fluence with a power law $\langle N\rangle \propto \phi^q$ with $q \leqslant 1$.

(iii) Mode-selective excitation is possible by a high-power short-pulse laser in which the excitation rate of the selectively-pumped mode is comparable or faster than the relaxation rate, i.e., the energy leakage rate from the pumped mode to the bath modes.

(iv) For long-pulse laser excitation of a system with very strong mode-mode coupling, the photon energy is rapidly randomized to all the modes, and an effective vibrational temperature of the excited molecule is defined

by the conservation of energy as follows:

$$S\bar{N}_m = \langle N \rangle \hbar\omega, \tag{II.19a}$$

where S is the total number of vibrational modes (e.g., S = 15 for the SF_6 molecule), and $\bar{N}_m$ is the overall occupation number of the molecule given by the Bose-Einstein function

$$\bar{N}_m = [\exp(\hbar\bar{\omega}/kT_{eff}) - 1]^{-1}. \tag{II.19b}$$

Here all the intramolecular modes are assumed to be in thermal equilibrium with an effective temperature T_{eff} and a mean vibrational frequence $\bar{\omega}$. We note that the average molecular excitation $\langle N(t) \rangle$ given by Eq. (II.18) in general is time dependent through the temporal profile of the laser pulse, I(t). Therefore $T_{eff}(t)$ is also time dependent and reaches a peak value at the end of the pulse, e.g., a square pulse, and gradually decays to the initial temperature after the pulse is off. Further discussion of T_{eff} will be given later when a thermal population is introduced by the solution of the rate equation.

The heat-bath model may be extended to a system consisting of several subgroups in which the mode-mode coupling is more significant within each subgroup than between the subgroups. In this situation the specifically-excited subgroup may be characterized by a higher T_{eff} than the others and in turn opens the selective channels of laser-induced rate processes which, e.g., are governed by an Arrhenius form $\exp(-E_A/kT_{eff})$, where E_A is an activation energy of the specific channel. We note that the rate processes are determined

by the ratio of E_A/kT_{eff} and not simply by E_A, so that the "easier channel" is not necessarily the one with a lower E_A.

2. Quasi-Continuum Model -- Rate Equation Approach

We now discuss the second quantum approach, with treats all vibrational modes on an equal footing, with the eigenstates of the system being mixtures of all the normal modes. Due to the high density of vibrational states at high-excitation energy, the molecule can easily absorb more photons through resonant incoherent transitions between so-called quasi-continuum levels, where rate equations have been widely used for collisionless[16-23] and collisional[24-26] MPD.

A well-accepted qualitative model for MPD of SF_6 has provided a general picture where the molecular energy levels are divided into three regions (see Fig. 2): (I) the discrete region characterized by coherent excitation, where the ν_3 (active) mode absorbs 3 to 6 photons and the anharmonicity of the vibrational potential is nearly compensated for by allowed rotational transitions; (II) the quasi-continuum region where the level density is very high and incoherent excitation is essential; and (III) the true continuum region. Region (I) processes are responsible for isotopic selectivity, coherent effects (multiphoton resonance, photon echoes, coherent wave propagation, etc.) and the intensity dependence of MPE with high selectivity. For the excitation processes in regions (II) and (III) it has been shown experimentally for SF_6 that high laser fluence (energy), not high laser power (intensity), is necessary for driving the molecule through the quasi-continuum and

is the important parameter for determining the dissociation yield.[17] However, later experiments on other molecules have shown that both laser fluence and intensity determine the dyanmics of MPD.[2(c)]

For multiphoton excitation in the quasi-continuum region, the Fermi Golden Rule is valid and the full Schrödinger equation reduces to a set of incoherent rate (master) equations. For the collision-free condition (low pressure), the rate quation for the energy population is

$$\frac{dP_n}{dt} = W^a_{n-1}P_{n-1} + W^e_n P_{n+1} - (W^a_n + W^e_{n-1})P_n - k_n P_n, \qquad \text{(II.20)}$$

where P_n is the population in the n-th level (n photons absorbed). W^a_n (W^e_n) is the transition rate constant for absorption (emission) from level n to n+1 (n+1 to n) and is related to the absorption cross section (σ_n) and frequency of the field (with intensity I) by $W^a_n = \sigma_n I/\hbar\omega$ and $W^e_n/W^a_n = g_n/g_{n+1}$, where g_n is the molecular density of states at energy $n\hbar\omega$. k_n, the unimolecular decomposition rate constant, can be calculated by RRKM theory[27] or quantum RRK theory.[28] From Eq. (II.20) we realize that collisionless MPE and MPD are characterized by the laser intensity and frequency, the absorption cross section, the density (or degeneracy) of states and the unimolecular reaction constant. During the past several years, the rate equations describing MPD have been studied by different approaches, such as a thermal model for Boltzmann-type energy populations,[20] diffusion model for continuum populations,[22] exact stochastic model,[23] the model of restricted intramolecular relaxation[25] and the random coupling model.[29]

Depending on the form of the absorption cross section and the density of states in the quasi-continuum, the solution of the above rate equation gives us different populations and corresponding dissociation probabilities. For example, various types of n-dependence of the absorption cross section have been considered: $\sigma_n = \sigma_0/n$, $\sigma_n = \exp(-\alpha n+\beta)$ and σ_n = constant in Refs. 19, 20 and 16, respectively. A "thermal model" with suitable functional forms for σ_n and g_n (and neglecting the dissociation rate k_n) has been studied in which the population is governed by the rate equation[21]

$$\frac{dP_n}{dt} = \frac{AI}{S}(n+S-1)P_{n-1} + \frac{AI}{S}(n+1)P_{n+1} - \frac{AI}{S}(2n+S), \tag{II.21}$$

where the constant A is proportional to the absorption cross section and S is the number of vibrational modes involved in the process. The above rate equation can be solved in closed form to give the thermal population[30]

$$P_n = Ng_n \exp[-n\hbar\omega/kT_{eff}], \tag{II.22}$$

where N is a normalization constant and g_n is the quantum degeneracy given by

$$N = \left[\sum_{n=0}^{\infty} P_n\right]^{-1} = [1 - \exp(\hbar\omega/kT_{eff}]^S, \tag{II.23a}$$

$$g_n = (n+S-1)!/[n!(S-1)!], \tag{II.23b}$$

and the effective temperature T_{eff} as a function of time is given by the conservation of energy

$$S\hbar\omega\bar{n} = \sigma\int_0^t I dt = \sigma\phi, \tag{II.24a}$$

$$\bar{n} = [\exp(\hbar\omega/kT_{eff}) - 1]^{-1}, \tag{II.24b}$$

where σ is the absorption cross section and ϕ is the fluence of the laser radiation. For multiphoton absorption processes, for $kT_{eff} >> \hbar\omega$ and for $n >> S$, we obtain the high-temperature or classical limit of the population,

$$P_n = \left[\frac{n^{S-1}}{(S-1)!(<n>/S)^S}\right] \exp\left[\frac{nS}{<n>}\right], \tag{II.25}$$

where $<n>$ is the mean numbers of photon absorbed per molecule, i.e., $<n> = \sum_{n=0} nP_n$. We note that in this classical limit $kT_{eff} = \hbar\omega<n(t)>/S$, which follows the time dependence of $<n(t)>$, and we may obtain a power law $T_{eff} \propto \phi^q$ according to Eq. (II.18). Furthermore, the corresponding dissociation probability is found to be

$$P_d = \sum_{n=n^*}^{\infty} P_n \propto \exp(-Sn^*/<n>), \tag{II.26}$$

which is the usual Arrhenius form.

A "continuum model" was also developed for more general functional forms of σ_n and g_n:

$$\sigma_n = \sigma_0(n+C)^{\alpha}, \tag{II.27a}$$

$$g_n = g_0(n+C)^{S-1}, \tag{II.27b}$$

where σ_0, g_0, C and α are suitable constants. For high excitations n>>1, the difference equation (II.20) reduces to a classical diffusion equation where n becomes a continuous variable,[31]

$$\frac{\partial P_n}{\partial \phi} = g_n^{-1} \frac{\partial}{\partial n} (g_n \sigma_n \frac{\partial P_n}{\partial n}). \tag{II.28}$$

Using the expression of Eq. (II.27), the population can be solved in a closed form, and the corresponding dissociation probability is also given in closed form as[22]

$$P_d = \exp(\frac{\phi_0}{\phi})[1 + \sum_{j=1}^{J} (\frac{\phi_0}{\phi})^j/j!], \tag{II.29}$$

$$\phi_0 = (n^*)^\beta/(\beta^2 \sigma_0), \tag{II.30a}$$

$$J = (S/\beta)-1, \quad \beta = 2-\alpha, \tag{II.30b}$$

for integer values of S/β. This model results in a set of "universal curves" which may be used for data analysis in various experimental situations. We note that the thermal results shown in Eq. (II.25) represent a special case of Eq. (II.29) with $\alpha = 1$, i.e., a harmonic model. From the solution of Eq. (II.28), we may calculate the average excitation (photon quanta per molecule). The result shows a power law $\langle n \rangle \propto \phi^q$, where $q = (2-\alpha)^{-1}$. It is seen that $\langle n \rangle \propto \phi$ for a harmonic model (α=1) and $\langle n \rangle \propto \phi^{1/3}$ for an anharmonic model (α= -1).[22] These results are in agreement with that of the heat-bath model, Eq. (II.17).

The dynamics of MPE and MPD has been investigated by a molecular beam method, and the experimental results have been analyzed by an

improved rate equation where the intensity dependence of excitation over the discrete levels is included.[18] These dynamical features are summarized as follows: (i) Both the laser intensity and the fluence are important in determining the MPD yield. (ii) Excitation over the discrete levels into the quasi-continuum is mainly governed by the laser intensity. (iii) Excitation through the quasi-continuum to the dissociation level depends only on the laser fluence. (iv) Above the dissociation level, the excess energy of the dissociated molecule is determined by the balance between the up-excitation rate and the dissociation rate. Therefore, in the case of long laser pulses, the excess energy is determined by the laser intensity, while for short pulses case it is determined by the laser fluence. For SF_6, the excess energy was shown to be laser fluence dependent when the laser pulse has energy higher than 5 J/cm^2. (v) The photon energy deposited in the active mode is rapidly randomized among all the vibrational modes on a time scale of 10^{-8} s, which is much faster than the dissociation lifetime. The observed dissociation rates and the overall dynamics of MPD are in good agreement with the results predicted by RRKM theory. (vi) The population distribution P_n in the quasi-continuum predicted by a model with $\sigma_n \propto \exp(-\alpha n)$ is narrower than a thermal distribution. Another model based on a dephasing broadening in the quasi-continuum also shows this narrower population which is governed by a Poisson distribution (see Fig. 3).[32] More recently, a model of quasi-continuum absorption has been developed to provide a more precise meaning for the term "quasi-continuum".[33] This theory accounts for unimolecular dipole dephasing and partial dipole recorrelation, and it predicts the collapse and revival phenomena based on the concept that the level spacing of the quasi-continuum is close enough that some continuum-like behavior is

evident in the transition dynamics, but also far enough apart so that the actual discreteness of the upper "band" of the final levels is not completely smeared.

3. Excitation of Intramolecular Modes[12]

In the previously discussed heat-bath model of MPE, the active mode is singled out as the pumped system and all other modes are treated as a heat bath. The coupling between the system and the bath modes provides the relaxation mechanism where the many-body effects due to the anharmonic mode-mode coupling are phenomenologically treated by the energy (γ_1) and phase (γ_2) relaxation factors. This damping model, while providing a simple picture of the energy transfer processes and focusing on the active-mode excitation, is not able to provide the detailed individual excitations within the intramolecular modes. To describe the dynamical excitations and evaluate the intramolecular vibrational relaxation (IVR) rate, we shall now present a microscopic model which includes the anharmonic mode-mode coupling, in contrast to the damping model where only the active-mode excitation was included.

Before investigating IVR for the SF_6 molecule, we shall develop general formulas for describing the dynamics of intramolecular mode-mode coupling for any polyatomic system. The total Hamiltonian for an anharmonic quantum oscillator subject to infrared radiation may be written as

$$H(t, Q_1, Q_2, \ldots Q_N) = H_0^{eff} + \lambda H_{anh} = H'(t), \qquad \text{(III.31)}$$

where H_0^{eff} is the effective unperturbed Hamiltonian of the system (with N normal modes), λH_{anh} is the intramolecular anharmonic coupling, and H'(t) is the laser field interaction Hamiltonian. In a second-quantization representation, the individual terms of the total Hamiltonian may be expressed by[12]

$$H_0^{eff} = \sum_j \hbar\omega_j a_j^\dagger a_j - i\sum_j \hbar\Gamma_j/2, \tag{II.32}$$

$$H_{anh} = \sum_{i\neq j\neq k} \sum_{\ell,m,n=1}^{p} [F_{\ell mn}^{ijk}(a_i^\dagger a_i)^\ell (a_j^\dagger a_j)^m (a_k^\dagger a_k)^n$$

$$+ G_{\ell mn}^{ijk}(a_i^\dagger)^\ell (a_j^\dagger)^m (a_k)^n] + \ldots, \tag{II.33}$$

$$H'(t) = \sum_j V_j(t)(a_j^\dagger + a_j). \tag{III.34}$$

In Eq. (II.32) the imaginary part of the complex effective Hamiltonian Γ_j takes account of the level broadening of the open system due to factors such as collisional (pressure) broadening for a homogeneous system or surface-phonon-induced damping for a heterogeneous system. In Eq. (II.33), two typical terms of the anharmonic coupling are shown: the first term representing T_2 phase relaxation processes, where no vibrational energy among the intramolecular modes is exchanged, and the second term representing the T_1 energy relaxation processes where the photon energy is deposited in the active mode(s) and populated in all the other inactive mode via anharmonic coupling. In Eq. (II.34), $V_j(t) \propto V_{j0}\cos(\omega t)$ is proportional to the derivative of the dipole moment

and the effective local electric field of the j-th mode with laser frequency ω. We note that the anharmonic coupling factors $F^{ijk}_{\ell mn}$ and $G^{ijk}_{\ell mn}$ are related to the p-th derivatives of the anharmonic potential energy (with respect to the normal coordinates) with $p = \ell + m + n$ being the order of the multiquantum coupling.

The solution of the time-dependent Schördinger equation

$$i\hbar[\partial\Psi/\partial t] = H\Psi, \tag{II.35}$$

with the total Hamiltonian given by Eq. (II.31), may be written as[14]

$$\Psi(t) = \exp\left\{-\frac{i}{\hbar} H_0^{eff} t + A(t) + \sum_j (B_j(t)a_j^\dagger - B_j^*(t)a_j)\right\}\Psi(0), \tag{II.36}$$

where A(t) and B(t) are time-dependent coefficients to be determined by the equations of motion. Since the energy population and the excitations of the system are only characterized by the amplitude functions $B_j(t)$ and are independent of A(t), we shall focus on the equation of motion for $B_j(t)$, which can be obtained by the substitution of Eq. (II.31) into Eq. (II.35) together with the expression of Eq. (II.36) for the wave function:

$$i\hbar \frac{dB_j}{dt} = \lambda \sum_{i\neq j\neq k} \sum_{\ell mn} m\{F^{ijk}_{\ell mn}(B_i^* B_i)^\ell (B_j^*)^{m-1} B_j^m (B_k^* B_k)^n$$

$$+ G^{ijk}_{\ell mn}(B_j^*)^\ell (B_j^*)^{m-1}(B_k)^n \exp(i\Delta_I t)\}$$

$$+(V_{j0}/2)\exp(i\Delta_E^j t) - (i\Gamma_j/2)B_j, \tag{II.37}$$

where the external detuning (Δ_E^j) and the internal detuning (Δ_I) are defined by $\Delta_E^j = 2\pi(\nu_{j+1} - \nu_j) - \omega$ and $\Delta_I = 2\pi(\ell\nu_i + m\nu_j - n\nu_k)$. In deriving Eq. (II.37), we have used the usual rotating-wave approximation and operator algebra such as[14]

$$[\exp(B^*a)]F(a^\dagger)[\exp(-B^*a)] = F(a^\dagger + B_j^*), \tag{II.38}$$

where $F(a^\dagger)$ is any operator function and B_j are c-numbers.

The important features of the quantum equations of motion [Eq. (II.37)] are: (i) The j-th normal mode of the system is strongly coupled to the laser field when $V_{j0} \neq 0$ and the external detuning is not far-off the resonance condition $\Delta_E^j = 0$ (due to the anharmonicity, we shall find later that the optimal detuning is red shifted, i.e., $\Delta_E^j > 0$). (ii) The intramolecular coupling is governed by the coupling strengths $\lambda F_{\ell mn}^{ijk}$, $\lambda G_{\ell mn}^{ijk}$ and the internal detuning Δ_I. For the intramolecular coupling to be significant, we shall expect a near resonance $\Delta_I \simeq 0$, which was also shown by a classical treatment.[35] (iii) By Eq. (II.37) and its complex conjugate, we find that the equation of motion for $B_j^* B_j$ contains no T_2 dephasing term, i.e., no vibrational energy is exchanged among the intramolecular modes due to the T_2 dephasing processes. (iv) The amplitude function is related to the average excitation in the Poisson distribution

$$P_{nj}(t) = \exp(-\bar{n}_j)\bar{n}_j^{n_j}/n_j!, \tag{II.39}$$

where P_{nj} is the energy population of a harmonic oscillator (for $\lambda = 0$), and n_j and $\bar{n}_j$ are the vibrational quantum number and the average

excitation of the j-th mode, respectively, where

$$\bar{n}_j(t) = |B_j(t)|^2 = \sum_{nj} n_j P_{nj}(t). \tag{II.40}$$

Therefore the average excitation $\bar{n}_j = |B_j|^2$ is a relevant quantity in describing the energy distribution among the intramolecular modes, as we initially expected.

We have shown that IVR will be significant only when the internal resonance condition is met, i.e., the photon energy deposited in the active mode will be rapidly shared by those modes which have frequencies close to that of the active mode with the frequency combination resonant or near resonant with that of the active mode. Furthermore, from the concept of the energy-gap law,[36] we know that IVR is dominated by those low-order combinations, i.e., small values of p, since it is a strongly decreasing function of p when p increases. We therefore may truncate the order of IVR in the sum of Eq. (II.37), which otherwise cannot be numerically solved with a reasonable amount of computer time, particularly for a large molecule system with a large number of vibrational modes like SF_6.

To show the role of the external and internal detunings in IVR, we now consider the SF_6 system in the collisionless low-pressure regime (i.e., $\Gamma_j = 0$) and focus on the case of the fourth-order anharmonic coupling $\varepsilon Q_3 Q_2^2 Q_6$, i.e., p = 4, where ε is the anharmonicity and Q_3, Q_2 and Q_6 are the normal coordinates of the ν_3 (active), ν_2 and ν_6 modes. It is known that SF_6 has an O_h symmetric group, and the frequency spectrum of the 15 normal modes (some are degenerate) is (in cm^{-1}):

$\nu_1 = 773.6$, $\nu_2 = 642.1$, $\nu_3 = 947.97$, $\nu_4 = 615.03$, $\nu_5 = 522.9$ and $\nu_6 = 364$. The corresponding internal detuning then is $\Delta_I = 2\pi(\nu_3 - 2\nu_2 - \nu_6)$ and the external detuning is $\Delta_E = 2\pi\nu_3 - \omega$, where ω is the frequency of the tunable CO_2 TEA laser which is near resonant with the ν_3 mode. The quantum coupled equations of motion [Eq. (II.37)] for this case become

$$i\hbar\dot{B}_1 = \lambda' C_1^4 B_1^* B_1^2 + \lambda' C_1 C_2^2 C_3 B_2^2 B_3^* \exp(i\Delta_I' t) + (V_{10}/2)^2 C_1 \exp(i\Delta_E' t), \qquad \text{(II.41a)}$$

$$i\hbar\dot{B}_2 = \lambda' C_2^4 B_2^* B_2^2 + 2\lambda' C_1 C_2^2 C_3 B_1 B_2^* B_3 \exp(-i\Delta_I' t), \qquad \text{(II.41b)}$$

$$i\hbar\dot{B}_3 = \lambda' C_3^4 B_3^* B_3^2 + \lambda' C_1 C_2^2 C_3 B_1^* B_2^2 \exp(-i\Delta_I' t). \qquad \text{(II.41c)}$$

$B_j (j=1,2,3)$ are the related amplitude functions of the normal modes ν_3, ν_2 and ν_6 respectively; $\lambda' = 12\lambda$, $\Delta_I' = 2\pi(\nu_3' + \nu_6' - 2\nu_2')$ and $\Delta_E' = 2\pi\nu_3' - \omega$, where $\nu_j' (j=2,3,6)$ are the anharmonic-corrected frequencies, i.e., $\nu_j' = \nu_j - \lambda' C_j/\hbar$; and C_j are the quantization constants, $C_j = (\hbar/2m_j\omega_j)^{1/2}$. The above system, for the case of exact resonance, $\Delta_E' = 0$, has been discussed and the related IVR has been estimated.[37] Here we shall show the dynamical features of IVR and find the optimal external and internal detunings by solving the coupled equations of motion numerically. We investigate the time evolution of the average excitations, $\bar{n}_1 = |B_1|^2$, $\bar{n}_2 = |B_2|^2$ and $\bar{n}_3 = |B_3|^2$, governed by Eq. (II.41) with the initial Boltzmann populations at room temperature (T = 300K) $B_1(0) = 0.10$, $B_2(0) = 0.214$ and $B_3(0) = 0.417$, and the initial phases $\tan^{-1}[I_j(0)/R_j(0)] = 0$, where I_j and R_j are the imaginary and real parts of $B_j (j = 1,2,3)$.

Fig. 4 shows the peak values of the average excitations of the active mode ($\bar{n}_1^*$) and of the ν_2 mode ($\bar{n}_2^*$) vs. the external (Δ_E') and internal (Δ_I') detunings, respectively. It is seen that the optimal detuning $\Delta_E^* \simeq 17$ cm^{-1}, and the value of $\bar{n}_1^*$ decreases for Δ_E' larger than Δ_E^*. Similar behavior can also be seen for $\bar{n}_2^*$. This "red-shift" behavior of the optimal detuning is a general feature of any laser-excited anharmonic system where the energy spacings are closer for higher levels. Furthermore, these nonlinear effects due to the anharmonicity show the "bistability" transition in the diagram of steady-state average excitation vs. laser intensity. (See Section III for more detailed discussion.)

Fig. 5 shows that the time evolution of the excitations of various modes for exact resonance, far-off resonance and the optimal detuning. It is seen that, by comparison of A with B, the active-mode excitation (n_1) is coupled to the other modes more significantly for the resonance situation than for the far-off resonance situation, as we predicted from the internal resonance criterion. Note that the peak value of the ν_2 mode ($\bar{n}_2^*$) decreases from 0.4 (for $\Delta_I' = 0$) to 0.1 (for $\Delta_I' = 63$ cm^{-1}). From these numerical results we estimate that the rising times of the average excitations t_1^* [defined by the first peak values of the average excitation $\bar{n}_1^*(t^*)$] range from $t_1^* = 27$ picoseconds (ps) to $t_1^* = 70$ ps depending on the internal detuning Δ_I'. However, the rising times of the ν_2 mode, i.e., the IVR times, are on the order of $t_2^* \simeq 10$ ps (or 3.3 cm^{-1}). A typical excitation diagram is shown in Fig. 5(C) for the case of $(\Delta_E'/2\pi, \Delta_I'/2\pi) = (2.71, 1.00)$.

4. Selectivity in Multiphoton Processes

Selectivity is characterized not only by the coherent properties of the laser field but also by the molecular properties of the excited system.

Therefore, the types of selectivity in infrared MPE can be classified according to the relation between the various relaxation times of the excited system and the energy pumping rate of the laser field. Let us first define R_{intra} and R_{inter} as the intra- and intermolecular vibrational energy transfer rates, respectively, R_{VT} as the relaxation rate for molecular vibrational-translation coupling, i.e., R_{VT}^{-1} is the time for complete thermal equilibrium to be reached in the molecular mixture, and W_{exc} as the rate of vibrational multiphoton excitation of the molecule. We can distinguish four different types of selectivity depending on the relative magnitudes of the relaxation rates and the laser excitation rate (note that the relaxation rates R_{inter} and R_{VT} are pressure dependent, although for low pressures we shall expect that $R_{VT} << R_{inter} << R_{intra}$).

(I) Mode (bond)-selective excitation ($W_{exc} >> R_{intra}$). A certain mode or a functional group of a polyatomic moleclue is in a nonequilibrium state which has a higher vibrational temperature T_{eff} [defined by Eq. (II.24)] as compared with the remaining modes or functional groups. This is the situation of a long lifetime or high pumping rate.

(II) Molecular-selective excitations ($R_{intra} >> W_{exc} >> R_{inter}$). In this case, the absorbed photon energy is rapidly randomized within the excited molecule in which the local vibrational temperature is higher than the overall translational temperature of the mixture of different molecules.

(III) Vibrational-selective excitation ($R_{inter} >> W_{exc} >> R_{VT}$). In this more moderate condition, vibrational equilibrium among all the mixed molecules is reached, but there is still no overall thermal relaxation. This situation prevails for low pressures, where

vibration-translation relaxation rates are lower than vibration-vibration relaxation rates.

(IV) Nonselective thermal excitation ($R_{VT} >> W_{exc}$). This is the situation of thermal excitation of all the molecules in a mixture by a low-power CW laser. This area of infrared thermal chemistry is of interest for a heterogeneous system, e.g., species adsorbed on a solid surface, where the laser radiation is used to excite the adsorbed gas molecules without significantly heating up the solid surface (assuming the phonon coupling to be small). We shall discuss this type of excitation in Section III.

The attraction of infrared laser chemistry is that if the photon energy can be deposited and maintained in a specific vibrational mode (or functional group), a selective reaction channel may be induced by that mode (functional group). Therefore, one of the critical questions concerning MPD processes is whether the photon energy remains localized in the pumped mode (or molecule) long enough to result in a mode-selective (or molecule-selective) reaction. Most theoretical models of MPD assume that IVR is very fast (on the order of a picosecond), and statistical approaches such as RRKM theory have been applied successfully to a number of experimental results.[17,20] Recently, however, several experiments examining product branching ratios in relatively complex molecules, e.g., cyclopropane, have shown that the laser selectivity cannot be explained by the statistical theory.[38] The evidence suggests that the laser-induced reactions could result from a nonergodic or partially mode-selective excitation. Several research groups have also examined the bond localization character of large molecules, e.g., benzene, both experimentally[39-41] and theoretically.[42] This nonstatistical behavior is explained by a local-mode model in which

the total system is divided into two groups of vibrational modes. Within each group, the vibrational modes are strongly coupled and the photon energy quickly randomized. Between groups, however, the coupling is considerably weaker, and intergroup randomization rates are therefore appreciably slower by the concept of the energy-gap law.[36]

Another theory called the "restricted IVR model" has been recently proposed for the possibility of laser selective photochemistry.[43] This model provides a basis for a quantitative description of MPD when IVR processes occur on a time scale competitive with the unimolecular reaction and radiative pumping rate. Note that the statistical theories of unimolecular decay, like the RRKM theory, preclude any possibility of selectivity because of their assumption of very fast IVR rates. For MPD of the SF_6 molecule, the IVR rate is estimated on the order of 10^{12} sec^{-1}, so that selective bond breaking (or mode selection) is possible only when one uses laser radiation with very short pulse duration and about two orders of magnitude more intense than currently available lasers.[20] However, for laser-induced decomposition of cyclopropane, the experimental results strongly indicates a selective mechanism[38] and may be analyzed by the restricted IVR model in which a slower IVR rate (10^{10} sec^{-1}) is estimated. According to this model, the vibrational modes of the system are divided into two groups with an intragroup relaxation rate R_{intra} and an intergroup rate $R_{inter} = \beta R_{intra}$. The theory then allows for a smooth transition from the RRKM theory (with $\beta \to 1$) to the Slater theory (with $\beta >> 1$), and group-selective processes are possible when $\beta << 1$.

5. Multiple-Frequency Laser Excitation

Recent experiments using two infrared lasers simultaneously have demonstrated that MPD can be produced at significantly reduced intensities compared to single-laser excitation, and consequently a sharper isotopic selectivity can be achieved.[44] In these experiments, a lower intensity near-resonant radiation and a higher-intensity off-resonant radiation, neither of which produces dissociation by itself, together give dissociation. Both classical and quantum models have been proposed to analyze MPD enhanced by two or many infrared lasers.[45-48] The effect of laser polarization was also investigated, and it was found that the excitation is more effective when the polarizations of the two lasers are parallel than when they are perpendicular.[49] More recently, the interaction of a diatomic molecule with two near-resonant lasers was studied by a classical anharmonic model.[50]

Within a heat-bath treatment, the total Hamiltonian of an anharmonic quantum oscillator subject to two infrared lasers may be expressed in the same form as that of a single-laser excitation, Eq. (II.12), except that the interaction term H_{AF} is now extended to the form

$$H_{AF} = \hbar[V_1(t) + V_2(t)]\ (a^{+}+a), \tag{II.42}$$

where $V_{1,2}(t)$ are the pumping rates of the laser radiations with frequencies $\omega_{1,2}$. By the same procedures as previously introduced for Eq. (II.15), we obtain the rate equation for the average excitation via two-laser processes as

$$\frac{d\langle n\rangle}{dt} = \frac{\sigma_1 I_1}{\hbar\omega_1} + \frac{\sigma_2 I_2}{\hbar\omega_2} + F(I_1 I_2)^{1/2} - \gamma_1(\langle n\rangle - \bar{N}). \tag{II.43}$$

$F(I_1 I_2)^{1/2}$ is the interference term, with an appropriate function F related to the oscillatory functions $\sin(\Delta_i t)$ and $\cos(\Delta_i t)$, where $\Delta_i = \omega_0 - \omega_i$ $(i = 1,2)$, and the absorption cross sections σ_i are given by, similarly to Eq. (II.16), as

$$\sigma_i = \frac{A_i(\gamma_1+\gamma_2)\hbar\omega_i}{(\Delta_i - 2\epsilon^*\langle n\rangle)^2 + (\gamma_1+\gamma_2)^2/4} \cdot \tag{II.44}$$

For lack of temporal mutual coherence of the two laser sources, we may neglect the interference term and focus on the cooperative effects of these two different lasers on the average excitation of the system. As shown in Fig. 6, we see that at the optimal detuning with $(\Delta_1, \Delta_2) = (2, 8)$ in the unit of $(\gamma_1+\gamma_2)$, the system has a maximum excitation (curve A).[47] It is also interesting to note that a single-laser excitation, where the pumping rate equals the sum of the individual rates, is less effective than the two-laser simultaneous excitations. These cooperative effects of MPE by two different lasers are characterized by the nonlinearity of the absorption cross section through the anharmonic potential of the system.

The above results based on a quantum heat-bath model may also be obtained by a classical approach.[48] The equation of motion is given by an extension of Eq. (II.3),

$$\langle\ddot{Q}\rangle + \gamma\langle\dot{Q}\rangle + \omega_{eff}^2\langle Q\rangle = \sum_{i=1,2} [eE_i \cos(\omega_i t)]/m, \tag{II.45}$$

and the corresponding power absorption is given by the extended expression of Eq. (II.5)

$$\left\langle \frac{dE}{dt} \right\rangle = \sum_{i=1,2} \left(\frac{e^2 E_i^2}{4m} \right) \left[\frac{\gamma}{(\Delta_i - K^* A_i^2)^2 + \gamma^2} \right] + P_I(t), \tag{II.46}$$

where the interference term is given by

$$P_I(t) = \left(\frac{e^2}{4m} \right) E_1 E_2 \sum_{i=1,2} \frac{\gamma \overline{\cos[(\omega_1 - \omega_2)t]} - (\Delta_i - K^* A_i^2) \overline{\sin[(\omega_1 - \omega_2)t]}}{(\Delta_i - K^* A_i^2)^2 + \gamma^2}. \tag{II.47}$$

To compare the above classical results with those of the quantum models, we note that the interference term $F(I_1 I_2)^{1/2}$ of Eq. (II.43) is proportional to $E_1 E_2$ in Eq. (II.47), since the intensity is related to the electric field by $I_i = E_i^2/(8\pi/c)$. Furthermore, the classical and quantum correspondence may be easily obtained by the following quasi-quantum relations:

$$e = \mu'(0), \tag{II.48a}$$

$$\frac{1}{2} m \omega_0^2 A^2 = \langle n \rangle \hbar \omega_0, \tag{II.48b}$$

where e is a classical charge, $\mu'(0)$ is the matrix element of the derivative of the dipole operator, evaluated at the equilibrium point, and $\langle n \rangle \hbar \omega_0$ is the photon energy absorbed by the quantum oscillator and hence equals the energy of the classical osicllator with amplitude A.

The enhancement of MPE via multiple-frequency lasers has been investigated.[45,46] It was suggested that if a single laser of intensity I produces a maximum excitation of frequency ω, then the same maximum

excitation may be produced by N lasers of intensity I/N^3 and frequencies $\omega_k = \omega_0 + k(\omega-\omega_0)/N$, with k = 1, 2, ...N. The enhancement of MPE or the reduced power law of the laser intensity, I/N^3, compared with that of the separate N-laser excitation, I/N, in principle can be achieved if one can modulate the phases of the laser pulses such that the Rabi frequencies are synchronized with the excitations between pairs of the anharmonic energy levels, i.e., π pulses are required in addition to the resonance condition ω_k.[45]

B. Molecular Collisions

1. Resonance Formation, Chemical Reactions and Transition-State Spectroscopy

In recent years there has been an upsurge of interest in gas-phase laser-induced collisions. While much of the excitement has been due to the tantalising prospect of selectively altering the dynamics of chemical reactions, it remains true that the literature (both experimental and theoretical) is generally characterised by the assumption of very intense laser fields, and these are somewhat impractical for two reasons. First, intense fields have a habit of producing stray side effects that may interfere with the process of interest (gas breakdown due to ionisation is a typical example). Second, and perhaps more important, is that intense fields are consistent only with pulsed lasers, and these are unfortunately "switched off" most of the time they are operating: the pulse length is typically extremely short compared to the time between pulses. Thus, any cross section which one calculates is effectively "reduced" by many orders of magnitude in a realistic experiment. In our opinion, this is one of the most serious limitations posed to conventional laser-induced chemistry.

Of course, one could use the radiation in a theoretically trivial way, to excite the reactants into quantum states that make the desired reaction more feasible. However, in many cases this may not be desirable. For example, it may not be possible to excite the reactants because the available lasers are not resonant with the transition. Moreover, even after the reactants are excited, one still has only a relatively crude control over the outcome of the reaction: undesirable side reactions may also take place, or the quantum efficiency for the reaction of interest may turn out to be low.

One can to a large extent get around these problems by taking advantage of the huge numbers of molecular states that are formed during the collision. This means that a far greater range of experimental conditions, such as collision energy and laser frequency, can in principle give rise to a reaction. However, one again runs into the problem that, since many collisions are short-lived, any photons that are to be absorbed during the collision have to be absorbed in a relatively short period of time. This of course means that in order to observe any reaction at all, one must provide more photons, and this raises the intensity requirements of the laser to levels that may be impractical for the reasons we have given. [The kind of intensity that has been discussed in the literature is typically greater than, and usually much greater than, 1 MW/cm^2.]

There are two related factors by which radiative collision cross sections can be increased. The first is resonance formation, and the second is low-energy collisions. They are related since the effect in both cases is to increase the time of collision, thus allowing the colliding partners more chance of absorbing a photon. It is perhaps not surprising that resonance formation leads to an enhancement of the cross section, but it may seem rather paradoxical that a decrease in collision energy should have a similar effect. After all, the Arrhenius Law implies that chemical reactions proceed at a slower rate as the temperature is lowered. However, it must be remembered that in a chemical reaction there is always an activation energy barrier, and the reason that reactions become faster at higher energies is simply that more reactants have sufficient energy to overcome this barrier.

But if the activation energy is supplied by a photon, there is then no need for a high collision energy--indeed low energies are favored since they entail longer collision times. At exceptionally low collision temperatures (less than a few degrees Kelvin), the collision must be treated quantum mechanically since the scattering wavelengths become comparable to the molecular dimensions, except for very heavy atomic and molecular reactants. We shall first consider an atom-atom collision in the presence of laser radiation and investigate the ramifications of radiative resonance formation when more than one laser is employed. Later, we shall sketch some work which is underway to investigate the feasibility of driving certain chemical reactions with lasers of low intensity.

We consider an atom-atom collision in the presence of two lasers, L1 and L2. The total Hamiltonian is given in atomic units as

$$H = -\frac{1}{2\mu}\nabla^2 + H^{el} + H^{so} + H^{rad} + H_1^{int} + H_2^{int} , \qquad \text{(II.49)}$$

where μ is the reduced mass of the system, and H^{el} is the electronic Hamiltonian in the absence of spin-orbit coupling, with eigenvalues (in the Born-Oppenheimer approximation) which are the molecular potentials. H^{so} is the spin-orbit Hamiltonian. H^{rad} is the Hamiltonian of the radiation fields,

$$H^{rad} = \sum_i \omega_i \, a_{i\sigma}^{\dagger} \, a_{i\sigma} \qquad \text{(II.50)}$$

where ω_i is the frequency of laser i, and σ is its polarization state

in spherical coordinates: σ = 0, +1 and -1 denotes, respectively, light plane polarized in the z-direction, and right and left circularly polarized and propagating along z. The eigenvectors of H^{rad} are the Fock states $|n_{i\sigma}>$, such that $a_{i\sigma}|n_{i\sigma}> = \sqrt{n_{i\sigma}}|n_{i\sigma}-1>$ and $a_{i\sigma}|n_{i\sigma}> = \sqrt{n_{i\sigma}}|n_{i\sigma}+1>$. The radiative interaction Hamiltonians within the dipole approximation are

$$H_i^{int} = \varepsilon_i \Sigma_\sigma [a_{i\sigma}\, \mu_\sigma + a_{i\sigma}^\dagger\, \mu_\sigma^*] \,, \tag{II.51}$$

where μ_σ is the space-fixed component of the dipole operator and $\varepsilon_i = (\frac{2\pi\omega_i}{V_i})^{1/2}$, with V_i as the quantization volume of the field i. Note that μ_σ can be related to the molecule-fixed components of the dipole operator, μ_η, by the transformation

$$\mu_\sigma = \Sigma_\eta\, \mu_\eta\, D^1_{\eta\sigma}(\hat{R}), \tag{II.52}$$

where $D^1_{\eta\sigma}(\hat{R})$ is the Wigner rotation matrix.

We are particularly interested in the two curve-switching processes which are shown in Fig. 7. Process I has been called the "photon-catalytic effect".[51] This is because there is no net loss of photons from the field, since for each absorption there is an emission of the equivalent photon (same frequency, polarisation and direction). Such a process would therefore appear to hold some promise for laser-induced chemistry. However, from a practical point of view, laser cavity losses are far more important than losses to and from a molecular system. Therefore,

the efficiency of the process is hardly affected by the few photons that are returned to the radiation field by the molecular systems. Moreover, the overall cross sections are not in general very high. Process II on the other hand, while apparently a more contrived means of achieving the same result, turns out to have two advantages. First, it allows the colliding species to approach at exceptionally low energies, since the energy defect for curve switching is made up by absorption of the second photon from L2. Second, it provides greater scope for optimization of the collision conditions: by changing the bound-to-bound transition it is possible to optimize the bound-continuum interactions so that the overall cross section can be maximized.[52]

In order to treat resonance scattering, we consider a Breit-Wigner separation of the T-matrix. The radiative interaction gives rise to resonances in the scattering spectrum, while the field-free interaction may be considered to be a slowly-varying function of the scattering energy. It is therefore convenient to separate the T-matrix into slowly and rapidly varying parts:

$$T = T^P + T^R ,$$

where T^P is the slowly varying, potential scattering T-matrix and T^R represents the resonance scattering. Following the formulation of Feshbach,[53] we define the following projection operators:

$$P = \sum_\alpha \int | \psi_{\alpha E'} \rangle \langle \psi_{\alpha E'} | dE' \qquad \text{(II.53)}$$

$$Q = \sum_n |\phi_n\rangle\langle\phi_n| . \qquad \text{(II.54)}$$

Here, α is a complete set of angular momentum quantum numbers, and E' is the energy of the continuum state specified by α. The n index is a set of vibrational and angular momentum quantum numbers which specify a bound state of the system. The space of Q can be further subdivided into R and S, such that R + S = Q:

$$R = \sum_m |\phi_m\rangle\langle\phi_m| \tag{II.55}$$

$$S = \sum_{n'} |\phi_{n'}\rangle\langle\phi_{n'}| \ , \tag{II.56}$$

It is now possible to write the T-matrix for resonance scattering as[52]

$$T^R_{fi} = \langle\psi^-_f | H_{PR}\Omega H_{RP} | \psi^+_i\rangle \tag{II.57}$$

where $$\Omega = (E - H_{RR} - H_{RP}\, G^+_p\, H_{PR})^{-1} \tag{II.58}$$

$$H_{XY} = XHY \ . \tag{II.59}$$

G^+_p is the Green's function for potential scattering, i.e., with the radiative interaction switched off and the scattering determined by the term H^{el} in the Hamiltonian. This term has off-diagonal elements in a diabatic basis which are indirectly due to spin-orbit coupling, reflecting a curve-switching even in the absence of radiation. The scattering eigenfunctions ψ^+_i and ψ^-_f are, respectively, the out-wave for this potential scattering problem, starting in the initial state i, and the in-wave starting in the final state f. These are <u>total</u> potential scattering wavefunctions consisting of a plane wave in the specified channel and spherical waves in all channels. These may be written

in terms of the standing-wave solutions of the potential scattering, $|\Phi_{\alpha E}^{-}\rangle$ by using the orthogonal matrix W which diagonalises the potential scattering S-matrix.[52] The result is

$$T_{fi}^{R} = \sum_{mm'} \sum_{\alpha\beta} W_{f\alpha} H_{\alpha m} \Omega_{mm'} H_{m'\beta} W_{\beta i} , \tag{II.60a}$$

$$T_{fi}^{R}(\text{DWBA}) = \sum_{mm'} H_{fm} \Omega_{mm'} H_{m'i} , \tag{II.60b}$$

where m and m' are bound intermediate states of the collision complex, and

$$H_{\alpha m} = \langle \Phi_{\alpha E}^{-} | H | m \rangle , \tag{II.61}$$

where $\Phi_{\alpha E}^{-}$ is a standing-wave eigenfunction of H. In the distorted-wave Born approximation (DWBA), W is the unit matrix, and furthermore, $T_{fi}^{P} = H_{fi}$. Therefore, we have for the total T-matrix

$$T_{fi}\ (\text{DWBA}) = H_{fi} + \sum_{mm'} H_{fm} \Omega_{mm'} H_{m'i} \tag{II.62}$$

The quantity of central interest is Ω since it contains the detailed information about radiative couplings. Possible kinds of laser-induced resonance scattering illustrated in Fig. 8. By defining $\Omega_{mm'}$, we also define a particular pathway: for example, in Eq. (II.60b) $H_{\beta s}\Omega_{st}H_{t\alpha}$ is the amplitude for Process 2 in Fig. 8. Notice, however, that all the ancillary absorptions and emissions induced by L2 are implicitly taken into account in the inversion of Ω^{-1}; that is, Ω_{st} depends not only on $|s\rangle$ and $|t\rangle$ but also on $|u\rangle$. We first evaluate Ω^{-1} by expanding G_{p}^{+} in terms of its open channel eigenfunctions:

$$\Omega^{-1}(E) = E - H_{RR} + P \sum_{\alpha} \frac{H_{RP}|\psi^{+}_{\alpha E'}><\psi^{+}_{\alpha E'}|H_{PR}}{E-E'} - i\pi \sum_{\alpha} H_{RP}|\psi^{+}_{\alpha E}><\psi^{+}_{\alpha E}|H_{PR} \qquad \text{(II.63)}$$

Because of the symmetry of W in (3.12), $|\psi^{+}_{\alpha E}>$ can be replaced by $|\Phi_{\alpha E}>$ in (II.63). With this in mind, the matrix representation of Ω^{-1} in the space of R may be determined by a superposition of a linewidth matrix Γ, a level-shift matrix F, and a radiative interaction matrix V, which describes the bound-to-bound transitions induced by L2:

$$\Omega^{-1}_{st}(E) = E - V_{st} + F_{st}(E) - \frac{i}{2}\Gamma_{st}(E) \ , \qquad \text{(II.64)}$$

where

$$V_{st} = <n_2|<s|H_2^{int}|t>|n_2 - 1> \qquad \text{(II.65a)}$$

$$\Gamma_{st}(E) = 2\pi <n_2 - 1|<s|H_2^{int}|\Phi_{\gamma E}>|n_2><n_2|<\Phi_{\gamma E}|V|t>|n_2> \quad \text{(5.4b)} \qquad \text{(II.65b)}$$

$$F_{st}(E) = \frac{1}{2\pi} P\int dE' \frac{\Gamma_{st}(E')}{E-E'} \qquad \text{(II.65c)}$$

$$V_{tt} = 0 \qquad \text{(II.66a)}$$

$$\Gamma_{tt}(E) = 2\pi\Sigma_{\alpha}|<n_2-1|<t|H_1^{int}|\Phi_{\alpha E}>|n_2>|^2+2\pi|<t|V|\Phi_{\gamma E}>|^2+\Gamma_{se} \qquad \text{(II.66b)}$$

$$F_{tt}(E) = \frac{1}{2\pi} P\int dE' \frac{\Gamma_{tt}(E')}{E-E'} \ , \qquad \text{(II.66c)}$$

where V is the nonradiative interaction operator (e.g., spin-orbit coupling), and Γ_{se} is the width due to spontaneous emission. The 3x3 matrix Ω^{-1} is now inverted to give the following result:

$$\Omega_{st} = \frac{\Omega_{st}^{-1}(\tilde{\Delta}_u - \frac{i}{2}\Gamma_u)}{(\tilde{\Delta}_s - \frac{i}{2}\Gamma_s)[(\tilde{\Delta}_t - \frac{i}{2}\Gamma_t)(\tilde{\Delta}_u - \frac{i}{2}\Gamma_u) - (\Omega_{tu}^{-1})^2] - \Omega_{st}^{-1}(\tilde{\Delta}_t - \frac{i}{2}\Gamma_t)} , \tag{II.67}$$

where $\tilde{\Delta}_i = E - E_i - F_{ii}$, and E_i is the unperturbed energy of the bound state i.

Using Eqs. (II.60) and (II.67), we can now write down the T-matrix for Processes I and II in Fig. 7. We assume no predissociation channel and neglect spontaneous emission:

$$\text{Process I:} \quad T_{fi} = T_{fi}^{P} + \sum_{m} \sum_{\alpha\beta} \frac{W_{f\alpha} H_{fm} H_{m\beta} W_{\beta i}}{\tilde{\Delta}_m - \frac{i}{2}\Gamma_m} , \tag{II.68}$$

where

$$\Gamma_m = 2\pi \sum_{\gamma} |H_{m\gamma}|^2 ,$$

$$\text{Process II:} \quad T_{fi} = \sum_{mm'\alpha\beta} \frac{W_{f\alpha} H_{\alpha m} V_{mm'} H_{m'\beta} W_{\beta i}}{(\tilde{\Delta}_f - \frac{i}{2}\Gamma_m)(\tilde{\Delta}_i - \frac{i}{2}\Gamma_{m'}) - V_{mm'}^2} . \tag{II.69}$$

It is noteworthy that as the energy defects Δ of the dressed states approach zero, the processes have the same order of magnitude. Indeed, the actual magnitude of Process II might even greatly exceed that of Process I, even though Process II is a three-photon process. We have shown by means of a detailed calculation on the XA + F system that this is indeed the case, provided the initial kinetic energy is low.[52] Moreover, the intensity requirements on the radiation are also very low -- LI operating at 3 kw/cm^2 can give rise to gas kinetic cross sections for Process II. On the other hand, calculations have shown Process I to

give rise to a relatively small cross section (around 0.05 $\mathring{A}^2$) even though the intensity of L1 is large (0.3 MW/cm^2). We emphasize that large effects can be obtained from low-intensity lasers, provided resonances are involved and the initial collision energy is extremely low.

Recently, there have been a number of interesting experiments which appear to have demonstrated chemical reactions that are induced by lasers resonant with any asymptotic states.[54-58] Although this is an encouraging start, many of these reactions seem to have a very small total cross section. It would be useful to have a theory of laser-driven chemical reactions which would enable us to decide what kind of reactions may be feasible, and to perform some quantitative estimates of cross sections. To this end we may consider a model of chemical reaction which is based on the theory of the atom-atom collision discussed above and which conforms to the criteria we have established. An important condition is the ability to form resonances during the collision. We have so far considered radiative resonance formation, but it may be useful to begin by considering systems which form resonances in the absence of radiation. An important class of such systems, which are readily obtained experimentally, are van der Waals molecules (VDWM) formed in their ground electronic state.[59-62] We may, for example, be interested in the reaction

$$He + I_2 + \hbar\omega \longrightarrow HeI^* + I^* \ , \tag{II.70}$$

where the asterisk signifies an excited electronic state.

Consider a collinear reaction, $A + BC + \hbar\omega \longrightarrow BC^* + C^*$, where the bonds BC and AB* are strong and the bonds AB and BC* are relatively weak (see Fig. 9). This kind of condition would be expected

in a typical VDWM. In the absence of radiation, resonances occur in each individual electronic state. For example, the BC bond may gain a quantum of vibrational energy through coupling to the AB bond, which then enters a bound state of motion. The atoms A, B and C then co-exist in a quasibound state which is, however, unstable with respect to the reverse process, predissociation of atom A. This effect is known as "vibrational predissociation".[63-65]

Let us outline the construction of a scattering theory in which the predissociation takes the form of a Feshbach resonance. The radiative interaction between electronic states could be handled in much the same way as for the atom-atom problem. The two electronic states have the coordinate representation $x_1([\rho]; R,r)$ and $x_2([\rho]; R,r)$, respectively, where $[\rho]$ are the electronic coordinates and r and R are, respectively, the length of the strong bond [I-I in the above reaction] and the distance from the more weakly-bound atom (He) to the center of mass of the two strongly-bound atoms (see Fig. 9). Averaging the total Hamiltonian H over the electronic coordinates, we obtain the effective (Born-Oppenheimer) Hamiltonian for the nuclear degrees of freedom:

$$\langle x_1|H|x_2\rangle = V_{12}(R,r) \tag{II.71a}$$

$$\langle x_1|H|x_1\rangle = T_{AB} + T_{C,BA} + m_1(R) + p_2(r) + V_1(R,r) \tag{II.71b}$$

$$\langle x_2|H|x_2\rangle = T_{A,BC} + T_{BC} + m_2(R) + p_2(r) + V_2(R,r) \tag{II.71c}$$

Here, T stands for the kinetic energy operator of the subscripted species,

and m and p are Morse functions representing the potential energy associated with the two "bonds" (strictly speaking, the weak bond is not a conventional bond since its length is measured to the center of mass of the other bond). V_1 and V_2 represent the three-body portions of the ground and excited potential surfaces, which are coupled only through the radiative coupling V_{12}.

We wish to write the T-matrix for the chemical reaction in terms of the operators P and Q which project, respectively, onto the open channels and the eigenvectors of a zeroth-order Hamiltonian defined to be the effective Hamiltonian of Eq.(II.71) minus V_1 and V_2. These are then given by

$$P = \sum_{n_1} \int dE_1 |n_1 E_1^+\rangle\langle n_1 E_1^+| + \sum_{v_2} \int dE_2 |n_2 E_2^-\rangle\langle n_2 E_2^-| \tag{II.72a}$$

$$Q = \sum_{n_1 v_1} |n_1 v_1\rangle\langle n_2 v_2| + \sum_{n_2 v_2} |n_2 v_2\rangle\langle n_2 v_2|, \tag{II.72b}$$

where $|n_j E_j^+\rangle = |n_j\rangle|E_j^+\rangle$, etc., j being the electronic state index. $|E_1^+\rangle$ is the state vector for inelastic scattering in the ground electronic state, consisting of a plane wave in the channel labeled by the asymptotic energy E, plus outgoing spherical waves in all other channels. Similarly, $|E_2^-\rangle$ is an incoming wave for the rearrangement channel. The quantum numbers n_j and v_j label, respectively, the quantum states of the Morse oscillators m_j and p_j. We consider in addition the projectors R and S such that R + S = Q. The space of R is defined by those bound-state vectors which give rise to strong resonances (these can be called "doorway states"[66]), where S is comprised of all other bound-state vectors. It is now possible to write the general T-matrix element connecting the initial and final states:

$$T_{fi} = \langle E_f^-|H_{PR}\Omega H_{RP}|E_i^+\rangle. \tag{II.73}$$

Equation (II.73) contains all the information relevant to a chemical reaction, including the effect of the radiation field. It may at first sight appear analogous to the DWBA picture of a chemical reaction, but it is not. It does in fact represent the exact solution to the Lippmann-Schwinger equation, with the complication that the effective (optical) potential, $H_{PR}\Omega H_{RP}$, is not only complex but also nonlocal in the coordinates R and r. The problem hinges on the representation of $\underset{\approx}{\Omega}$. This is given in terms of the width matrix Γ, the level-shift matrix F and the matrix V whose off-diagonal elements describe radiative bound-bound transitions. The off-diagonal elements of Γ consist of the (nuclear) bound-continuum interaction (both radiative and nonradiative). In other words, Γ couples the open and closed channels. Under certain conditions we expect these matrices to be representations of local operators, where these conditions might hinge on the validity of the Markov approximation used in time-dependent many-body theory. Here a nonlocal kernel $K(t,t')$ in the rate equation for a subsystem is replaced by a local function of time: $K(t,t') \simeq \kappa(t)\delta(t-t')$. This means physically that the motion of the subsystem at one time is completely uncorrelated with its motion at some other time, i.e., there is no memory in the motion (due to randomization on a very short time scale). Similar situations are expected to pertain for long-lived resonances in three-body collisions, which is quite different from what would be expected in, say, a direct collision or stripping reaction where the initial and final states are much more correlated and the nonlocality of the potential is more important.[67]

We could initially assume a local optical potential. Then the matrix representation of Ω in the space projected by R will consist of radiative bound-bound transitions between reactant and product states; it will also consist of nonradiative predissociation widths which couple the bound and scattering states

for either the product or the reactant channels taken separately. Roughly speaking, the probability of reaction may be regarded as the probability of association multiplied by the probability of dissociation into a particular product channel. [This picture should not be carried too far, however, because it is essentially perturbative and we are not using perturbation theory.] The rather complicated effect of nonlocality will eventually have to be addressed, especially since there is already evidence that nonlocality becomes more important at low energies,[68-70] and this is just the scattering regime we are interested in. A simplifying feature is that nonlocality appears to be separable at low energies, i.e., $f_E(R,R') \overset{E\to 0}{=} g_E(R)h_E(R')$.[69,70]

Finally, we would like to say a brief word about transition-state spectroscopy in the light of what has been discussed in this section. There has recently been interest in, and experimental evidence for, such spectroscopy.[71,72] We wish to emphasize that the transition state may be regarded as a set of resonance states formed during a collision. Spectroscopy of the transition state then involves radiative transitions between such states. Spectroscopy and energy transfer are distinguishable only according to what one wishes to detect: if one chooses to detect emitted (or absorbed) photons, then it is spectroscopy, and if particles are detected then it is energy transfer (scattering). The spectroscopic "probe" may thus be regarded merely as one contributor to the total S-matrix for particle scattering. Thus, the methodology for treating spectroscopy of the transition state would be essentially what we have outlined for radiative collisions. We note that L2 acts not only as a spectroscopic probe but also as the agent of energy transfer within the manifold of transition states. Thus, when L2 has a significant effect on the overall scattering event, the distinction between these two functions is unclear. They are, however, to be thought of in a unified way, as we have mentioned.

2. Isotopic Selectivity

An intriguing potential application of radiative resonance scattering is to isotope separation. Consider the radiative velocity-changing collision depicted in Fig. 10. We may represent the event depicted in the top part as

$$A + B(E_i) \xrightarrow{+\hbar\omega_1} AB(v,\ell) \xrightarrow{+\hbar\omega_2} AB(v'\ell') \xrightarrow{-\hbar\omega_1} A + B(E_f) \qquad (II.75)$$

where $+\hbar\omega$ denotes absorbtion and $-h\omega$ denotes emission. The vibration-rotation level of the AB complex is denoted by (v,ℓ). The selectivity of such a process arises from the different vibration-rotation spacings for systems of different isotopic composition.[73] Clearly, only certain colliding pairs could then undergo the above three-photon event. For such systems the final translational energy has been increased by an amount equal to the energy of a single photon from L2 (i.e., $\hbar\omega_2$). From the previous considerations we might expect such an event to be extremely efficient at low collision energies. The extra translational energy picked up would be very much greater than the relative translational energy of the unexcited molecules in the beam, and comparable to the forward translational energy. Thus, the excited molecules will tend to be scattered out of the beam. Experimentally the collision partners can be prepared in the same beam which is formed by supersonic expansion. At some point downstream of the source, where the kinetic energy of relative motion is extremely low (1K), the beam may be crossed by the two lasers L1 and L2. The desired products which are scattered out of the beam may then be skimmed off and collected.

We have used the formalism of the previous section to calculate the importance of this effect for the XeF system. Let us define a separation p for separation of the heavy isotope ^{130}Xe:

$$p = \frac{\bar{\sigma}_{130}}{\bar{\sigma}_{129}+\bar{\sigma}_{130}} \qquad ((II.75)$$

where $\bar{\sigma}_{129}$ and $\bar{\sigma}_{130}$ are the kinetic-energy-averaged cross sections for ^{129}Xe and ^{130}Xe collisions with ^{19}F, respectively. When L2 is tuned to the appropriate frequency for resonance in $^{130}Xe^{19}F$, p is found to be as high as 0.996. While certain aspects not taken into account in our calculations might reduce the efficiency, such as finite laser bandw'dths and possible elastic collisions experienced by the deflected molecules before leaving the beam, it is clear that these velocity-changing radiative collisions could provide an efficient means of isotope separation. Furthermore, the high cross section of the event (about 20 $\mathring{A}^2$ in our specific example[73]) is achieved with the relatively lower laser intensity of 5 kW/cm^2.

The advantage such a process has over more conventional techniques like photodissociation or photoionization is, in the main, one of flexibility: first, there is almost unlimited control over the initial scattering energy, and second, depending on the tunability of L2, there is a large choice of bound intermediate states. This flexibility allows for optimization of conditions. The other techniques are limited to using initial states which belong to a limited number of bound states. Under these circumstances, the available dissociation pathways may often be unfavorable, requiring intense lasers. We would like to add that a chemically reacting system (such as was outlined in the previous section) might be even more appropriate for isotope separation. In this instance, only one laser is required to drive the reaction. Finally, we summarize by noting that all of the ideas we have discussed in Part B of Section II lead to our belief that laser-induced chemistry is eminently viable provided one stresses resonance formation and low collision energies.

III. Surface Processes

While the influence of laser radiation on homogeneous gas-phase systems has been intensely studied,[1,2] much less has been done on heterogeneous, e.g., gas/solid, systems either theoretically[35,74-93] or experimentally.[94-101] The effects of laser radiation on adspecies/surface systems depend upon the nature of the surface (metal, insulator or semiconductor, smooth or rough, etc.), the coherent properties of the laser radiation (frequency, intensity, pulse duration, polarization, etc.) and the electronic and vibrational structure of the adspecies/surface system. Depending upon the laser frequency, the electronic, vibrational or vibronic states of the adspecies and/or the substrate may be perturbed with susequent energy flow among the various modes of the system. In this section, we shall focus on the infrared vibrational excitation of the adspecies/surface system in which the direct electronic excitation of the adspecies, which could only be affected by, e.g., visible radiation, will be ignored. However, indirect types of excitations such as substrate heating, migration and desorption of the adspecies will be considered.

We shall first investigate the field-free system where species (atoms or molecules) are adsorbed (physisorbed or chemisorbed) on a solid surface. The combined interface system, adspecies/surface, is significantly different from the homogeneous, i.e., gas-phase or clean surface, systems as follows:

(i) The adspecies (consisting of n atoms) has 3n so-called "frustrated" librational degrees of freedom instead of 3n-6(5) as in the gas phase. For example, there are six vibrational modes for CO adsorbed on a solid surface whereas the surface-free CO molecule has only one vibrational mode.

(ii) Due to the substrate, the excited adspecies usually has a shorter lifetime as compared with that in the gas phase, because of its strong coupling to the phonon modes, particularly for chemisorbed species.

(iii) The energy spectrum of the species is changed in the presence of the substrate. The frequency shift and level broadening may be caused by many surface-induced phenomena such as:[82] (1) energy flow between the adspecies and the substrate and among the internal modes of the adspecies; (2) fluctuation of the effective dipole moment of the adspecies caused by, e.g., the charge transfer between the adspecies and the adsorbent surface and the dynamic coupling between the adspecies dipole and its image; (3) fluctuation of the conformations of the adspecies caused by the libration of the adspecies, particularly when the system is subjected to laser radiation; (4) migration-induced broadening via inelastic scattering among the adspecies (particularly for physisorbed states) and their collision with the surface atoms; and (5) other phase-relaxation-induced broadening, i.e., T_2 broadening.

(iv) The quasi-continuum region, available in the gas phase only for polyatomic molecules, may be usually achieved even for diatomic molecules when adsorbed on a solid surface. The frustrated degrees of freedom, as defined in (i), have very high densities of states, and the overlap of these individual states will lead to a quasi-continuum of the overall vibrational potential of the adspecies and/or the surface potential.

When the adspecies/surface system is subjected to IR radiation, item (iii) above will most likely play a particularly important role, due to processes such as laser-enhanced migration and desorption. Furthermore, when the adspecies is highly excited and reaches the quasi-continuum, further excitation resulting in bond-breaking (desorption) may be achieved by quasi-resonant laser excitation in this region and/or thermal-phonon-assisted excitation. The concept of the quasi-continuum is essential for understanding the mechanism of desorption; without this concept, one must resort to unrealistically high laser powers to overcome the anharmonicity of, e.g., a Morse potential. Detailed discussion on this aspect will be given later.

The influence of IR radiation on the adspecies/surface system is more complicated to describe than for gas-phase unimolecular dynamics as described in Part A of Section II. The following important mechanisms will be addressed:

- How is the laser photon energy selectively transferred to the active mode of the adspecies with consequent relaxation to the bath modes?
- What is the energy relaxation dynamics and how are the (single-phonon and multiphonon) relaxation rates governed by systems parameters, such as frequency spectrum, interaction potential and masses of the adspecies/surface system?
- What is the nature (selective and nonselective) of the photon energy deposition in the system? How is the selectivity characterized by the damping rate, pumping rate and the rate of intramolecular vibrational relaxation?
- How does the nature of energy flow from the excited mode to the other modes depend upon mathematical treatments, e.g., Markoff approximation, continuum-density-of-states approximation and the feedback mechanisms achieved by memory effects and/or the substrate heating effects?
- How are the isotope effects for a system consisting of a mixture of isotopic adspecies characterized by, e.g., the frequency difference of the isotopes, the direct dipole-dipole interaction and the phonon-mediated coupling?
- How does the laser radiation affect the rate processes via field-induced dynamics such as desorption, migration, decomposition, recombination and desoption? In other words, how do the laser and surface synergistically affect heterogeneous catalytic reactions?

None of the above addressed aspects of laser-induced surface processes (LSSP) has been completely investigated, either experimentally or theoretically. However, some qualitative and/or semi-quantitative results, will be discussed in this section, which consists of two parts: (A) energy flow in adspecies-surface systems where microscopic treatments, types of selectivity, photon

energy population, isotope effects and dynamic effects (migration and desorption) will be investigated; and (B) laser/surface-catalyzed reactions where applications of the theoretical aspects of LSSP and some recent experimental work on LSSP will be reviewed.

A. Energy Flow in Adspecies-Surface Systems

Considering a group of species (atoms or molecules) adsorbed on a solid surface and subjected to IR radiation, the most general total Hamiltonian describing the energy flow within the adspecies/surface system may be written as

$$H = H_0 + \sum_{i\neq j} H_{ij} + \sum_{i} H_{ii} + \sum_{i\neq j} H_{iji} + \sum_{i\neq j\neq k} H_{ikj} + \sum_{i} H_{iF}(t) \quad . \qquad \text{(III.1)}$$

H_0 represents the unperturbed Hamiltonian of the system (adspecies, substrate phonons and laser photons); H_{ij} and H_{ikj} represent the direct interaction and the k-mode-mediated interaction between the i-th and j-th modes, where i, j and k may be the adspecies, adbond or phonon modes; and H_{iF} is the interaction between the i-th mode of the system and the field (laser photon). In the following discussion, we shall assume only one active mode in the adspecies to be excited by the IR radiation, except for when we discuss isotope effects, in which case there will be two active modes.

The microscopic Hamiltonian including heat-bath effects will be used to calculate the excitations for both single-phonon and multiphonon processes. A more complicated system consisting of A, B and C subgroups will be investigated, where the memory function of the interaction between A and B and their common damping to C is included. Energy populations in a multilevel system will be studied, and the mechanism of excitation (selective vs nonselective) will be numerically examined. Numerical results will also be shown for the adbond excitations in the H/W system. By solving the rate equation in energy space in the quasi-continuum, several types of photon energy populations and the associated desorption probabilities will be calculated. Extension of the single adspecies to a system consisting of two isotopes will be investigated, and finally, the dynamic effects (migration and desorption) will be studied. While much of the work presented in this section has already been published or

is in press (with references cited), some unpublished concepts and results are also included, e.g., the discussions in Parts A.2.a, A.4 and A.5.

1. Microscopic Treatment

a. Single-Phonon Processes

Consider a heterogeneous system consisting of atoms or molecules adsorbed on a uniform solid surface and subjected to infrared laser radiation. The vibrational degrees of freedom of the adspecies-surface system can be divided into two groups, namely, the pump mode (resonant infrared-active vibrational mode of the selectively-driven adspecies) and the bath modes (all other modes including adspecies inactive modes and the surface phonon modes). The radiation feeds energy into the pump mode, and the heat bath provides a relaxation mechanism. The microscopic model Hamiltonian describing this relaxation dynamics can be written in the following second-quantized form, corresponding to the simplest case of Eq.(III.1) consisting of only H_0, H_{ij} and H_{iF} with i=A:[82]

$$H = H_A + H_B + H_{AB} + H'(t) \quad , \tag{III.2a}$$

$$H_A = \hbar\omega_A a^\dagger a + \sum_{p=3} \hbar\beta_p (a^\dagger + a)^p \quad , \tag{III.2b}$$

$$H_B = \sum_j \hbar\omega_j b_j^\dagger b_j \quad , \tag{III.2c}$$

$$H_{AB} = \sum_j \hbar(K_j a^\dagger b_j + K_j^* a b_j^\dagger) \quad , \tag{III.2d}$$

$$H'(t) = \hbar V \cos(\omega t)\ (a^\dagger + a) \quad , \tag{III.2e}$$

$$V = (2\hbar m_A \omega_A)^{-\frac{1}{2}} \mu'(0) E \cos(\theta) \quad . \tag{III.2f}$$

H_A and H_B are the unperturbed Hamiltonians (vibrational energy) of the pump mode and the bath modes, respectively; H_{AB} is the interaction Hamiltonian coupling the pump mode and the bath modes; and $H'(t)$ is the adspecies-field effective interaction Hamiltonian. The operators $a^\dagger$,a and $b^\dagger$,b are the usual harmonic vibrational ladder operators (with fundamental frequencies ω_A and ω_j) of the pump mode and the bath modes, respectively; β_p is the anharmonicity of the nonlinear quantum oscillator (pump mode); $\mu'(0)$ is the derivative of the effective dipole moment of the pump mode evaluated at the equilibrium point; E is the electric field of the radiation with frequency ω, linearly polarized at an angle θ with respect to the effective dipole moment; and m_A is the reduced mass associated with the active mode. In Eq. (III.2d), K_j represents the coupling between the active mode and the j-th bath mode. We note that the laser field defined in the expression of Eq. (III.1e) was assumed to be a single-mode classical field; the case of a quantized multimode laser excitation will be investigated later. [We should also mention that θ=0 in Eq. (II.12e), which is why the cosine term is absent there.]

The equation of motion for an operator $O(t)$ in the Heisenberg picture,

$$O(t) = \exp(iHt/\hbar)\, O\, \exp(-iHt/\hbar) \quad , \tag{III.3}$$

where the time-independent operator O is defined in the Schrödinger picture, is

$$\frac{dO(t)}{dt} = \frac{1}{i\hbar}[O(t)\,,\,H] \quad , \tag{III.4}$$

employing the operator algebra[14]

$$[a(t)\,,\,H] = \partial H/\partial a^\dagger(t) \quad , \tag{III.5a}$$

$$[b(t)\,,\,H] = \partial H/\partial b^\dagger(t) \quad , \tag{III.5b}$$

we obtain the following set of coupled equations:

$$\dot{a}(t) = i\omega_{eff}a(t) - i\sum_j K_j b_j(t) - iV\cos(\omega t), \tag{III.6a}$$

$$\dot{b}_j(t) = -i\omega_j b_j(t) - iK_j^* a(t) \quad , \tag{III.6b}$$

where ω_{eff} is the effective frequency obtained by the contact transformation,[82] including anharmonicity up to fourth order in Eq. (III.2b),

$$\omega_{eff}(t) = \omega_A - 2\varepsilon^* a^\dagger(t)a(t) \quad , \tag{III.6c}$$

$$\varepsilon^* = 30\beta_3^2/\omega_A - 6\beta_4 \quad , \tag{III.6d}$$

We solve for the phonon operators $b_j(t)$ by formally integrating Eq. (III.6b) to obtain

$$b_j(t) = b_j(0)\exp(-i\omega_j t) - iK_j^* \int_0^t dt'\, a(t')\exp[-i\omega_j(t-t')]. \tag{III.7a}$$

Substituting Eq. (III.7a) in Eq. (III.6a), we get

$$\dot{a}(t) = i\omega_{eff}(t)a(t) + A_1(t) + A_2(t) - iV\cos(\omega t) \ , \tag{III.8a}$$

where

$$A_1(t) = -i \sum_j K_j^* b_j(0)\exp(-i\omega_j t) \quad , \tag{III.8b}$$

$$A_2(t) = -\int_0^t dt' A(t')\, M(t-t') \quad , \tag{III.8c}$$

and $M(t)$ is the memory (kernel) function given by

$$M(t) = \sum_j |K_j|^2 \exp(-i\omega_j t) \ . \tag{III.8d}$$

To solve the above equation and hence the average excitation, the unknown function $A(t)$ and the many-body effects due to the phonon modes in $A_2(t)$ must be decoupled. Depending on the memory function $M(t)$, which is characterized by the time evolution of the active mode and the density of states (or frequency spectrum) of the phonon modes, the excitation and relaxation may behave quite differently. For example, the relaxation of the active mode may be irreversible in one way or reversible in another, i.e., there may be energy feedback to the active mode in the other way. There are several techniques to deal with the aforementioned many-body problem. We shall first discuss those for irreversible relaxation, and the feedback mechanism resulting from different features of the memory function will be investigated later.

Within a Markoff process where the correlation time of the phonon operators is much faster than that of the active mode and the excitation rate, the zeroth-order active-mode operator $a(t)=a(0)\exp[-i\int dt'\omega_{eff}(t')]$ may be used to evaluate $A_2(t)$. There are several alternatives to evaluate the integral in Eq. (III.8c): (i) extending the upper time limit from t to infinity and working out the time integral first; (ii) assuming a continuum phonon spectrum and factoring out the coupling strength K and the density of states ρ; (iii) assuming the memory function is a delta function in time. Either of these methods gives [14,84]

$$A_2(t) = -(\gamma_1/2 + i\delta\omega)a(t) \ , \tag{III.9}$$

where the damping factor, γ_1, and the frequency shift, $\delta\omega$, are given by

$$\gamma_1 = 2\pi|K(\omega_A)|^2 p(\omega_A) \ , \tag{III.10a}$$

$$\delta\omega = P\left[\sum_j |K_j|^2/(\omega_A-\omega_j)\right], \tag{III.10b}$$

where P stands for "principal part".

Substituting the result of Eq. (III.9) into Eq. (III.8a), we decouple the phonon modes and obtain a single equation

$$\dot{a}(t) = i(\omega_{eff}+\delta\omega-i\gamma_1/2)a(t) + A_1(t) - iV\cos(\omega t) \ . \tag{III.11}$$

The effects of the phonon modes have thus been incorporated into a damping factor, γ_1, and a frequency shift, $\delta\omega$, of the active mode. Another technique to treat the multimode phonon effects is the Wigner-Weisskoff single-pole approximation, which we shall discuss later when dealing with multiphonon relaxation processes.

The above nonlinear equation cannot be solved analytically due to the excitation-dependent anharmonicity in $\omega_{eff}(t)$ [see Eq. (III.6)]. However, for low excitation, we may ignore the anharmonicity and solve Eq. (III.11) to obtain the ensemble-averaged (on the active- and bath-mode coordinates) excitation $\langle n(t)\rangle \equiv \langle\langle a^{\dagger}(t)a(t)\rangle\rangle$ for the harmonic case ($\varepsilon^*=0$),

$$\langle n(t)\rangle = \left[\frac{(V/2)^2}{\Delta^2+(\gamma_1/2)^2}\right]\left[1+e^{-\gamma_1 t}-2e^{-\gamma_1 t/2}\cos(\Delta t)\right] + \bar{n}\left[1-e^{-\gamma_1 t}\right] , \qquad \text{(III.12)}$$

where $\Delta=\omega_A+\delta\omega-\omega$ is the phonon-shifted detuning and $\bar{n}$ is the phonon occupation number given by the Bose-Einstein function, evaluated at the active-mode frequency,

$$\bar{n} = \left[\exp(\hbar\omega_A/kT)-1\right]^{-1} . \qquad \text{(III.13)}$$

Here we assumed that the phonon modes provide an infinite energy "sink" and the initial surface temperature (T) remains constant. This is not necessarily always true when one considers a more complicated system consisting of several subgroups of bath modes, where some of the subgroups may have finite numbers of modes rather than an infinite sink. Further discussion on this will be given later.

So far we have discussed only the situation where the damping or level width of the excitation is governed by the so-called T_1(energy) relaxation rate, γ_1. To include the effects of T_2(phase) relaxation on the excitation, we investigate the ensemble-averaged (over the phonon-bath coordinates) equation of motion for the active-mode operator, $\hat{O}(t)=a(t)$ or $a^{\dagger}(t)a(t)$, in the Heisenberg-Markoff picture (HMP).[14,81]

$$\frac{d\langle\hat{O}(t)\rangle}{dt} = \left\langle [iV\cos(\omega t)/\hbar]\left[\frac{\partial\hat{O}(t)}{\partial a^{\dagger}(t)} - \frac{\partial\hat{O}(t)}{\partial a(t)}\right] - (\gamma_1/2)\left[\frac{\partial\hat{O}(t)}{\partial a(t)}\, a(t) + a^{\dagger}\frac{\partial\hat{O}(t)}{\partial a^{\dagger}(t)}\right]\right\rangle + \gamma_1\bar{n}\frac{\partial^2\hat{O}(t)}{\partial a(t)\partial a^{\dagger}(t)} + \left\langle\frac{d\hat{O}(t)}{dt}\right\rangle_{T_2} . \qquad \text{(III.14)}$$

The last term involving the dephasing (T_2 processes) is characterized by the dephasing-induced broadening factor γ_2 as follows:

$$\left\langle \frac{d\hat{O}}{dt} \right\rangle_{T_2} = \gamma_2 \left\langle \left[a^\dagger(t)a(t),O(t)\right]a^\dagger(t)a(t) - a^\dagger(t)a(t)\left[a^\dagger(t)a(t),\hat{O}(t)\right] \right\rangle , \quad \text{(III.15)}$$

which is mathematically constructed such that, for $\hat{O}(t)=a(t)$ and $a\dagger(t)a(t)$,

$$\left\langle \frac{da(t)}{dt} \right\rangle_{T_2} = -\gamma_2 a(t), \quad \left\langle \frac{d[a^\dagger(t)a(t)]}{dt} \right\rangle_{T_2} = 0 . \quad \text{(III.16)}$$

This assures that the T_2 dephasing changes only the phase of the active mode without changing its vibrational energy. By analogy with the above phenomena, in collisional phenomena the T_1 and T_2 relaxation correspond to inelastic and elastic scattering, respectively, and the overall collisional broadening is then given by $\gamma_1+\gamma_2$.

By using Eq. (III.14) and the rotating-wave approximation, the ensemble-averaged equations of motion in the HMP are found to be

$$\langle\dot{\tilde{a}}(t)\rangle = -\left[i(\Delta-2\epsilon^*\langle a^\dagger(t)a(t)\rangle) + (\gamma_1+\gamma_2)/2\right]\langle\tilde{a}(t)\rangle - iV/2 , \quad \text{(III.17a)}$$

$$\langle\dot{\bar{n}}(t)\rangle = (iV/2)\,\langle\langle\tilde{a}^\dagger(t)-\tilde{a}(t)\rangle\rangle - \gamma_1(\langle n(t)\rangle-\bar{n}) , \quad \text{(III.17b)}$$

where we have used the rotating frame defined by $\tilde{a}(t)=a(t)\exp(i\omega t)$. For long laser-pulse excitation, we may employ the adiabatic limit, $|\dot{\tilde{a}}|<<(\gamma_1+\gamma_2)|a|$, to obtain the energy rate equation from Eq. (III.17) with $\dot{\tilde{a}}=0$,

$$\frac{d<n>}{dt} = \frac{\sigma I}{\hbar\omega} - \gamma_1 \left(<n>-\bar{n}\right) \quad , \tag{III.18}$$

where σ and I are the absorption cross section of the whole system (active plus bath modes) and laser intensity (with photon energy $\hbar\omega$). $\sigma I/\hbar\omega$ therefore denotes the total excitation rate of the system given by [81]

$$\frac{\sigma I}{\hbar\omega} = \frac{AI(\gamma_1+\gamma_2)}{[\Delta-2\epsilon^*<n>]^2+(\gamma_1+\gamma_2)^2/4} \quad , \tag{III.19}$$

and $A=(V/E)^2(4\pi/c)$ is a constant resulting from $I=E^2/(8\pi/c)$.

The steady-state average excitation, X, for a cold surface, i.e., neglecting $\bar{n}$, is seen from Eq. (III.18) to be governed by a cubic equation,

$$X = \frac{AI(\Gamma_+/\gamma_1)}{(\Delta-2\epsilon^*X)^2+(\Gamma_+/2)^2} \quad , \tag{III.20}$$

where $\Gamma_+=\gamma_1+\gamma_2$ is the total damping factor resulting from the T_1 (energy) and T_2 (phase) relaxation. The optimal detuning then occurs at the maximum ($dX/d\Delta = 0$) and is given by $\Delta^* = 2\epsilon^*X^*$ (note - the single asterisk which was already attached to ϵ does not signify an optimal condition as it does for Δ and X). At the other extreme where $dX/d\Delta \to \infty$, we obtain a quadratic equation for the detuning, whose two roots correspond to a "bistability" in X as a function of Δ. By equating the two roots, we obtain the critical pumping rate $I^*=\gamma_1\Gamma_+^2/(8A\epsilon^*)$, implying that the existence of the bistability is a consequence of the condition $I>I^*$. For

a fixed laser intensity, which is proportional to V^2 (or the pumping rate), the bistability criterion may also be stated in terms of the anharmonicity as $\varepsilon^* > \varepsilon^{**} = (\gamma_1\Gamma_+)/(4AI)^{\frac{1}{2}}$. This "bistability" feature of the steady-state excitation is shown in Fig. 11. It is seen that when the anharmonicity ε^* is larger than the critical value, ε^{**}, the excitation profile shows the bistable transition from P to Q as the detuning increases, and from R to S as the detuning decreases. We note that the maximum excitation is red-shifted to $\Delta^* > 0$, which is a general property of any nonlinear oscillator with $\varepsilon^* > 0$. A classical analogy of this nonlinear quantum oscillator will be shown later.

A remark on the relaxation rate of the single-phonon processes must be made before we discuss multiphonon processes. We have shown that the many-body effects of the phonon modes on the excitations of the active mode may be reduced to an energy relaxation factor (γ_1) and frequency shift ($\delta\omega$) as shown by Eq. (III.10). In the Markoff approximation the single-phonon relaxation rate is given by [14,78]

$$\gamma_1 = \mathrm{Re} \sum_j |K(\omega_j)|^2 \int_0^\infty d\tau \exp[-i(\omega_j-\omega_A)\tau]$$

$$= \int_0^\infty d\omega_j |K(\omega_j)|^2 \rho(\omega_j)\pi\delta(\omega_j-\omega_A), \qquad \text{(III.21)}$$

which vanishes when $\omega_A > \omega_j$, a situation in which the active-mode frequency is usually greater than that of the bath modes. This unrealistic zero relaxation rate may be avoided if one includes the finite lifetime of the phonon modes, γ_B, which turns the delta function in Eq. (III.21) into a Lorentzian.[87] For an Einstein spectrum $\rho(\omega_j) = \delta(\omega_j-\omega_D)$, we obtain

$$\gamma_1 = \left(\frac{m_A}{m_S}\right)\left(\frac{\omega_A^3}{\omega_D}\right)\left[\frac{\gamma_B/2}{(\omega_A-\omega_D)^2+(\gamma_B/2)^2}\right], \qquad \text{(III.22)}$$

which is significantly different from the result for zero phonon width $\gamma_B = 0$. For a Debye model, $\rho(\omega_j) = 3\omega_j^2/\omega_D^3$ and $\gamma_B = 0$, we have

$$\gamma_1 = \left(\frac{3\pi}{2}\right)\left(\frac{m_A}{m_S}\right)\left(\frac{\omega_A^4}{\omega_D}\right) \quad , \tag{III.23}$$

where m_A and m_S are the reduced masses of the adspecies and the surface atoms, respectively.[78,93]

b. Multiphonon Processes

We have shown that a single-phonon relaxation rate may be achieved by the finite lifetime (or level width) of the phonon modes if the frequency difference $\omega_A - \omega_D$ is not significantly greater than the phonon width γ_B. This is for the situation that the active-mode frequency is close to the phonon spectrum. However, for an IR-active system the active-mode frequency is usually much higher than that of the phonon modes, e.g., for CO/Ni, $\omega_A \sim 2\pi \times 1000 cm^{-1}$, $\omega_j \sim 2\pi \times 300 cm^{-1}$ and $\gamma_B \sim 50 cm^{-1}$, which results in a very small single-phonon relaxation. Therefore, for those systems with a big energy gap between the active and bath modes, the relaxation mechanism is dominated by multiphonon processes and neither Eq. (III.22) nor (III.23) is an appropriate expression for γ_1. To find the power law for the ratios (m_A/m_S) and (ω_A/ω_D), we shall investigate the thermally-averaged (on both the active- and bath-mode coordinates) golden rule for the multiphonon relaxation rate,[87]

$$\gamma_1 = \left(\frac{2}{\hbar^2}\right) \mathrm{Re} \int_0^\infty dt \, \langle\langle H_{AB}(t) \, H_{AB}(0) \rangle\rangle \quad , \tag{III.24}$$

which is governed by the autocorrelation function of the interaction Hamiltonian between the active mode and the bath modes.

Consider a Morse surface potential

$$V(Q,U) = D\left[e^{-2\alpha(Q-U-r_0)} - 2e^{-\alpha(Q-U)}\right], \qquad \text{(III.25a)}$$

$$\approx 2\alpha DQ[e^{2\alpha U} - e^{\alpha U}], \qquad \text{(III.25b)}$$

where D and α are the appropriate parameters of the Morse potential, and Q and U are the position of the adatom and of the surface atom with equilibrium position r_0. Since the frequency of the adatom is much higher than that of the phonon spectrum, we have used the linear expension $\exp(\alpha Q) \approx 1 + \alpha Q$ and dropped the constant terms which do not conserve energy in Eq. (III. 25b). The interaction Hamiltonian is then given by the fluctuation of the adatom-surface potential, i.e.,

$$H_{AB} = V(Q,U) - \langle V(Q,U)\rangle, \qquad \text{(III.26)}$$

where $\langle V(Q,U)\rangle$ is the thermally-averaged (over the bath-mode coordinates) surface potential. Employing the identities

$$\langle e^{\alpha U(t)} e^{\alpha u(0)}\rangle = \langle e^{\alpha U(t)}\rangle\langle e^{\alpha U(0)}\rangle e^{\langle \alpha^2 U(t)U(0)\rangle}, \qquad \text{(III.27a)}$$

$$\langle e^{\alpha U}\rangle = e^{\langle \alpha^2 U^2/2\rangle}, \qquad \text{(III.27b)}$$

we obtain the autocorrelation function

$$\langle\langle H_{AB}(t)H_{AB}(0)\rangle\rangle = (2\alpha D)^2\langle\langle Q(t)Q(0)\rangle\rangle\{E_0(E_t+1) + E_0^4(E_t^4+1) - 2E_0^{5/2}(E_t^2+1)\}, \qquad \text{(III.28a)}$$

$$E_0 = \exp(\alpha^2 \langle\langle U^2 \rangle\rangle) \quad , \tag{III.28b}$$

$$E_t = \exp(\alpha^2 \langle\langle U(t)U(0) \rangle\rangle) \quad . \tag{III.28c}$$

Eq. (III.28) together with Eq. (III.24) enables us to evaluate the multiphonon relaxation rate up to any order. Note that the linear term of the potential $V(Q,U) \approx 4\alpha^2 DQU$ gives us the single-phonon relaxation rate, Eq. (III.22), when $2\alpha^2 D = m_A \omega_A^2$. Furthermore, the relaxation rates may behave differently for different choices of the interaction potential and/or phonon spectrum. To evaluate the multiphonon relaxation rate for a very strong coupling case, the steepest descent method is usually used.[87,89]

For a p-phonon process with $\omega_A \approx q\omega_q + (p-q)\omega_p$, where ω_A, ω_q and ω_p are the frequencies of the active mode and of the acoustic and optical phonons, respectively, the interaction Hamiltonian includes the term $[\alpha^{2(p+1)} QU^p/p!]$. Transforming the coordinates Q and U into the second quantization operators, the integral of Eq. (III.24) may be worked out for an Einstein spectrum to give[77]

$$\gamma_1 \propto \frac{\omega_A^2}{[p!(p-q)!]^{\frac{1}{2}}} \left(\frac{\omega_A}{q\omega_q}\right)^q \left(\frac{\omega_A}{(p-q)\omega_p}\right)^{p-q} \left(\frac{m_A}{m_q}\right)^q \left(\frac{m_A}{m_p}\right)^{p-q} \quad , \tag{III.29}$$

where m_A, m_q and m_p are the reduced mass of the active mode and of the acoustic and optical phonons. We note that the multiphonon relaxation rate is strongly decreasing with increasing the order parameters p and q, since $m_A \ll m_p, m_q$. Therefore, for systems with a small mass ratio, $m_A/m_q, m_q \ll 1$, and/or a high active-mode frequency, $\omega_A \gg \omega_p, \omega_q$, we expect a long lifetime of the excited adspecies. The above results, which provide us with a quantitative description of the power laws of the mass and frequency, are in agreement with that of the energy-gap law.[37] The relaxation rate for the N/Si system has been estimated to be $\gamma_1 \approx 10^{11} s^{-1}$, where for H/Pt, $\gamma_1 \approx 10^4 s^{-1}$. The latter is much lower due to the smaller mass ratio, m_H/m_{Pt}, and $\omega_A \approx 2000$ cm^{-1}, $\omega_q \approx 150$ cm^{-1} and $\omega_p \approx 400$ cm^{-1}.[77]

To obtain the average excitation of the active mode and temperature dependence of the multiphonon relaxation rate, we shall consider the microscopic Hamiltonian[81]

$$H = H_A + H_B + H_{AB} + H'(t) \quad , \tag{III.30}$$

which is the same as that of the single phonon case except that the interaction Hamiltonian H_{AB} describing multiphonon relaxation is now given by

$$H_{AB} = \sum_{\nu} (\hbar G_\nu B_\nu a^\dagger + \hbar G_\nu^* B_\nu^\dagger a) \quad , \tag{III.31a}$$

where we define a multiphonon operator

$$B_\nu \equiv \prod_{j_1,j_2,\cdots j_N}^{j_\nu} b_{j_1} b_{j_2} \cdots b_{j_N} , \tag{III.31b}$$

and G_ν is the coupling strength. It is seen that H_{AB} reduces to Eq. (III.2d) and describes single-phonon relaxation when N=1 and $G_\nu = K_j$. The Heisenberg equations of motion are

$$\dot{a}(t) = i[\omega_{eff}(t)+\tilde{\omega}(t)]a(t) - i \sum_{\nu} G_\nu B_\nu(t) - iV\cos(\omega t), \tag{III.32a}$$

$$\dot{B}_\nu(t) = -i\Omega_\nu B_\nu(t) - iN_\nu G_\nu^* a(t), \tag{III.32b}$$

where

$$\Omega_\nu = [B_\nu(t),H_B]/B_\nu(t) = \sum_{j=j_1}^{j_\nu} \omega_j \quad , \tag{III.33a}$$

$$N_\nu = [B_\nu(t),B_\nu^\dagger(t)] \quad , \tag{III.33b}$$

and $\tilde{\omega}(t)$ is a stochastic frequency modulation which accounts for dephasing effects.

By employing the Markoff approximation as used in the single-phonon case, Eq. (III.32) is decoupled and results in the ensemble-averaged equations of motion in the HMP[14,84]

$$\langle\dot{\tilde{a}}(t)\rangle = -[i(\Delta - 2\varepsilon^*\langle a^\dagger(t)a(t)\rangle) + (\gamma_1+\gamma_2)/2]\langle\tilde{a}(t)\rangle - iV/2 \quad , \tag{III.34a}$$

$$\langle\dot{n}(t)\rangle = -(iV/2)\langle\langle\tilde{a}^\dagger(t) - \tilde{a}(t)\rangle\rangle - \gamma_1(\langle n(t)\rangle - \bar{N}) \quad , \tag{III.34b}$$

which have the same structure as for the single-phonon case [Eq. (III.17)], except that we now have the multiphonon equilibrium occupation $\bar{N} = \prod_j \bar{n}_j$, and the

relaxation factor is given by

$$\gamma_1 = 2\pi \sum_{\nu} |G_\nu|^2 \bar{N}_\nu \delta(\omega_A - \Omega_\nu) \quad , \tag{III.35a}$$

where

$$\bar{N}_\nu = \prod_{j=j_1}^{j_N} (\bar{n}_j + 1) - \prod_{j=j_1}^{j_N} \bar{n}_j . \tag{III.35b}$$

In deriving Eq. (III.35), the phonon-induced frequency shift was neglected and we assumed that the stochastic frequency obeys the simple correlation $\langle \tilde{\omega}(t)\tilde{\omega}(t') \rangle = \gamma_2 \delta(t-t')$. We note that the significant difference between single-phonon and multiphonon processes lies in the nature of the relaxation factor, γ_1, which is temperature independent [Eq. (III.21)] for single-phonon relaxation but strongly temperature dependent for multiphonon relaxation. For example, for an Einstein spectrum with $\rho(\omega_j) = \delta(\omega_j - \omega_D)$ and $\Omega_\nu = p\omega_D$ (p-phonon process), we find the temperature dependence of the relaxation rate as

$$\gamma_1 \propto [\exp(\hbar\omega_A/kt - 1] \; / \; [\exp(\hbar\omega_D/kt) - 1]^p \quad , \tag{III.36}$$

which, for low temperature ($kT << \hbar\omega_D$) becomes almost temperature independent,

$$\gamma_1 \propto 1 + p\exp(\hbar\omega_D/kT) \quad , \tag{III.37a}$$

whereas for high temperature $(\hbar\omega_A > kT >> \hbar\omega_D)$, (III.37b)

$$\gamma_1 \propto (kT/\hbar\omega_D)^p [\exp(\hbar\omega_A/kT) - 1] \; ,$$

which shows a strong temperature dependence.

We have also assumed the coupling factor G_ν to be independent of temperature and the spectrum of the phonon modes to be governed by a delta function. Furthermore, only the single term in Eq. (III.35) which provides the dominant contribution to the relaxation rate is considered. When considering many atoms of the substrate, the order parameter p should be split into several parts, i.e.,

$\omega_A \simeq \sum q\omega_q$, with $\sum q=p$, and the associated compound density of states should be expressed in terms of a convolution of the single-phonon density of states.[36] To evaluate the multiphonon relaxation rate for an actual system, a realistic phonon spectrum is needed, and information on the crystal structure of the substrate is required for a first-principles calculation.[102]

We have so far investigated the microscopic Hamiltonian based on a single-mode classical field, invoking the assumption that the number of photons in the laser field is so large such that the electric field (or intensity) of the radiation is kept constant even in the presence of the absorbing medium. Depending on the initial states of the system, the active mode may absorb or emit photons corresponding to the excitation and de-excitation of the adspecies. Similarly, the phonon modes may behave as a thermal field when the adspecies is initially "cooler" than the bath modes. For instance, if the substrate is heated by a laser or other thermal source but the adspecies is not, then energy could flow from the phonons to the adspecies. To study these cooling or heating processes of the adspecies, we shall consider a microscopic Hamiltonian similar to that of Eq. (III.1), except that the adspecies-laser interaction, $H'(t)$, is non-quantized into a multimode field form,

$$H'(t) = \hbar \sum_k (V_k c_k^\dagger a + V_k^* c_k a^\dagger) \quad , \tag{III.38}$$

where $c_k^\dagger$ and c_k are the harmonic ladder operators for the k-th mode of the quantized field, and V_k is proportional to the electric field due to radation and may be referred to as the Rabi frequency of the excitation. The Heisenberg equations of motion, previously given by Eq. (III.32), now become

$$\dot{a}(t) = i\omega_{eff}(t)a(t) - i \sum_\nu G_\nu B_\nu(t) - i \sum_k V_k^* c_k(t) \quad , \tag{III.39a}$$

$$\dot{B}_\nu(t) = - i\Omega_\nu B_\nu(t) - iN_\nu G_\nu^* a(t) \quad , \tag{III.39b}$$

$$\dot{c}_k(t) = i\omega_k c_k(t) - iV_k a(t) \quad . \tag{III.39c}$$

The above coupled equations can be solved by using the Markoff approximation to include the many-body effects due to the phonon modes and the laser as developed in the previous sections. Here we shall present an alternative technique.

Taking the Laplace transform of Eq. (2.35), we get

$$a(s) = U(s)a(s) + \sum_{\nu} V_{\nu}(s)B_{\nu}(s) + \sum_{k} W_{k}(s)c_{k}(s), \qquad \text{(III.40)}$$

where $a(s)$, $B_{\nu}(s)$ and $c_{k}(s)$ are the Laplace transforms of $a(t)$, $B_{\nu}(t)$ and $c_{k}(t)$, respectively, and $U(s)$, $V_{\nu}(s)$ and $W_{k}(s)$ are the appropriate functions obtained from the Laplace transform of Eq. (III.39). Employing the Wigner-Weisskopf single-pole approximation, i.e., $s \approx 0$ in Eq. (III.40), the inverse Laplace transform of Eq. (III.40) can be obtained to evaluate the average excitation of the active mode,

$$\begin{aligned} \langle n(t)\rangle \equiv \langle\langle a^{\dagger}(t)\, a(t)\rangle\rangle = \langle n(0)\rangle\, e^{-\Gamma t} + \\ \sum_{\nu} \left[\frac{|G_{\nu}|^2}{\Delta_{\nu}^2+(\Gamma/2)^2}\right]\left[1+e^{-\Gamma t}-2e^{-\Gamma t/2}\cos(\Delta_{\nu} t)\right] \prod_{j} \bar{n}_{j}(0) \\ + \sum_{k} \left[\frac{|V_{k}|^2}{\Delta_{k}^2+(\Gamma/2)^2}\right]\left[1+e^{-\Gamma t}-2e^{-\Gamma t/2}\cos(\Delta_{k} t)\right]\bar{n}_{k}(0) \quad , \end{aligned} \qquad \text{(III.41)}$$

where $\langle n(0)\rangle$, $\bar{n}_{j}(0)$ and $\bar{n}_{k}(0)$ are the initial occupation numbers of the active, phonon and photon modes, respectively, defined by a Bose function with the same temperature but at a different frequency. The detunings are defined by $\Delta_{\nu}=\omega_{A}-\Omega_{\nu}$ and $\Delta_{k}=\omega_{A}-\omega_{k}$, where Ω_{ν} is the multiphonon frequency and ω_{k} is the k-th mode laser frequency. Finally, $\Gamma=\gamma_{1}+\gamma_{0}$ is the total damping factor describing the effects of the parallel nonradiative (phonon) and radiative (photon) relaxation of the quantum oscillator into two independent, noninteracting multimode baths. We note that the multiphonon rate γ_{1} has a temperature dependence

given by Eq. (III.36), while the radiative factor γ_0 is independent of temperature since we consider dipole transitions of the active mode, i.e., the interaction Hamiltonian, Eq. (III.38), contains only linear coupling terms in the resonance excitation with frequency $\omega_k \approx \omega_A$.

Assuming an Einstein spectrum for both the phonon and photon modes, the average excitation at resonance, $\Delta_\nu = \Delta_k = 0$, becomes

$$\langle n(t) \rangle = \left(\frac{2}{\pi \Gamma^2} \right) \left(|G_E|^2 \rho_E \bar{N}_E + |V_F|^2 \rho_F \bar{n}_F \right) \left(1 - e^{-\Gamma t/2} \right)^2 + \langle n(0) \rangle e^{-\Gamma t}, \qquad \text{(III.42)}$$

which is characterized by the incoherent phonon field and the coherent laser field with initial occupations $\rho_E \bar{N}_E$ and $\rho_F \bar{n}_F$, respectively, and the initial occupation of the active mode is decaying with a total rate Γ through two parallel channels, the phonon and photon bath. We note that the active-mode excitation, with initial state $\langle n(0) \rangle = 0$, is built up by both the laser field and the phonon field, particularly when the initial phonon occupation $\bar{N}_E$ is high and/or is "heated up" by the laser field either directly or indirectly via mode-mode coupling.

2. Selective Excitation and Thermal Effects

So far the adspecies/surface system has been described microscopically by a Hamiltonian in which the active mode is singled out, with all the other (inactive) modes treated as a heat bath. The many-body effects of the bath modes were reduced to the damping factors γ_1 and γ_2 based on a Markoff approximation in which the kernel function, M(t) in Eq. (III.8c), was assumed to be a delta function. We shall now investigate the memory effects of the kernel function on the energy-flow dynamics (which up to now were assumed to be governed by an irreversible process with an infinite heat bath). To discuss the types of selectivity, the energy population of a multilevel system will be studied, and finally, the excitations of the adbond in the H/W system will be examined numerically.

a. Memory Function and Feedback Mechanisms

As illustrated in Fig. 12, in a simple heat bath model, the system consists of the active (A) mode and the bath (B) modes in which the B modes are treated as an infinite energy sink due to their large number of modes and the continuum phonon spectrum. The energy flow from A to B is irreversible (with a relaxation rate γ) within the spirit of Markoff processes. In a modified model, the system is divided into three groups: the active (A) mode, the quasi-continuum (B) modes and the true continuum (C) modes. For CO/Ni as an example, the ν_3 mode (with frequency $\sim$1000 cm^{-1}) is the active mode, and the adspecies internal and adbond modes ($\sim$300 cm^{-1}) are the B modes. We shall demonstrate that in the A-B-C model, although the energy flow from A to C and B to C are irreversible, the energy flow between A and B is not necessarily a one-way process. Depending upon the kernel function and the density of states associated with the quasi-continuum B modes, the interaction between A and B may be a two-way process, i.e., there can be a feedback from A to B. Furthermore, we shall show that there is an interference effect which causes an indirect coupling between A and B via the C modes.

The microscopic Hamiltonian describing the energy flow dynamics of the A-B-C system subjected to IR radiation may be best expressed as [Eq. (III.1) with i=A, j=B and k=C, where the C modes are inactive]

$$H = H_0 + H_{AB} + H_{AC} + H_{BC} + H_{AF} + H_{BB} + H_{AA} + H_{BF}, \qquad \text{(III.43)}$$

where $H_0=H_A+H_B+H_C$ is the unperturbed Hamiltonian of the system, $H_{ij}(i,j=A,B,C)$ represent the interactions among them, and H_{AF} and H_{BF} represent the A-mode-laser and B-mode-laser interactions. In the following discussion, we shall focus on the energy flow between A and B, and the last two terms in Eq. (III.43) will be ignored since our model system will consist of only one adspecies and one active mode. For simplicity, we further assume single-phonon processes (the extension to multiphonon processes may be done by techniques used earlier).

The equations of motion for the operators a, b_j and c_k for the A, B and C modes are given in the rotating frame by[14,84]

$$\dot{a} = -i\sum_j g_j\, b_j\, E_j - i\int d\omega_k\, K_{Ak}\, \rho_k\, c_k\, E_k - \frac{iV}{2}\, e^{i\Delta t} \qquad \text{(III.44a)}$$

$$\dot{b}_j = -ig_j a E_j^{-1} - i\int d\omega_k\, K_{jk}\, \rho_k\, c_k\, E_k/E_j - i\sum_{j\neq j'} V_{jj'} e^{i\Delta_{jj'}t}\,, \qquad \text{(III.44b)}$$

$$\dot{c}_k = -iK_{Ak}\, a E_k^{-1} - i\sum_j K_{jk}\, b_j\, E_j/E_k\,, \qquad \text{(III.44c)}$$

$$E_j = \exp(i\Delta_j t), \quad \text{etc.} \qquad \text{(III.44d)}$$

V is given by Eq. (III.2f); g_j, K_{Ak}, K_{jk} and $V_{jj'}$ represent the appropriate coupling factors associated with H_{AB}, H_{AC}, H_{BC}, and H_{BB}, respectively; the detunings are defined by $\Delta=\omega_A-\omega$, $\Delta_j=\omega_A-\omega_j$, $\Delta_k=\omega_A-\omega_k$, $\Delta_{kj}=\omega_j-\omega_k$, etc., where ω_A, ω_j and ω_k are the frequencies of the A mode, the j-th B mode and the k-th C mode with the continuum spectrum and density of states ρ_k. Employing the many-body techniques previously discussed, the effects due to the C modes may be replaced by the frequency shift and the damping factor, whereby Eq. (III.44) becomes

$$\dot{a} = -\gamma_A a - \sum_j iG_j\, b_j\, E_j - \frac{iV}{2}\, e^{i\Delta t}\,, \qquad \text{(III.45a)}$$

$$\dot{b}_j = -iG_j a E_j^{-1} - \sum_{j\neq j'} [iV_{jj'} + \pi\,|K_{j0}|^2\rho_0] e^{i\Delta_{jj'}t}\,. \qquad \text{(III.45b)}$$

$G_j=g_j+(G_1+iG_2)$ has two components--g_j resulting from the direct coupling and (G_1+iG_2) resulting from the indirect coupling between A and B via their coupling to the C modes, where $G_{1,2} \propto K_{j0}K_{A0}\rho_0$; and γ_A is the C-mode-induced damping factor. We note that in Eq. (III.45b), the B-B coupling is governed by the direct coupling factor $V_{jj'}$ (with $j\neq j'$), the C-mode-induced indirect coupling $\pi|K_{j'0}|^2\rho_0$(with $j'\neq j$) and the damping factor $\gamma_B=\pi|K_{j'0}|^2\rho_0$(with $j'=j$). For tractable results, we shall keep only the j'=j term in Eq. (III.45b), so that

$$\dot{b}_j = -\gamma_B b_j - iG_j\, a\, e^{-i\Delta_j t} \qquad \text{(III.45c)}$$

Eq.(III.45) has the same functional structure as Eq.(III.6), except that now the damping factor $\gamma_{A,B}$ has been introduced in the operators for the A and B modes due to their energy relaxation to the C modes. Substituting the formal solution of Eq. (III.45c) into Eq. (III.45a), we obtain, for $b_j(0)=0$,

$$\dot{a} = -\gamma_A a - \int^t dt' a(t') M(t-t') - \frac{iV}{2} e^{i\Delta t} \quad , \tag{III.46}$$

where the kernel (memory) function is given by

$$M(t) = \sum_j |G_j|^2 \exp[(i\Delta_j - \gamma_B)t] \quad . \tag{III.47}$$

To solve for a(t) with the boundary condition a(0)=0, we obtain the Laplace transform of a(t) from Eq.(III.46) as

$$\bar{a}(s) = \frac{-i(V/2)/(s-i\Delta)}{(S+\gamma_A)+\bar{M}(s)} \quad , \tag{III.48}$$

which is characterized by the Laplace transform of the kernel function, $\bar{M}(s)$, given from Eq. (III.47) by

$$\bar{M}(s) = \sum_j \frac{|G_j|^2}{(s+\gamma_B)-i\Delta_j} \quad . \tag{III.49}$$

In our earlier discussions involving the Markoff or continuum spectrum approximation, $M(t) \propto \delta(t)$, the dynamics of the B mode were simply damped due to the A mode. To investigate non-Markoff processes or reversible processes between A and B, we shall now evaluate $\bar{M}(s)$ without assuming a continuum spectrum. From the concept of the energy-gap law and the multiphonon relaxation rate discussed earlier, we know that the coupling strength $|G_j|^2$ is strongly decreasing with the increasing of the multiphonon order parameter. For only finite numbers of modes in B, we then may truncate the sum in Eq.(III.49) and further assume the mean value $\Delta_j=\bar{\Delta}$ and $\sum_j |G_j|^2 = N|\bar{G}|^2$ to obtain

$$\bar{M}(s) = \frac{N|\bar{G}|^2}{s+\gamma_B-i\bar{\Delta}} \quad , \tag{III.50}$$

which yields

$$a(s) = \frac{-i(V/2)(s+\gamma_B-i\bar{\Delta})}{(s-\lambda_1)(s-\lambda_2)(s-\lambda_3)} \quad , \tag{III.51a}$$

where $\lambda_3=i\Delta$ and $\lambda_{1,2}$ are the roots of

$$s^2+(\gamma_A+\gamma_B-i\bar{\Delta})s + \gamma_A(\gamma_B-i\bar{\Delta}) + N|\bar{G}|^2 = 0 \quad . \tag{III.51b}$$

We shall show that the nautre of the energy flow between A and B is characterized by these roots. For near resonance, $\bar{\Delta}<<\gamma_{A,B}$, when the damping of the B mode is in the range

$$\gamma_A-2\sqrt{N}|\bar{G}| < \gamma_B < \gamma_A+2\sqrt{N}|\bar{G}| \quad , \tag{III.52}$$

Eq.(III.52) has two complex roots (which otherwise are real). These complex roots yield the oscillatory behavior of a(t), and accordingly the active-mode excitation $\langle n(t)\rangle \equiv \langle\langle a^+(t)a(t)\rangle\rangle$ is an oscillating function. Therefore, Eq.(III.52) provides the criterion, in terms of the damping factors $\gamma_{A,B}$ and the coupling strength $\sqrt{N}|\bar{G}|$, for the energy flow from A to B and back to A. In the limit of $\gamma_{A,B}<<\sqrt{N}|\bar{G}|$, we readily obtain $\lambda_{1,2}=\pm i\sqrt{N}|\bar{G}|$, which provides the frequency of this back-and forth-flow. We note that in the single-mode limit, $s \approx 0$, $\bar{M}(0)\approx N|\bar{G}|^2/\gamma_B$, for $\bar{\Delta} \approx 0$, which gives the same results as that of the Markoff processes in which energy is irreversibly flowing from A to B and C with a total rate of $\gamma_A+\bar{M}(0)$. The active-mode excitation for arbitrary values of γ_B is given by

$$\langle n(t)\rangle = |a(t)|^2 = \left|\sum_{n=1}^{3} C_n e^{-\lambda_n t}\right|^2 \quad , \tag{III.53a}$$

where $\lambda_{1,2}$ are the roots of Eq. (III.52), $\lambda_3 = i\Delta$ and

$$C_n = \frac{-i(V/2)(\gamma_B - i\bar{\Delta} + \lambda_n)}{(\lambda_n - \lambda_{n'})(\lambda_n - \lambda_{n''})} \quad , \tag{III.53b}$$

with $n,n',n''=1,2,3$.

In addition to the above, there is a second type of energy feedback based on the periodicity of the kernel function in the quasi-continuum and the memory effects of the bound-continuum coupling,[103] and a third type which we now consider corresponds to the feedback effects resulting from the direct heating of the substrate or indirect heating via phonon coupling. The substrate temperature obeys the heat diffusion equation, given in a one-dimensional approximation as

$$\frac{\partial T}{\partial t} = \frac{\partial}{\partial z}\left(D\frac{\partial T}{\partial z}\right) + S(z,t) \quad . \tag{III.54}$$

D is the diffusivity and the heating source is $S(z,t) = (\alpha/\rho C_V)(1-R)I(z,t)$, where α, ρ and C_V are the absorption coefficient, mass density and specific heat of the substrate, respectively, and R is the reflectivity. We note that the substrate temperature is governed by the volume source of the laser radiation, I(z,t), with the boundary condition $D\rho C_V(\partial T/\partial z) = 0$ on the surface (z = 0). The solution of Eq. (III.54) is in general only available numerically. Except for the situation where the substrate is heated by a high-power short pulse, e.g., gigawatt picosecond pulse, the above diffusion equation, may be replaced by[104]

$$\frac{\partial T}{\partial t} = \frac{\partial}{\partial z}\left(D \frac{\partial T}{\partial z}\right) \tag{III.55a}$$

and the boundary condition

$$K \left(\frac{\partial T}{\partial z}\right)_{z=0} = -(1-R)\, I(0,t) \quad , \tag{III.55b}$$

where $K = D\rho C_v$ is the thermal conductivity of the substrate.

In an indirect heating process for the aforementioned A-B-C system (Fig. 13), the boundary condition is given by [instead of Eq. (III.55b]

$$K \left(\frac{\partial T}{\partial z}\right)_{z=0} = -F(t), \tag{III.56}$$

where $F(t)$ is the rate of energy flux (W/cm^2) from the (A+B) modes to the C modes whose temperature increases by an indirect channel through the laser excitation of (A+B). We note that the energy flux rate $F(t)$ in general is time dependent since the excitation and relaxation of (A+B) are time dependent. However, when the excitation of (A+B) saturates to steady state, the rate of energy flow from the radition into (A+B) equals the rate of leakage from (A+B) to C. In this situation, the steady-state energy flow $F_{s.s.}(t) = \sigma I/\hbar\omega$, where σ is the steady-state total absorption cross section of (A+B) and may be written as [see Eq. (III.19)]

$$F_{s.s.} = \frac{f\, A\, I\, \Gamma}{(\Delta - 2\varepsilon^* X)^2 + (\Gamma/2)^2} \quad , \tag{III.57}$$

where f is a fraction relating the microscopic number of modes to the macroscopic thermal parameter, e.g., thermal conductivity of the substrate, and Γ is the damping factor of (A+B).

In general, the damping factor is time dependent and given by the thermally-averaged golden rule, similar to Eq. (III.24),

$$\Gamma(t) = (\frac{2}{\hbar^2})\mathrm{Re}\int_0^t d\tau \ \langle\langle H_{ABC}(\tau)\ H_{ABC}(0)\rangle\rangle \quad , \tag{III.58}$$

where the interaction Hamiltonia H_{ABC} is related to the power series of the correlation function of the C-mode coordinate, $\langle\langle Q_C(t)\ Q_C(0)\rangle\rangle$, which generally depends on time through the time-dependent occupation number $\langle n_C(t)\rangle$. In view of the fact that $\Gamma(t)$, $\langle n_{A,B}(t)\rangle$ and $\langle n_C\rangle$ are all varying in time, the functional form of F(t) should be quite complicated. To find the temperature of the C modes, one should simultaneously solve the rate equation of (A+B) with a time-dependent damping factor $\Gamma(t)$ and the heat diffusion equation. However, when the excitation of (A+B) is saturated and when $\Gamma(t)$ is assumed to be a constant (or given by its mean value), the maximum surface temperature of the substrate, subject to the boundary condition of Eq. (III.56) with a steady-state flux $F_{s.s.}$, may be obtained by a Green's function technique to be[105,106]

$$T_s^* = T_0 + 2F_{s.s.}[t_p/\pi D)]^{\frac{1}{2}}/\rho C_v \quad . \tag{III.59}$$

From this result and the expression of $F_{s.s.}$ in Eq. (III.57), we can draw the following conclusions regarding the temperature behavior of the substrate due to indirect laser heating: (i) in contrast to direct heating, the indirectly-heated surface temperature is sensitive to the laser frequency through the Lorentzion of $F_{s.s.}$ vs detuning; (ii) T_s^* is linearly proportional to the laser intensity at low excitation, whereas $T_s^* \propto I^p$ with $1/3<p<1$, in general (iii) the increase of the substrate surface temperature will be significant only when the diffusivity is small; otherwise the thermal energy will diffuse into the bulk; (iv) the increase of T_s^* results in a higher occupation number

of the C modes, which in turn may provide energy feedback via their thermal phonons. Furthermore, the increase of $\langle n_C(t)\rangle$ leads to the decrease of the rate of energy flow from (A+B) to C given by $\Gamma(t)[\langle n_{AB}(t)\rangle - \langle n_C(t)\rangle]$. However, we also note that the overall effects of $\langle n_C(t)\rangle$ on the energy-flow dynamics of the system are not yet clear since the relaxation rate, $\Gamma(t)$, is also time dependent. The above results based on a square laser pulse tend to overestimate the surface temperature compared with that for an actual pulse which is close to a Gaussian. For better results, we may approximate the Gaussian by an isosceles triangle, which gives $T_s^* = 4/(27)^{\frac{1}{2}}$ ($\simeq 0.77$ of that for the square pulse).[105]

To further investigate the nonequilibrium behavior, we consider the rate equation

$$\frac{d\langle n_{AB}\rangle}{dt} = \frac{\sigma I}{\hbar\omega} - \Gamma(t)\left[\langle n_{AB}(t)\rangle - \langle n_C(t)\rangle\right], \tag{III.60}$$

which has the same structure as that of Eq. (III.18) except that the time dependence of $\Gamma(t)$ and $\langle n_C(t)\rangle$ are given by[107]

$$\Gamma(t) = \int_0^t d\tau e^{i\omega_0\tau} \langle\langle[\sum_j K_j C_j^\dagger(\tau), \sum_j K_j C_j(0)]\rangle\rangle \quad , \tag{III.61a}$$

and

$$\langle n_C(t)\rangle = \int_0^t d\tau e^{i\omega_0\tau} \langle\langle\sum_j |K_j|^2 C_j(0) C_j^\dagger(\tau)\rangle\rangle \quad , \tag{III.61b}$$

where ω_0 is the mean frequency of the (A+B) subsystem, $C_j = \prod_{i=1}^{j} c_i$ is the multiphonon operator for the C modes, and K_j is the coupling constant between (A+B) and C. We note that Eq. (III.60) reduces to the equilibrium expression, Eq. (III.18),

when the C-mode correlation time is much shorter than the inverse relaxation time and the upper time limit of Eq.(III.61) is extended to infinity. We finally note that the multiphonon relaxation rate given by Eq.(III.58) is a more general form than that of Eq. (III.61).

b. Multilevel System -- Selective vs Nonselective

So far we have assumed the active mode to be a harmonic "oscillator" without energy-level structure. For a true quantum system, the active mode should be treated as a multilevel system. As shown in Fig. 13, we consider a multilevel system in which the active mode is coupled to the B mode, which in turn couples to the continuum C modes with the damping factor γ. In the Heisenberg-Markoff picture (HMP) and within the rotating-wave approximation, the equations of motion for the Bose operators are given by[83]

$$\frac{dA_n(t)}{dt} = -\frac{i}{\hbar}\sum H_{mn}A_m(t)\exp[-(E_m-E_n)t/\hbar] \quad , \tag{III.62}$$

where H_{mn} are the matrix elements of the interaction Hamiltonian $H' = H_{AB}+H_{BC}+H_{AF}(t)$ given by

$$H_{mn} = \langle\Psi_m|H'|\Psi_n\rangle = \langle\phi_i^A\,\phi_j^B\,\phi_k^F|(H_{AB}+H_{BC}+H_{AF})|\phi_{i'}^A,\phi_{j'}^B,\phi_{k'}^F\rangle \quad , \tag{III.63}$$

ϕ_{ijk}^{ABF} being the eigenstates of the A, B and photon modes with the corresponding probabilities $P_m(t)=|A_m(t)|^2$. For example, in a two-photon process the eigenstates $|002\rangle$, $|200\rangle$ and $|020\rangle$ represent A and B both in their ground states, only A excited and only B excited, respectively. Considering the A mode as a three-level system with excited states, coupled to the m-th and 2m-th level of B which is in turn decaying to C, the equations of motion for

the Base operators -- $a_{1,2,3}$ for the A mode and $B_{1,2}$ for the B mode -- in the HMP are given from Eq. (III.62) as

$$\dot{a}_1(t) = - iV_1\, a_2(t)\, \exp(-i\Delta t) \quad , \tag{III.64a}$$

$$\dot{a}_2(t) = -iV_1\, a_1(t)\, \exp(i\Delta_1 t) - ig_1\, B_1(t)\, \exp(-i\Delta_1' t) - iV_2 a_3(t)\, \exp(-i\Delta_2 t), \tag{III.64b}$$

$$\dot{a}_3(t) = - iV_2\, a_2(t)\, \exp(-i\Delta_2 t) - ig_2\, B_2(t)\, \exp(-i\Delta_2' t), \tag{III.64c}$$

$$\dot{B}_1(t) = -ig_1^*\, a_2(t)\, \exp(i\Delta_1' t) - (\gamma_1/2)\, B_1(t), \tag{III.64d}$$

$$\dot{B}_2(t) = - ig_2^*\, a_3(t)\, \exp(i\Delta_2' t) - (\gamma_2/2)\, B_2(t) \quad , \tag{III.64e}$$

where $\Delta_1 = \omega_A - \omega$, $\Delta_2 = \Delta_1 - 2\varepsilon^*$, $\Delta_1' = m\omega_B - \omega_A$, $\Delta_2' = m\omega_B + 2\varepsilon^* - \omega_A$, ε^* is the anharmonicity of the A mode, and V, g, γ are the pumping rates, coupling factors and the damping rates for the related levels, respectively. The above coupled equations are numerically solved for $V_1 = V_2 = V$, $g_1 = g_2 = g$ and $\gamma_1 = \gamma_2 = \gamma$ to obtain the level populations

$$P_1 = |a_1(t)|^2,\ P_A = |a_2(t)|^2 + |a_3(t)|^2 \text{ and } P_B = |B_1(t)|^2 + |B_2(t)|^2. \tag{III.65}$$

P_A and P_B describe the population dynamics of the photon energy deposited in the A and B modes, respectively, while $P_C = 1 - (P_1+P_A+P_B)$ describes the population loss of the (A+B) modes and represents thermal heating, i.e., the portion of the photon energy randomized in the phonon bath C modes. The energy populations are shown in Fig. 14(A) for selective excitation of the A mode with $(V,g,\gamma) = (4,0.1,0.4)$ and in Fig. 14(B) for nonselective heating of the C modes with $(V,g,\gamma) = (4,1,1)$. We see that for fixed laser pumping

rates the selective excitation of the active mode (A) requires a small multiphonon coupling factor, g, and small energy leakage rates, γ, out of the B mode, while appreciable nonselective thermal heating of the bath modes (C) is achieved when the coupling factor and the damping rate are comparable to the pumping rate.

c. Adbond Excitation -- Hydrogen/Tungsten

In the heat-bath treatments, we have focused on the excitation of the active mode and treated all the other modes as a heat bath, which leads to a damping factor and the frequency shift for the active mode. To investigate the energy flow within the adspecies or the adbond, the vibrational modes should be rigorously treated rather than singling out the active mode from the bath modes. The intramolecular vibrational relaxation (IVR) rate of SF_6 molecule in the gas phase has been addressed in Part A.3 of Section II, and now we shall extend that study to the excitation of a heterogeneous system, namely hydrogen atom adsorbed on a tungsten surface. As shown in Fig. 15, there are total of six (3n, with n=2) possible librational modes in the C_{2v} point group bridge site adsorption of H/W(100). These consist of two-fold degenerative pairs of lateral modes (ν_2 and ν_3) and vertical modes (ν_1 in-phase and out-of-phase modes).[108] In view of the frequency spectrum ν_1 = 1038.6, ν_2 = 645.3 and ν_3 = 1290.6 cm^{-1}, we shall consider the fourth-order anharmonic coupling potential, proportional to $Q_1^2Q_2Q_3$, which dominates the vibrational relaxation rate with the internal detuning $\Delta_I = 2\pi(2\nu_1-\nu_2-\nu_3)$, where $Q_{1,2,3}$ are the normal coordinates of the $\nu_{1,2,3}$ modes. By the concept of the energy-gap law and the multiphonon relaxation rate discussed earlier, we presume that the fourth-order anharmonic coupling is the lowest order we can use since the detuning Δ_I is not far off resonance.

The Hamiltonian describing the fourth-order anharmonic coupling among the intra-bond modes of H/W in which the ν_1 mode is subjected to IR radiation

is given by[83]

$$H = \sum_{i=1}^{3} \hbar\omega_i a_i^\dagger a_i + \lambda H_{anh} + \hbar V\cos(\omega t)(a_1^\dagger + a_1) \quad , \qquad \text{(III.66)}$$

where V is given by Eq. (III.2f), and the anharmonic coupling is $H_{anh} = (Q_1+Q_2+Q_3)^4$. The diagonal terms of this coupling give the anharmonic components of the modes, whereas the off-diagonal terms provide the mode-mode coupling with the fourth-order coupling term $\lambda' Q_1^2 Q_2 Q_3$, where $\lambda' = 12\lambda$. Referring to Eq.(III.41), we can write the equation of motion for the amplitude functions B_j as [12]

$$i\hbar\dot{B}_1 = \lambda' C_1^4 B_1^* B_2^2 + 2\lambda' \bar{C} B_1^* B_2 B_3 E_+ - (V_{10}/2)^2 C_1 E_f \quad , \qquad \text{(III.67a)}$$

$$i\hbar\dot{B}_2 = \lambda' C_2^4 B_2^* B_2^2 + \lambda' \bar{C} B_1^2 B_3^* E_- \quad , \qquad \text{(III.67b)}$$

$$i\hbar\dot{B}_3 = \lambda' C_3^4 B_3^* B_3^2 + \lambda' \bar{C} B_1^2 B_2^* E_- \quad , \qquad \text{(III.67c)}$$

$$E_\pm = \exp(\pm i\Delta_\pm' t), \quad E_f = \exp(i\Delta_E' t) \quad , \qquad \text{(III.67d)}$$

$$\Delta_I' = 2\pi(2\nu_1' - \nu_2' - \nu_3'), \quad \Delta_E' = 2\pi\nu_1' - \omega \quad , \qquad \text{(III.67e)}$$

where $\bar{C} = C_1^2 C_2 C_3$ and other parameters are defined as in Eq. (II.41). The above coupled equations have been numerically solved by the fourth-order Runge-Kutta method (using a DEC-10 computer connected to the NCAR graphics software). The dynamical feature of the excitations which show the energy flow among ν_2, ν_3 and the active mode (ν_1) are illustrated in Fig. 16.

3. Photon Energy Population

In the heat-bath treatments, we have shown that the laser radiation may selectivily excite the active mode while the bath modes are kept "cold" if the pumping rate is greater than the relaxation rate; otherwise, there is nonselective thermal heating of the whole adspecies and/or the substrate surface. We have also demonstrated that in the H/W system, the IVR rate could be very fast ($\sim 10^{12}$ s^{-1}) when the internal resonance condition is not within the low-order anharmonic coupling. For systems with a very fast IVR rate, the photon energy initially deposited in the active mode may be randomized among all the adspecies and adbond modes. In this situation, the master (rate) equation, which treats all the vibrational modes in the subsystem, e.g., (A+B) in Fig. 13, on an equal footing, is more appropriate than that of the heat-bath treatments. We should note that, from the concept of energy-gap law, the subsystem involved in the master equation is defined by those modes which are strongly coupled, e.g., (A+B) modes in Fig. 13, and usually excludes those low-frequency phonon modes (C) which are separated far in frequency from the A and B modes. Therefore, the energy space of the master equation is defined by the number of photons absorbed by the whole adspecies, or (A+B) modes, rather than the vibrational quantum number of the active mode.

Before presenting the master equation which involves the pumping (relaxation) rates, we shall first calculate the associated absorption (stimulated emission) cross section for the adspecies. This may be obtained by a generalization of the total cross section of an anharmonic oscillator in Eq. (III.19),

$$\sigma_n = \frac{A(n+1)\bar{\Gamma}_n}{(\Delta-2\varepsilon^*X)^2+(\bar{\Gamma}/2)^2} \quad , \qquad \text{(III.68)}$$

where the n dependence of the transition dipole matrix element $\mu_{n,n+1} = \langle n+1, \cdot | x | n \rangle = \sqrt{(n+1)}\mu_{0,1}$ has been included. σ_n represents the cross section for a transition between the m-th and (m+1)-th levels with level widths Γ_n and Γ_{n+1}; $\bar{\Gamma}_n = (\Gamma_n+\Gamma_{n+1})/2$ is the mean width; and X is the steady-state excitation of the active mode. Noting that both $\bar{\Gamma}_n$ and X in general are n-dependent, e.g., $\bar{\Gamma}_n=(n+1)\Gamma_0$ for the transition pair (n, n+1) and $X \propto (n+1)$ at low active-mode excitations, the cross section may be written in the general form

$$\sigma_n = (n+1)^{\alpha}\sigma^* \quad , \tag{III.69}$$

where σ^* and α are correlated parameters depending on the relative magnitudes of the anharmonicity and the bandwidth. For example: $\alpha=1$ and $\sigma^*=\Gamma_0/[\Delta^2+\Gamma_0^2]$. for $\varepsilon^*=0$ (harmonic oscillator) and $\bar{\Gamma}_n=\Gamma$ (constant bandwidth); $\alpha=-1$ and $\sigma^* = \Gamma_0/(2\varepsilon^*)^2$ for an anharmonic oscillator, $\bar{\Gamma}_n=\Gamma_0 << 2\varepsilon^*X$, $X=n+1$ and $\Delta=0$; $\alpha=0$ and $\alpha^*=A/\Gamma_0$ for $\varepsilon^*=\Delta=0$ and $\bar{\Gamma}_n = (n+1)\Gamma_0$.

The master equation describing the photon energy population in the energy (n) space can be written as[80]

$$\frac{dP_n}{dt} = -(I\sigma_n/\hbar\omega)[P_n-(g_n/g_{n+1})P_{n+1}] + (I\sigma_{n-1}/\hbar\omega)[P_{n-1}-(g_{n-1}/g_n)P_n] \quad . \tag{III.70}$$

P_n is the population (adspecies/cm^2) of the level of energy $n\hbar\omega$, i.e., absorbing n laser quanta, and g_n is the degeneracy of the n-th level, related to the number of vibrational modes S in the adspecies [or (A+B) modes] by

$$g_n = g_0(n+1)^{S-1} \quad , \tag{III.71}$$

and $\sigma_{n,n-1}$ are the quantum cross sections for transitions between the level pairs (n, n±1) given by Eq. (III.69). We note that, as discussed in Part A.2.a, the transition rates or the cross sections are in general time dependent, and the above master equation with constant cross sections is the limiting case of the generalized master equation[84]

$$\frac{dP_n}{dt} = \frac{I}{\hbar\omega}\int_0^t dt' \sum_{n'} [\sigma_{n'n}(t-t')\, P_{n'}(t') - \sigma_{nn'}(t-t')\, P_n(t')] \ , \quad \text{(III.72)}$$

which reduces to Eq. (III.70) when we assume just the dipole transition, i.e., $\sigma_{n'n} = \sigma_n \delta_{n',n\pm1}$, and a Markoff process, i.e., $\sigma_n(t-t') = \delta(t-t')$. We note that within the harmonic model the dipole transition is a selection-rule-allowed process, but if the anharmonic potential is considered, the high-order transitions with $\sigma_{n'n} = \sigma_n \delta_{n',n\pm j}$ $(j \geq 2)$ are also allowed .

The exact solution of the quantal master equation for general forms of σ_n and g_n is not available. However, we shall discuss two limiting cases which are physically interesting and can be analytically solved.

(1) <u>α=S-1 (single-mode harmonic oscillator)</u>. Eq. (III.70) becomes

$$\frac{dP_n}{dt} = -(I\sigma^*/\hbar\omega)[(n+1)P_{n+1} + nP_{n-1} - (2n+1)P_n] \ , \quad \text{(III.73)}$$

which has the solution, with the initial condition $P_n(t=0)=N_0\delta(t)$,

$$P_n(t) = N_0 W^n(t)/[1+W(t)]^{n+1} \ , \quad \text{(III.74a)}$$

$$W(t) = \sigma^*\phi/\hbar\omega \ , \quad \text{(III.74b)}$$

$$\phi = \int_0^t dt\, I = \text{laser fluence } (J/cm^2) \ . \quad \text{(III.74c)}$$

The corresponding average excitation (quanta/adspecies) is

$$\langle n(t)\rangle = \frac{1}{N_0}\sum nP_n = W \propto \phi \quad . \tag{III.75}$$

(2) <u>α=0 (constant cross section), S=1</u>. For this case Eq. (III.70) becomes

$$\frac{dP_n}{dn} = -(I\sigma^*/\hbar\omega)[2P_n - P_{n+1} - P_{n-1}] \quad . \tag{III.76}$$

With the same initial condition as in case (1) and by using the recurrence relation of the modified Bessel function, we obtain the population function

$$P_n(t) = NN_0 \exp(-2W) I_n(2W) \quad , \tag{III.77}$$

where N is a normalization constant, I_n is the modified Bessel function, and W is again given by Eq. (III.74b). The corresponding average excitation for this population is

$$\langle n(t)\rangle = 2(W/\pi)^{\frac{1}{2}} \propto \phi^{\frac{1}{2}} \quad . \tag{III.78}$$

We note that the average excitation is proportional to the square root of the laser fluence, whereas in case (1) it is linearly proportional.

To investigate the population function and the associated average excitation for the general forms of σ_n and g_n, we shall now assume that P_n, σ_n and g_n are smooth functions in n-space. Within this continuum assumption, which is a good approximation when n is large, the quantal master equation, Eq. (III.70), is then converted into the classical diffusion equation[31]

$$\frac{\partial P_n}{\partial t} = \frac{I}{\hbar\omega}\frac{\partial}{\partial n}\left[\sigma_n g_n \frac{\partial}{\partial n}(P_n/g_n)\right] . \qquad \text{(III.79)}$$

Substituting Eqs. (III.69) and (III.71) into Eq. (III.79), a particular solution of Eq. (III.79) consistent with the initial condition $P_n(t=0) = N_0\delta(t)$ is

$$P_n(t) = NN_0 g_n \exp[-n^\beta/(\beta^2 W)] \quad , \qquad \text{(III.80)}$$

$$N = (\beta/g_0)(\beta^2 W)^{-S/\beta}/\Gamma(S/\beta) \quad , \qquad \text{(III.80b)}$$

$$\beta = 2 - \alpha \quad , \qquad \text{(III.80c)}$$

where W is again given by Eq. (III.74b) and N is the normalization factor. The average excitation for this classical population function can then be calculated as

$$\langle n(t)\rangle = N_0^{-1}\int_0^\infty dn\ P_n n = (\beta^2 W)^{1/\beta}\Gamma[(S+1)/\beta]\Gamma(S/\beta) \quad , \qquad \text{(III.81)}$$

which is proportional to $\sigma^{1/\beta}$ (since $W \propto \phi$) and consistent with the quantal results of Eqs. (III.75) and (III.78) for $\beta = 1$ (α=1) and $\beta = 2$ (α=0). It is worth noting that for $\alpha = -1$ (anharmonic oscillator), $\langle n(t)\rangle \propto \phi^{1/3}$ in this classical diffusion model, whereas the steady-state excitation of the active mode $\langle n_A(t)\rangle_{s.s.} \propto I^{1/3}$ in the quantal Heisenberg-Markoff model Eq. (III.20). Combining Eqs. (III.71), (III.80) and (III.81), we can express the population function in terms of the average excitation as

$$P_n = \frac{N_0^\beta}{\Gamma(S)}\left(\frac{F(S)}{\langle n(t)\rangle}\right)^S (n+1)^{S-1}\exp\left[-\left(\frac{nF(S)}{\langle n(t)\rangle}\right)^\beta\right] \quad , \qquad \text{(III.82a)}$$

$$F(S) = \Gamma[(S+1)/\beta]\Gamma(S/\beta) \quad . \qquad \text{(III.82b)}$$

For a comparison with the above classical diffusion model, we now consider a Boltzmann thermal distribution $P_n^*(t)$ which is characterized by the effective temperature T_{eff} and the quantal degeneracy g_n^* [g_n in Eq. (III.71) is a classical degeneracy] as follows:

$$P_n^*(t) = NN_0 g_n^* \exp[-n\hbar\omega/kT_{eff}] \quad , \tag{III.83a}$$

where

$$N = \left[\sum_{n=0}^{\infty} P_n^*/N\right]^{-1} = [1-\exp(-\hbar\omega/kT_{eff})] \quad , \tag{III.83b}$$

$$g_n^* = (n+S-1)!/[n!(S-1)!] \quad , \tag{III.83c}$$

and the effective temperature T_{eff} is defined as the average excitation energy per vibrational mode and is governed by energy conservation as

$$\hbar\omega\bar{n} = \hbar\omega\langle n(t)\rangle/S \quad , \tag{III.84a}$$

$$\bar{n} = [\exp(\hbar\omega/kT_{eff}) - 1]^{-1} \quad . \tag{III.84b}$$

For a multiphoton process ($\langle n(t)\rangle >> 1$), we obtain the high effective temperature limit ($kT_{eff} >> \hbar\omega$), and for $n >> S$, Eqs. (III.83) and (III.84) reduce to

$$\bar{n} \approx kT_{eff}/\hbar\omega, \quad kT_{eff} = \hbar\omega\langle n(t)\rangle/S \quad , \tag{III.85a}$$

$$N \approx (kT_{eff}/\hbar\omega)^S \quad , \tag{III.85b}$$

$$g_n^* \approx n^{S-1}/(S-1)! = g_n \quad . \tag{III.85c}$$

The population function reduces to

$$P_n^*(t) = \left[\frac{N_0 n^{S-1}}{(S-1)!(\langle n(t)\rangle/S)^S}\right] \exp\left(-\frac{ns}{\langle n(t)\rangle}\right) \quad , \tag{III.86}$$

which is identical to the result of the classical diffusion equation, Eq. (III.82a), for the case $\alpha = 1$ (harmonic oscillator).

Another important population function, the Poisson distribution, which follows from a solution of the Schrödinger equation,[82] has the form

$$P_n = (\langle n\rangle^n/n!)\exp(-\langle n\rangle) \quad , \tag{III.87a}$$

where $\langle n\rangle$ is the average excitation of the adspecies assumed to be harmonic with equal energy spacings. We note that $\langle n\rangle$ in general is time dependent and is given by[14]

$$\langle n(t)\rangle = \frac{AI}{\Delta^2+(\Gamma/2)^2}\left[1+e^{-\Gamma t}-2e^{-\Gamma t/2}\cos(\Delta t)\right] \quad , \tag{III.87b}$$

where A is a constant proportional to the transition dipole of the adspecies and Γ is the overall level width. The above result is identical to Eq. (III.12) with $\bar{n} = 0$; however, $\langle n\rangle$ here represents the photon quanta absorbed by the adspecies (as a whole) rather than that of the active mode. Moreover, $\langle n(t)\rangle_{s.s.} \propto I$ in the Poisson distribution which is quite different from the fluence dependence $\langle n(t)\rangle \propto \phi^q$ in the other types of distributions aforementioned. For a comparison of the Poisson function and those obtained from the diffusion equation and the Boltzmann-type distribution, we plot the results for various values of S and α in Fig. 17. The associated desorption probabilities P_d, shown in Fig. 18, are defined by

$$P_d = \frac{1}{N_0}\sum_{n=n^*}^{\infty} P_n \text{ (quantal population)}, \tag{III.88a}$$

$$P_d = \frac{1}{N_0}\int_{n^*}^{\infty} dn\, P_n \text{ (classical population)}, \tag{III.88b}$$

AD-A134 426 LASER-INDUCED MOLECULAR DYNAMICS: RATE PROCESSES IN THE GAS PHASE AND AT..(U) ROCHESTER UNIV NY DEPT OF CHEMISTRY J LIN ET AL. NOV 83 UROCHESTER/DC/83/TR-42 2/2

UNCLASSIFIED N00014-80-C-0472 F/G 7/4 NL

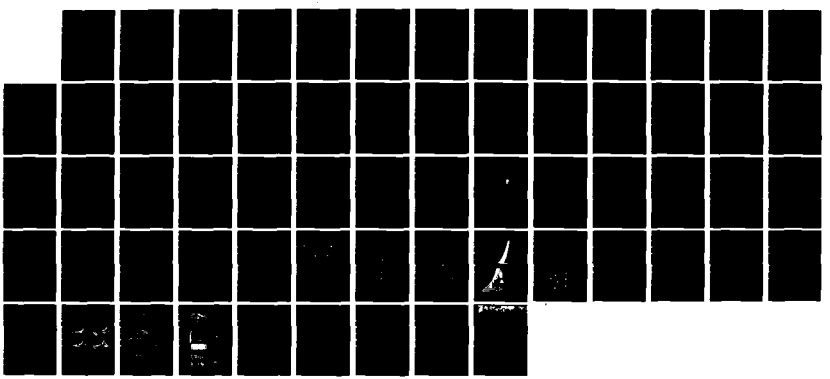

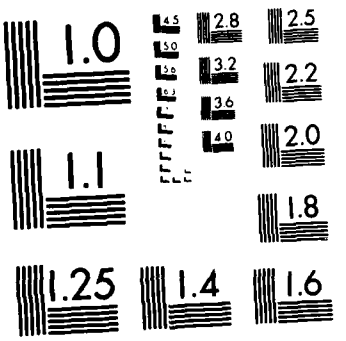

MICROCOPY RESOLUTION TEST CHART
NATIONAL BUREAU OF STANDARDS-1963 A

where n* is the desorption threshold. The adspecies will be desorbed from the solid surface through the channel of a direct bond breaking, indirect migration-induced desorption or Fano-type autodesorption via mode-mode coupling within the adspecies. We note that with a knowledge of the energy population together with the measured quantity n*, we should be able to evaluate the desorption probability. The reverse procedure, namely knowing the measured n* and the desorption yield (probability and/or rate of desorption) will provide the information about P_n, i.e., how good are the calculated populations for various systems. More discussion on the dynamics of desorption will be given later.

4. Isotope Effects

Infrared isotope separation of species in the gas phase has been successfully carried out both theoretically and experimentally.[2] However, the isotope effects of species adsorbed on a solid surface have only been recently studied either experimentally[100,109] or theoretically.[86] Unlike gas-phase isotopes whose absorption cross sections are governed mainly by their frequency difference, the collective excitations of isotopic adspecies are characterized by many other surface-induced effects: (i) direct dipole-dipole interactions among the identical and isotopic adspecies; (ii) indirect adspecies-adspecies interaction due to their common coupling to the substrate phonons, i.e., the phonon-mediated interaction; (iii) frequency shift and level broadening of the adspecies induced by such effects as substrate heating, multiphonon relaxation and dephasing; and (iv) dynamic effects such as migration and desorption. The above effects all influence the absorption cross sections of the isotope adspecies and usually smear out the "frequency separation" of different isotopes when they are co-adsorbed on a solid surface. For systems like $C^{12}O^{16}$ and $C^{12}O^{18}$ adsorbed on a copper surface, the frequency difference of the C-O stretching is about 47 cm^{-1} and their dynamic dipole-dipole coupling is rather large.[109] Therefore, it is more difficult to observe the

isotope effects for adsorbed CO than for adsorbed H_2 and D_2, which have weaker intermolecular coupling and a larger frequency difference. We shall suggest below some possible mechanisms for isotope separation of adspecies using a model based on a previously-developed theory.[86]

The ensemble-averaged equations of motion for a system consisting of a mixture of two isotopic adspecies may be obtained by extending those for the single adspecies, Eq. (III.34), as follows:

$$i\dot{a}(t) = \left[\omega^{A}_{eff}(t)-\omega\right]a(t) + V_A/2 + D'b(t) \quad , \tag{III.89a}$$

$$i\dot{b}(t) = \left|\omega^{B}_{eff}(t)-\omega\right|b(t) + V_B/2 + D'a(t), \tag{III.89b}$$

$$\langle\dot{n}_A(t)\rangle = -V_A\langle\langle Im[a(t)]\rangle\rangle - 2D\langle\langle Im[a(t)b^{\dagger}(t)]\rangle\rangle - \gamma_1^A\left[\langle n_A(t)\rangle - n_C/2\right], \tag{III.89c}$$

$$\langle\dot{n}_B(t)\rangle = -V_B\langle\langle Im[b(t)]\rangle\rangle + 2D\langle\langle Im[a(t)b^{\dagger}(t)]\rangle\rangle - \gamma_1^B\left[\langle n_B(t)\rangle - n_C/2\right], \tag{III.89d}$$

where V_A and V_B are the pumping rates for the A and B modes, n_C is the Bose-Einstein distribution for the C modes, Im denotes the imaginary part, and ω^{A}_{eff} and ω^{B}_{eff} are the effective frequencies of the isotopic adspecies A and B whose ensemble averages are given by

$$\langle\langle\omega^{A,B}_{eff}\rangle\rangle = \omega_{A,B} - 2\varepsilon^{*}_{A,B}\langle n_{A,B}(t)\rangle - i\Gamma_{A,B}/2 \quad , \tag{III.90a}$$

$$\Gamma_{A,B} = \gamma_1^{A,B} + \gamma_2^{A,B} \quad . \tag{III.90b}$$

In the above equations, a new adspecies-adspecies coupling strength, D', is introduced,

$$D' = D-i(D_1+iD_2), \tag{III.91}$$

which consists of two components, the direct dipole-dipole coupling strength D and the phonon-mediated coupling $(D_1 + iD_2)$, where D_1 and D_2 are given by the real and imaginary parts, respectively, of the integral[110]

$$\frac{1}{b(t)}\int_0^t dt'\ b(t') \sum_j n_C G_j^A G_j^B \exp[i(\Delta_{Aj}t - \Delta_{Bj}t')] \quad . \tag{III.92}$$

For the Markoff process or for a continuum C-mode spectrum, the real part of the integral reduces to the simple expression

$$D_1 = \pi n_C \rho_0 G_0^A G_0^B \quad , \tag{III.93}$$

which is proportional to the multiphonon occupation number, $n_C = \pi(\bar{n}_j+1) - \pi\bar{n}_j$, the density of states of the C-modes, ρ_0, and product of the coupling strengths between the isotopic adspecies and the C-modes, $G_0^A G_0^B$. Here we have approximated $\rho_j G_j^A G_j^B$ by $\rho_0 G_0^A G_0^B$.

The coupled equations [Eq. (III.89)], which are highly nonlinear due to the anharmonic corrections $2\varepsilon^* \langle n_{A,B}(t)\rangle$ and the isotope coupling strength D', can only be solved numerically. However, one can obtain the steady-state excitatations for the weak-coupling case, $D' \approx 0$, as

$$\langle n_{A,B}(t)\rangle_{s.s.} = \frac{\left[V_{A,B}/2\right]^2 \left[\Gamma_{A,B}/\gamma_1^{A,B}\right]}{\left(\langle\langle\omega_{eff}^{A,B}\rangle\rangle - \omega\right)^2 + \left(\Gamma_{A,B}/2\right)^2} \quad , \tag{III.94}$$

which show that one of the adspecies may be selectively excitated without significant excitation of the other when the laser frequency, ω, is tuned to one of the optimal values, i.e., $\Delta_{eff}^{A,B} \equiv \langle\langle\omega_{eff}^{A,B}\rangle\rangle - \omega = 0$, for either adspecies A or B.

To demonstrate the effect of the coupling strength, D', on the dynamics and the steady-state excitations, we plot the numerical solutions of Eq.(III.89) for the harmonic case ($\varepsilon_{A,B}^* = 0$) in Fig. 19. It is seen that $\langle n_A(t)\rangle$ is higher than $\langle n_B(t)\rangle$ for $\Delta_A < \Delta_B$, where $\Delta_{A,B} = \omega_{A,B} - \omega$, with $D' = 0$ [Fig. 19(A)]. As D'

increases, both excitations decrease [Fig. 19(B)]. Increasing the coupling strength to the transition value, i.e., $D' = D^* = (\Delta^B+\Delta^A)/2$, causes the steady-state excitations to become identical [Fig. 9(C)]. For large coupling strength, $D'>D^*$, both excitations are low and $\langle n_B(t)\rangle$ is higher than $\langle n_A(t)\rangle$ (Fig. 19(D)]. These numerical results for the steady-state excitations are seen to be in accord with analytical results. Such results can be obtained by defining the "difference excitation" $N_- \equiv X - Y$, where X and Y are the steady-state excitations of the adspecies A and B, respectively. We obtain, from Eq. (III.89), for $\epsilon^*_{A,B}=0$, $V_A=V_B=V$, $\gamma_1^A=\gamma_1^B=\gamma_1$ and $\Gamma_A=\Gamma_B=\Gamma$,

$$N_- = V^2\Gamma\Omega_-(\Omega_+-2D')/\left[4\gamma_1\left(Z_1^2+Z_2^2\right)\right], \tag{III.95a}$$

$$Z_1 = \Delta_A\Delta_B - D'^2 - (\Gamma/2)^2 \quad , \tag{III.95b}$$

$$Z_2 = \Gamma\Omega_+/2 \quad , \tag{III.95c}$$

$$\Omega_\pm = \Delta_B \pm \Delta_A \quad , \tag{III.95d}$$

$$\Delta_{A,B} = \omega_{A,B} - \omega \quad . \tag{III.95e}$$

The above expression for the steady-state "difference excitation" N_- displays the following important features: (i) isotopic selectivity increases with decreasing coupling strength; (ii) when the coupling strength reaches the transition value $D' = D^* = \Omega_+/2$, there is zero selectivity, i.e., $N_- = 0$ as shown in Fig. 19(C).

For further investigation of the selectivity, we consider the reduced selectivity $\bar{S}$ defined by[86]

$$\bar{S} = \int_0^{t_p} dt\langle n_A(t)\rangle/\langle n_B(t)\rangle \quad , \tag{III.96}$$

where t_p is the laser pulse duration, and $\langle n_A(t)\rangle$ and $\langle n_B(t)\rangle$ are the excitations of the isotopes to be solved numerically from Eq. (III.89). The numerical results for non-interacting (D'=0) and interacting (D'≠0) isotopes are shown in Fig. 20, which reveals the following features: (i) for the harmonic case, with $\varepsilon^*_{A,B}=0$, $\bar{S}=1$ for $\Delta_A=|\Delta_B|$ [curve (E)], (ii) for the anharmonic cases, $\varepsilon^*_{A,B}\neq 0$, a higher selectivity is expected [curve (B)] than that of curve (E) due to the nonlinear feature of the excitation; (iii) the optimal condition for high selectivity is that the laser frequency has positive detuning for both the A and B adspecies [compare curve (C) with (E) and curve (A) with (B)]; (iv) curve (E') shows the effects of D' on the selectivity for the case of $\varepsilon^*_{A,B}=0$ at $D'=D^*=(\Delta_A+\Delta_B)/2$, where $\bar{S}=1$ at steady-state as predicted by the analytical expression, Eq. (III.95); (v) for $\varepsilon^*_{A,B}\neq 0$, D* is "blue shifted" toward $\bar{S}=1$ [curve (F')]; (vi) an increase in D' shows a decrease in $\bar{S}$ [curves (A) to (G')], and $\bar{S}<1$ when $D'<D^*$, corresponding to the situation of $\langle n_A\rangle < \langle n_B\rangle$ [curve (D) of Fig. 19 and curves (F') and (G') in Fig. 20]. We finally note that for a non-interacting system, D'=0, the greater the frequency difference, $\Delta_A-\Delta_B$, the higher the selectivity; however, for an intereacting system, an increase of the coupling strength, D', does not necessarily result in a decrease of the excitations. Numerical solutions of Eqs. (III.89 and (III.96) show that there is an optimal set of values (D^{**}, $\varepsilon^*_{A,B}$) which yield maximum excitations; e.g., for $\varepsilon^*_A=1$, $V_A=10$, $\gamma_1^A=\gamma_2^A=2$ and $\Delta_A=8.3$, $D^{**}\simeq 2.9$ yields the maximum value of $\langle n_A\rangle$.

For further demonstration of the effects of the coupling strength, we look at the total steady-state excitation $N_+=X+Y$. Some results are shown in Fig. 21.

5. Dynamic Effects

We shall end this section by discussing some dynamic effects resulting from the excitation of the adspecies and/or the substrate. These effects are associated with phenomena such as migration, recombination, decomposition and desorption. Here we shall focus on theoretical aspects of migration and desorption, while other processes will be looked at in Section IV.

a. Migration

To describe the individual behavior of the adspecies occupied at different lattice sites, we introduce another parameter, namely the site operator, in addition to the ladder operators for the normal modes in the dynamic Hamiltonian given by

$$H(t) = H_0(Q_1,Q_2,\cdots Q_j) + \sum_{k,k'} V_{kk'}(Q_1,Q_2,\cdots Q_j)c_k^{\dagger}c_{k'} + H_{AF}(t) \quad . \tag{III.97}$$

H_0 is the unperturbed Hamiltonian of the system (with normal coordinates Q_j), $V_{kk'}(Q_j)$ is the lattice-site-dependent interaction potential of the system, and $c_k^{\dagger}$ and $c_{k'}$ are the site operators of the Bloch states $|k\rangle$ and $\langle k'|$, respectively, which can be expressed in terms of Wannier functions in the site representation as

$$c_k^{\dagger} \equiv |k\rangle = \frac{1}{\sqrt{N}} \sum_n e^{i\vec{k}\cdot\vec{R}_n}|n\rangle \quad , \tag{III.98a}$$

$$c_{k'} \equiv \langle k'| = \frac{1}{\sqrt{N}} \sum_m e^{-i\vec{k}'\cdot\vec{R}_m}\langle m| \quad . \tag{III.98b}$$

Taylor expansion of the interaction potential,

$$V_{kk'}(Q_1,Q_2,\cdots Q_j) = V_0 + \sum_{j'=1}^{j}\left[\frac{\partial V}{\partial Q_{j'}}\right]_0 Q_{j'} + \cdots + \sum_{i,j'}\sum_p \frac{1}{(p+1)!}\left[\frac{\partial^{p+1}V}{\partial Q_i(\partial Q_{j'})^p}\right]_0 Q_i Q_{j'}^p + \cdots, \tag{III.99}$$

gives us the general forms for the intramolecular couplings, p being the order of

the multiphonon processes. Using the second-quantization expression of Eq. (III.99) and the Wannier site representation in Eq. (III.98), we obtain, from Eq. (III.97), the microscopic model Hamiltonian as follows:[79]

$$H(t) = H_A^0 + H_B^0 + H_C^0 + H_C' + H_1 + H_2 + H_3 + H_4 + H_{AF}(t) \quad , \tag{III.100}$$

$$H_A^0 = \hbar\omega_A a^\dagger a, \quad H_B^0 = \sum_j \hbar\omega_j b_j^\dagger, \quad H_C^0 = E_0 \sum_n c_n^\dagger c_n \quad . \tag{III.101a}$$

$$H_C' = \sum_{n,j} X_{nj} c_n^\dagger c_n (b_j^\dagger + b_j) + \sum_n Y_n c_n^\dagger c_n (a^\dagger + a) + \sum_{nj} Z_{nj} c_n^\dagger c_n (a^\dagger + a)(b_j^\dagger + b_j), \tag{III.101b}$$

$$H_1 = \sum_{n \neq m} J_{nm}\, c_n^\dagger c_m \quad , \tag{III.101c}$$

$$H_2 = \sum_{n \neq m} K_{mn}\, c_n^\dagger c_m (a^\dagger + a) \quad , \tag{III.101d}$$

$$H_3 = \sum_j \sum_{n \neq m} G_{nm}^j\, c_n^\dagger c_m (b_j^\dagger + b_j) \quad , \tag{III.101e}$$

$$H_4 = \sum_j \sum_{n \neq m} W_{mn}^j c_n^\dagger c_m (a^\dagger + a)(b_j^\dagger + b_j) + [\text{higher-order terms}], \tag{III.101f}$$

$$H_{AF}(t) = \sum_{n \neq m} V(t)\, K_{nm}\, c_n^\dagger c_m (a^\dagger + a) \quad . \tag{III.101g}$$

X, Y, Z, J, K and G are the appropriate coupling parameters proportional to the first derivative of the interaction potential ($V_{kk'}$), while W is proportional to the second derivative of $V_{kk'}$. The above dynamic Hamiltonian provides us with the following features: (i) the ground state site energy of the adspecies E_0 is perturbed by H_C', which includes changes in site n due to direct interactions with the lattice and due to active-mode excitation, as well as an indirect interaction with the phonons via the active mode; (ii) the terms H_C^0 and H_1 represent parallel motion of the adspecies, $|J_{nm}|^2$ in H_1 being related to the

intersite transition probability from site n to site m due to coherent motion; (iii) the terms H_2 and H_3 represent the perpendicular vibrational-motion-induced intersite transitions due to the active mode A and the bath modes B of the adspecies/surface system, respectively; (iv) H_4 is the A and B mode coupling-induced intersite transition; (v) finally, the excitation of the active mode, governed by $H_{AF}(t)$, provides the dominant driving force for intersite migration of the adspecies.

For the case of chemisorption on a lattice site, the equilibrium position of the adspecies is shifted due to the distortion of the lattice. In this case the adspecies-phonon interaction is very strong and perturbation theory cannot be used. It is posssible, however, to use a canonical transformation to go to lattice-dressed operators $A_n^\dagger$, A_n, $B_j^\dagger$, B_j and $C_n^\dagger C_n$ which take into account the shifted equilibrium position of the adspecies and the lattice distortion. The transformed total Hamiltonian is quite complicated, and for tractable results we shall investigate the single-phonon case, where the dressed Hamiltonian is

$$H(t) = \tilde{H}_0 + \tilde{H}_{AB} + \tilde{H}'_C + \tilde{H}_{AF}(t) \quad , \tag{III.102a}$$

$$\tilde{H}_0 = \tilde{E}_0 \sum_n C_n^\dagger C_n + \hbar\omega_{eff} A^\dagger A + \sum_j \hbar\omega_j B_j^\dagger B_j \quad , \tag{III.102b}$$

$$\tilde{H}_{AB} = \sum_{n\neq m,j} \hbar\tilde{W}^j_{nm}\, C_n^\dagger C_n \left[A^\dagger B_j + A B_j^\dagger\right] \quad , \tag{III.102c}$$

$$\tilde{H}'_C = \sum_{n,j} \hbar\tilde{Z}_{nj}\, C_n^\dagger C_n \left[A^\dagger B_j + A B_j^\dagger\right] \quad , \tag{III.102d}$$

$$\tilde{H}_{AF}(t) = \sum_{n\neq m} \tilde{V}_{nm}(t)\, C_n^\dagger C_n \left[A^\dagger + A\right] \quad , \tag{III.102e}$$

$$\omega_{eff} = \omega_A - 2\varepsilon^* A^\dagger A \quad . \tag{III.102f}$$

$\tilde{E}_0$ is the distortion energy, $\tilde{W}^j_{nm}$ and $\tilde{Z}_{nj}$ are the transformed coupling constants of W^j_{nm} and Z_{nj}, respectively, and $\tilde{V}(t)$ is the transformed laser-adspecies coupling constant of $V(t)K_{nm}$. Employing the many-body technique described in the previous sections, we obtain the equations of motion for the ensemble average $\langle\langle\langle\cdots\rangle\rangle\rangle$ (over the A and B modes and the lattice site coordinates) of the active (A) mode and the lattice site transition probability:

$$\frac{d\langle A\rangle}{dt} = -i\langle\omega_{eff}(t)\rangle\langle A\rangle - iV(t) - \left[\left[\gamma_1+\gamma_2+\gamma_M\right]/2\right]\langle A\rangle \quad , \tag{III.103a}$$

$$\frac{\langle\langle n_A\rangle\rangle}{dt} = -i\left\langle\left\langle V(t)A^{+} - V(t)A\right\rangle\right\rangle - \left[\gamma_1+\gamma_M\right]\left[\langle\langle n_A\rangle\rangle - \bar{n}_0\right] \quad , \tag{III.103b}$$

$$\frac{d\langle\langle P_n\rangle\rangle}{dt} = -2\gamma_m\left[\left[\langle\langle n_A\rangle\rangle+1\right]\bar{n}_B + \left[\bar{n}_B+1\right]\langle\langle n_A\rangle\rangle\right]\left[2\langle\langle P_n\rangle\rangle - \langle\langle P_{n+1}\rangle\rangle - \langle\langle P_{n-1}\rangle\rangle\right] . \tag{III.103c}$$

Here γ_2 is a dephasing factor, and γ_1 is the phonon-coupling-induced damping factor given by

$$\gamma_1 = \sum_j |\tilde{Z}^j|^2 \gamma_B \Big/ \left[\Delta_j^2 + \left[\gamma_B/2\right]^2\right] \quad , \tag{III.104a}$$

$$\Delta_j = \langle\omega_{eff}\rangle - \omega_j \quad , \tag{III.104b}$$

where γ_B is the decay factor of the phonon (B) modes due to anharmonic coupling. In Eq. (III.104) and in what follows, we assume only nearest-neighbor contributions, namely, $Z^j_{nm} = Z^j_{n,n\pm1} = Z^j$, etc. The migration-induced damping factor γ_M is given by

$$\gamma_M = \sum_j |\tilde{W}^j|^2 \left[\frac{\left[\gamma_B/2\right]\cos\left[d\lambda_j\right] - \Delta_j \sin\left[d\lambda_j\right]}{\Delta_j^2 + \left[\gamma_B/2\right]^2}\right] \quad , \tag{III.105}$$

where λ_j and d are the wavelength of the B-mode vibration and the lattice spacing of the substrate, respectively. We note that a simplified model[78] which assumes an infinite phonon lifetime, i.e., $\gamma_B=0$, results in $\gamma_1=\gamma_M=0$ for single-phonon processes and for $\omega_{eff} > \omega_j$. For systems with great energy gap, $(\omega_{eff}-\omega_j)>>\gamma_B$, the damping factors for the single-phonon processes are very small and multiphonon processes are dominant. Employing techniques similar to those used for obtaining Eq. (III.35), the expressions of γ_1 and γ_M for multiphonon processes may be obtained by setting Δ_j equal to $<\omega_{eff}>-\sum_j \omega_j$ and multiplying the coupling parameters $|\tilde{Z}^j|^2$ and $|\tilde{W}^j|^2$ by the multiphonon occupation number of the heat-bath modes in Eqs. (III.104) and (III.105).

From the coupled equations, Eq. (III.103), we can calculate the lattice site occupation probability $\langle\langle P_n(t)\rangle\rangle$, which in turn gives us the mean-square displacement of the adspecies

$$\langle R^2(t)\rangle \equiv d^2 \sum_n n^2 \langle\langle P_n(t)\rangle\rangle \quad . \tag{III.106}$$

and the diffusion (migration) coefficient

$$D = \lim_{t\to\infty} \left[\frac{\langle R^2(t)\rangle}{2t}\right] \quad . \tag{III.107}$$

The site probability function $\langle\langle P_n(t)\rangle\rangle$ is in general not analytically available due to the time-dependent excitation $\langle\langle n_A(t)\rangle\rangle$ which is nonlinearly coupled [Eq. (III.103)]. For tractable results, we investigate the large damping case, $\gamma_{1,2}>>\gamma_M$, such that the adspecies reaches its steady-state excitation $X \equiv \langle\langle n_A(t)\rangle\rangle_{s.s}$ which is governed by a cubic equation, Eq. (III.20). Using this steady-state excitation, we may solve Eq. (III.103C) to obtain the quasi-steady-state site probability,

$$\langle\langle P_n(t)\rangle\rangle = I_n(4Wt)e^{-4Wt} \quad , \tag{III.108}$$

where I_n is a modified Bessel function and

$$W = \left(2\bar{n}_B X + X + \bar{n}_B\right)\gamma_M \quad . \tag{III.109}$$

Thus, from Eq. (III.106) and using the recursion relation for the modified Bessel functions, we obtain the mean-square displacement, which in turn yie s the migration coefficient

$$D = 4Wd^2 \quad . \tag{III.110}$$

This is related to the laser intensity by a power law, I^p, $1 \le p \le 3$, since $W \propto I^p$; $p=1$ for low excitations for the harmonic case ($\epsilon^*=0$), and $p=1/3$ for high excitations. We note that the above laser-enhanced migration constant, $D \propto W$, is governed by an Arrhenius form for the high-temperature limit, $kT \gg \hbar\omega_j$,

$$D = D_0 \exp\left[-E_A/kT\right] \quad , \tag{III.111a}$$

$$E_A \propto \left[|\tilde{W}^j|^2 + |\tilde{Z}^j|^2\right]\hbar\omega_A \tag{III.111b}$$

is the "activation energy" for migration. We note that the above Arrhenius form for the migration coefficient resulting from single-phonon processes may be replaced by a non-Arrhenius function for multiphonon processes.

The master equation given in Eq. (III.103c) involves the assumptions of nearest-neighbor contribution and constant migration rate. Removing these two assumptions, we have the generalized master equation[84]

$$\frac{dP(m,n,j,t)}{dt} = \int_0^t dt' \sum_{m',n',t'} \left[W^{jj'}_{mm',nn'}(t-t')P(m',n',j',t') - W^{j'j}_{m'm,n'n}(t-t')P(m,n,j,t') \right] \quad \text{(III.112)}$$

where $P(m,n,j,t)$ is the site probability of finding the adspecies at the lattice site (m,n) and at the j-th vibrational level at time t, $W^{jj'}_{mm',nn}(t)$ is a time-dependent transition rate from state (m',n',j') to (m,n,j), and $W^{j'j}_{m'm,n'n}(t)$ is the associated reverse rate. We note that in the above general form the transition rates are not only time dependent but also governed by both the site coordinate (m,n) and the vibrational states of the adspecies (j) which are activated by the laser radiation. Depending on the migration barrier and the vibrational energy of the adspecies, there are at least three types of dynamical transitions.

Type (I): horizontal migration. The laser induces the transition from (m,n,j) to(m',n',j) with a change in lattice site but leaving the vibrational state unchanged. This is the situation that the adspecies is vibrationally excited to a mobile site followed by a horizontal migration, but returning to its initial vibrational state by energy relaxation to phonons. Mathematically, this process may be described by H_1 and H_4 in Eq. (III.101).

Type (II): vertical transition. This involves the transition from (m,n,j) to (m,n,j'), where the initial j-th vibrational state is promoted to the higher state $j'>j$ when the adspecies absorbs photons, but the energy level is still not high enough to cause intersite transitions. For this case the migration barrier is large, and the description involves H'_C in Eq. (III.101b).

Type (III): oblique transition. This involves simultaneous intersite and vibrational state transitions and may be described by H_2 and H_{AF} in Eq. (III.101).

We note that a type (I) transition usually involves a physisorbed state for highly mobile adspecies and may be thermally induced by either direct laser heating of indirect phonon excitation. A type (II) transition may cause direct

desorption when enough phonons are absorbed by the adspecies. The last type of transition may cause indirect desorption via surface rate processes such as recombination or decomposition or by the assistance of phonons.

We finally note that the laser-induced selective surface migration of adspecies has been theoretically proposed,[84] although no experimental work has been reported. In the model system of Lin and George,[84] the moble adspecies (usually in a physisorbed state) could migrate in a preferential direction which has a lower migration energy barrier and/or higher effective temperature [see Eq. (III.111)]. This laser-enhanced selective migration, either direction-selective or adspecies-selective (if isotope and/or mixture adspecies are involved), plays an essential role in the surface rate processes which are diffusion-limited.

b. Desorption

Desorption mechanisms have been recently studied, both theoretically[78,80-82,89-92] and experimentally.[94-101] First of all, we should note that none of the theories developed as far nor measured data are able to completely describe the desorption mechanisms which may be achieved through several channels. Depending upon the states of the adspecies (such as physisorbed or chemisorbed, adatom or admolecule, and the potential of the adbond) and the frequency spectrum of the system and the laser field, as shown in Fig. 22 the desorption may result from direct laser excitation or from indirect energy transfer processes. The desorption channels from type (I) to type (V) will be discussed separately.

Type (I): direct desorption via active-mode excitation. This type of desorption channel has been investigated by Slutsky and George in a harmonic model,[78] Lin and George in an anharmonic model[80,82] and Metiu et al in a Morse potential model[89] [see Fig. 22(I)]. In these models, the active mode is excited by multiphoton processes, while energy is leaking to the bath modes

which lead to a damping factor or level width of the active mode. When enough photon energy is absorbed by the active mode [or the adbond in the one-dimensional (1D) Morse potential model], the adspecies may be desorbed from the surface by overcoming the desorption energy. In a harmonic model, this threshold photon energy (or laser intensity) in order for desorption to occur has been underestimated by the harmonic model, where the absorption cross section is governed by a constant detuning $\Delta=\omega_A-\omega$, and has been overestimated by the 1D Morse potential model. While the anharmonic model of Lin and George (AMLG) should sometimes provide a good estimate of the desorption threshold energy, none of the above treatments will be appropriate when the IVR rate of the system is faster than or comparable to the laser excitation rate, since the photon energy is more likely randomized within the adspecies and/or substrate phonons. Overcoming the anharmonicity in the AMLG model, $\Delta'=\Delta-2\varepsilon^*\langle n\rangle$, or in the Morse potential model, and thus reaching the continuum, is quite unlikely to occur for this fast IVR situation. We also note that in the Morse potential model, the important concept of the "quasi-continuum" is excluded. Therefore, one might look for another type of desorption channel, such as the following suggestion.

Type (II): direct desorption via the quasi-continuum. The concept of the quasi-continuum and the mechanisms for level broadening have been proposed by Lin and George.[84] As shown in Fig. 22(II), the active (A) mode is pumped by near-resonant radiation and the photon energy is rapidly randomized within the admolecule(M) with a damping rate γ to the C modes. There we have introduced the quasi-continuum (QC) in the surface potential M-C bond. We note that for a small adspecies (e.g., single atom or diatomic molecule), the QC may not be achieved when one assumes an 1D potential. As discussed in Part A.3 of this section, the master (rate) equation treatment for the incoherent excitation in the regime of the QC is able to provide a quantitative description of the desorption mechanism.[80] We should also note that the level

broadening of the adspecies can be achieved by several factors such as the anharmonic coupling in the adbond, the surface-phonon-induced T_1 and T_2 relaxation and adspecies-adspecies interactions (static dipole coupling or dynamic scattering-induced pressure broadening). All of these broadening effects may achieve the QC even for small species where this is not possible in the gas phase.

Type (III): indirect desorption via tunneling. Desorption may also occur indirectly when the adspecies (particularly for a physisorbed state) is excited to a high vibrational level whose energy is degenerate with some continuum of the adbond. As shown in Fig. 22(III), the active mode of the admolecule is excited with its excited state coupled to the continuum of the adbond (B-C) to cause the desorption of A-B. This type of desorption channel essentially involves a Fano-type bound-continuum coupling and has been employed by Lucas and Ewing in their predissociation model for an adspecies and later by Kreuzer et al[92] and Casassa et al.[91] Although a Morse potential has been used for the adbond (B-C), the above authors have assumed either a single-photon process or a multiphoton process but with a harmonic potential for the active bond (B-C). This harmonic assumption again might overestimate the transition rate (or the absorption cross section) in the master equation.[92] Furthermore, a 1D Morse potential of the adbond (B-C) without the concept of the QC may cause errors in the estimation of the desorption rate.

Type (IV): indirect desorption via substrate heating. Shown in Fig. 22(IV) is a system in which the adspecies is not active to the radiation but the substrate can absorb photon energy either by phonon or electron excitation. The adbond may be broken by absorbing thermal energy from the heated substrate surface. This desorption channel may occur when the substrate with small diffusivity is highly heated and the adspecies is weakly bounded, e.g., physisorbed. However, this type of desorption is much less sensitive to the laser frequency than types (I)-(III) where the dipole transition is governed by the

detuning.

Type (V): phonon-assisted desorption in the QC regime. We propose another type of desorption channel, as shown in Fig. 22(V), which combines those mechanisms described for types (I)-(IV). The effective adbond potential (M-C) consisting of regions (i) and (ii) is coupled to the substrate phonons which may help desorption occur, particularly when the adbond is excited to region (ii) and near the true continuum. In the coherent excitations of region (i) with strong phonon coupling, the energy flow from the adspecies to the substrate is more likely irreversible. However, when the adspecies reaches region (ii), i.e., the QC,desorption may be assisted by the feedback energy from the thermal phonons. When the adspecies is highly excited into the QC region and in thermal equilibrium with the substrate, the desorption rate (k_D) may be approximated by

$$k_D = k_0 \exp[-(E^* - \hbar\omega\langle n\rangle)/k_B T_s^*] \quad , \tag{III.113}$$

where k_0 is the pre-exponential factor, k_B is Boltzmann's constant, and $\langle n\rangle$ is the mean number of photon absorbed by the adspecies [given by e.g., Eq.(III.75) or (III.78)] with the threshhold desorption energy E^* and maximum surface temperature T_s^* [given by Eq. (III.59)]. Another way of describing the phonon-assisted desorption rate is by the expression

$$k_D = k_0 \exp[-E^*/k_B(T_{eff} + T_s^*)] \quad , \tag{III.114}$$

where T_{eff} is an effective temperature of the adspecies [given by Eq. (III.84)]. We note that in either of the above expressions, Eq. (III.113) or (III.114), the desorption rate may be enhanced by the laser excitation through $\langle n\rangle$ and T_{eff} and further assisted by the thermal phonons via T_s^*, where $T_s^* \approx T_0$ (initial surface temperature) when the substrate surface is not heated.

A more rigorous expression for the desorption rate given now as time dependent is

$$k_D(t) = \int_0^\infty d\varepsilon \sum_n W_{n\varepsilon}(t)\, P_n(t) \quad , \tag{III.115}$$

where $P_n(t)$ is the probability that the adspecies is in the bound vibrational state $|n\rangle$, given by, e.g., a Poisson function [Eq.(III.87a)]. $W_{n\varepsilon}(t)$ is a thermal transition rate from the bound state $|n\rangle$ to the continuum state $|\varepsilon\rangle$ given by

$$W_{n\varepsilon}(t) = k_0 \exp\left[-(\varepsilon - E_n)/k_B T_s(t)\right] , \tag{III 116}$$

where E_n is the energy of the n-th vibrational state, and $T_s(t)$ is the time-dependent surface temperature which can be obtained from the diffusion equation, Eq. (III.55a), with the boundary condition Eq. (III.56).

Type (VI): indirect desorption by dynamics. The final desorption channel to be discussed is also an indirect type, which may be achieved by dynamic processes such as migration, scattering and reactions. An example is shown in Fig. 22(VI), where the initially chemisorbed adspecies may make a transition to the mobile physisorbed P-state by absorbing enough photon energy to overcome the transition barrier, but still not have enough energy to overcome the desorption barrier.[82] The mobile P-state may easily migrate on the surface and eventually desorb from the substrate by further absorbing photon energy via the direct desorption channel [types (I) and II)] or the indirect channel [types (III) and (IV)] or the phonon-assisted channel [type (V)].

B. Laser Applications to Surface Chemistry

We have discussed in Part A.5 two of the most important dynamical processes associated with the phenomenon of laser-stimulated surface processes (LSSP) --migration and desorption. In addition to these processes, LSSP in general should include rate processes such as diffusion, recombination, decomposition, dissociation and adsorption (or deposition). Before investigating

the experimental aspects of LSSP, we display in Fig. 23 a flow chart of the methodology of LSSP. Both classical and quantum treatments have been developed for the absorption cross section which, with the master equation in energy space, gives the energy population and the average excitation. Furthermore, by solving the master equation in the lattice-site space we may investigate laser-induced surface migration (which in the field-free case has been studied by random walk techniques.[111] We have shown that for large values of n, the discrete master equation reduces to a classical diffusion equation where the energy population can be analytically obtained. The energy flow and population of the adspecies/surface system provide the fundamental mechanisms of LSSP as discussed in Part A. In this second part we shall study the applications of LSSP to surface chemistry, which includes heterogeneous catalysis, chemical vapor deposition and laser annealing.

Some of the applications of lasers to surface chemistry and/or physics are:

(1) Enhancement of surface diffusion-limited reactions.

(2) Enhancement of the mobilities of selective species in a multi-component environment.

(3) Control of the concentration of reagents by selective desorption or excitation-induced migration of the species.

(4) Study of the decomposition and recombination rate processes on solid surfaces.

(5) Study of the catalytic properties and heterogeneity features of the adsorbents.

(6) Isotope separation and mass separation of adspecies via selective desorption (laser chromatography).

(7) Study of the composition and location of the active sites and the conformation structure of the adspecies.

(8) Fabrication of microelectronics via laser-induced chemical vapor deposition; microetching and laser annealing.

We first discuss laser applications to heterogeneous catalysis, which involve the following processes:[112] (1) adsorption (physical or chemical) and desorption of the species on the catalytic surface; (2) migration of adsorbed species and subsequent collisions; (3) interactions (via dipole-dipole, charge transfer, etc.) between the adspecies, either directly or surface-mediated; (4) scattering (reactive or nonreactive) of gas-phase species by the clean surface or adsorbed species.

A laser beam might influence the above processes in a number of ways depending upon the physical and chemical states of the excited species. Some examples are (where K denotes the catalytic substrate):

(i) Excitation of a reactant in the gas phase

$$A + K \rightarrow A/K \begin{cases} \rightarrow AK + K & (a) \\ \rightarrow B + C + K & (b) \end{cases}$$

(ii) Excitation of an intermediate adsorbed on the surface

$$(A + B)/K \xrightarrow{k_1} (AB)/K \xrightarrow{k_2} \begin{cases} \dashrightarrow AB + K & (c) \\ \dashrightarrow C + D + K & (d) \end{cases}$$

(iii) Excitation of a reaction product in the gas phase

$$A+B + K \dashrightarrow (AB)/K \dashrightarrow C + D \quad . \qquad (e)$$

In (i), laser radiation may enhance the adspecies-substrate reaction (a) and the decomposition processes catalyzed by the substrate (b). Laser/surface-catalyzed decomposition processes have been investigated for the chemisorption of CH_4 on Rh[113] and HCOOH on Pt,[97] where the vibrational excitation of the reactants has been chosen to change the rate of adsorption and the amount of products formed. The infrared laser-induced etching of a

semiconductor has been studied for SF_6/Si, where the gas-phase reactant SF_6 is excited and then chemsorbed on the Si surface to react and form the products SF_6(g) and SiF_4(g) desorbed from the substrate.[100]

In (ii), laser radation may influence the overall reaction rate in several ways: (1) by increasing the mobility of the reactant atoms (A or B) through photon excitation of the A-K or B-K bond with subsequent enhancement of the reaction rate k_1 [see type (VI) in Fig. 22]; (2) by removal of the excess energy from the unstable complex (AB) on the substrate surface via laser-stimulated emission accompanied by surface-phonon-mediated relaxation, thereby increasing the reaction rate k_2; and (3) by breaking the AB-K bond either directly through laser excitation of the adspecies or indirectly through thermal desorption by laser heating of the surface [see types (I) and (IV) in Fig. 22]. We note that the direct desorption of chemisorbed species from a solid surface usually requires multiphoton absorption, necessitating the use of high-power radiation. However, much lower powers may be sufficient for the desorption of a diatomic molecule adsorbed on a solid surface (A-B-K) if the photon energy absorbed by the A-B molecule can be easily transferred to the surface to break the B-K bond via anharmonic coupling [see type (III) in Fig. 22]. Laser desorption of OH radicals from a silica surface has been reported in which a low-power ($\approx$10 W/cm^2) CW CO_2 laser was used to excite the Si-OH stretching mode.[95] High-intensity ($\approx$MW/cm^2) pulsed CO_2 laser desorption processes have also been performed for CH_3F/NaCl,[99] C_5H_5N/Ag and the isotopes C_5H_5N and C_5D_5N coadsorbed on KCl.[100,101]

In (iii), we illustrate laser excitation of a reaction product after it is desorbed from the substrate. The detection of the OH radical desorbing from a Pt and Rh/Pt catalyst surface by laser-induced fluorescence has been recently reported.[97]

Another important aspect of laser applications is in laser-assisted chemical vapor deposition (LCVD), which could provide a new method in the fabrication of microelectronics. A typical sequence of events occurring in CVD are:

1. Diffusional transfer of the gaseous reactants to the surface.
2. Adsorption of reactants on the surface.
3. Events on the surface, e.g., reactions, migration, nucleation, etc.
4. Desorption of products from the surface.

Laser radiation can be used to decompose the gaseous molecules or heat the substrate in order to enhance adsorption. Examples of systems studied so far are: the decomposition of metal alkyls and metal carbonyls to deposit on metals and the decomposition of SiH_4 to deposit on silicon;[115] reactions of $SiCl_4$ with H_2 to deposit Si, and SiH_4 with NH_3 to deposit Si_3N_4.[116] We note that in the above mentioned examples, laser radiation may be used to induce CVD with many features which are not available from the conventional procedures, e.g., single-step processes, small-scale deposition with high homogeneity, remote procedure, and selective and local deposition.

We finally mention laser annealing. Both CW laser solid-phase recrystallization and pulsed laser liquid-phase epitoxy have been reported.[117] Furthermore, the controversy regarding the physical mechanisms responsible for annealing, namely the thermal melting model versus nonthermal plasma model, has been investigated by picosecond laser processes.[118]

Acknowledgments

This work was supported in part by the Air Force Office of Scientific Research (AFSC), United States Air Force, under Grant AFOSR-82-0046, the Office of Naval Research and the National Science Foundation under Grant CHE-8022874. The United States Government is authorized to reproduce and distribute reprints for governmental purposes notwithstanding any copyright notation hereon. TFG acknowledges the Camille and Henry Dreyfus Foundation for a Teacher-Scholar Award (1975-84) and the John Simon Guggenheim Memorial Foundation for a Fellowship (1983-84).

References

1. (a) N. R. Isenor and M. C. Richardson, App. Phys. Lett. 18, 224 (1971); (b) V. S. Letokhov, E. A. Ryabov and O. A. Tumanov, Sov. Phys. JETP 36, 1069 (1973).

2. Reviews of MPE and MPD are: (a) N. Bloembergen and E. Yablonovitch, Physics Today 31 (5), 23 (1978); (b) P. A. Shultz, Aa. S. Sudbo, D. J. Krajnovich, H. S. Kwok, Y. R. Shen and Y. T. Lee, Ann. Rev. Phys. Chem. 30, 379(1979); (c) A. H. Zewail, V. S. Letokhov, R. N. Zare, R. B. Bernstein, Y.T. Lee and Y. R. Shen, in A Special Issue on "Laser Chemistry," Physics Today 33 (11), 25-59 (1980); (d) C. D. Cantrell, V. S. Letkohov and A. A. Makarov, in Coherent Nonlinear Optics, Recent Advances, ed. by M. S. Feld and V. S. Letokhov (Springer, Heidelberg, 1980).

3. N. Bloembergen, Opt. Commun. 15, 416 (1975).

4. T. P. Cotter, W. Fuss, K. L. Kompa and H. Stafast, Opt. Commun. 18, 220 (1976).

5. B. Steverding, P. Dudel and E. P. Gibbon, J. Appl. Phys. 48, 1195 (1977); 49, 1260 (1978).

6. J. Lin, Phys. Lett. 70A, 195 (1979).

7. J. Lin and T. F. George, Phys. Lett. 80A, 296 (1980).

8. J. Lin and T. F. George, Phys. Rev. B 24, 65 (1981).

9. D. Poppe, Chem. Phys. 45, 371 (1980).

10. R. B. Walker and R. K. Preston, J. Chem. Phys. 67, 2017 (1977).

11. L. M. Narducci, S. S. Mitra, R. A. Skates and C. A. Coulter, Phys. Rev. A 16, 247 (1977).

12. J. Lin and T. F. George, Theoret. Chim. Acta (Berl.) 61, 243 (1982).

13. (a) D. W. Noid and R. A. Marcus, J. Chem. Phys. 67, 559 (1977); Chem. Phys. Lett. 23, 269 (1980); (b) R. Ramaswamy, P. Siders and R. A. Marcus, J. Chem. Phys. 74, 4418 (1981); (c) E. J. Heller, J. Chem. Phys. 72, 1337 (1980).

14. H. W. Louisell, Quantum Statistical Properties of Radiation (Wiley, New York, 1973), Chap. 7.

15. (a) D. O. Ham and M. Rothchild, Opt. Lett. 1, 28 (1977); (b) R. V. Ambartzumian, Yu. A. Gorokhov, V. S. Letokhov and G. N. Markarov, Sov. Phys. JETP 69, 1956 (1975).

16. J. L. Lyman, J. Chem. Phys. 67, 1868 (1977).

17. E. R. Grant, P. A. Schutz, Aa. S. Sudbo, Y. R. Shen and Y. T. Lee, J. Phys. Rev. Lett. 40, 115 (1978).

18. P. A. Schutz, Aa. S. Sudbo, E. A. Grant, Y. R. Shen and Y. T. Lee, Chem. Phys. 72, 4895 (1980).

19. M. Quack, J. Chem. Phys. 69, 1282 (1978).

20. J. G. Black, P. Kolodner, M. J. Shultz, E. Yablonovitch and N. Bloembergen, Phys. Rev. A 19, 704 (1979).

21. J. Scheck and J. Jortner, J. Chem. Phys. 70, 3016 (1979).

22. W. Fuss, Chem. Phys. 36, 135 (1979).

23. J. R. Barker, J. Chem. Phys. 72, 3686 (1980).

24. J. Troe, J. Chem. Phys. 66, 4745 (1977).

25. J. Stone, E. Theile and M. F. Goodman, J. Chem. Phys. 73, 2259 (1980).

26. A. C. Baldwin and H. van der Bergh, J. Chem. Phys. 74, 1012 (1981).

27. W. Forst, Theory of Unimolecular Reactions (Academic, New York, 1973).

28. M. J. Shutz and E. Yablonovitch, J. Chem. Phys. 68, 3007 (1978).

29. B. Carmeli and J. Jortner, J. Chem. Phys. 72, 2054; 2070 (1980).

30. E. W. Montroll and K. E. Shuler, J. Chem. Phys. 26, 454 (1957).

31. A. V. Eletskii, V. D. Klimov and V. A. Legasov, Dokl. Acad. Nauk. SSSR 237, 1196 (1978).

32. Y. Ben-Aryeh, J. Quant. Spect. Radiat. Transfer 23, 403 (1980).

33. (a) J. J. Yeh, C. M. Bowden and J. H. Eberly, J. Chem. Phys. 76, 5936 (1982); (b) E. Kyrola, Abstracts of the Fifth Rochester Conference on Coherence and Quantum Optics (Rochester, New York, 1983), p. 60.

34. J. Ford, J. Math. Phys. 2, 387 (1961).

35. J. Lin and T. F. George, Surface Sci. 108, 340 (1981).

36. A. Nitzan, S. Mukamel and J. Jortner, J. Chem. Phys. 60, 3929 (1974).

37. Z. Gan, G. Yang, X. Huang and K. Feng, Acta Physica Sinica (Peking) 29, 743 (1980).

38. R. Hall and A. Kaldor, J. Chem. Phys. 70, 4027 (1979).

39. J. W. Perry and A. H. Zewail, Chem. Phys. Lett. 65, 31 (1979).

40. K. V. Reddy and M. J. Berry, Chem. Phys. Lett. 66, 223 (1979).

41. J. C. Stephenson, D. S. King, M. F. Goodman and J. Stone, J. Chem. Phys. 70, 4496 (1979).

42. D. Heller and S. Mukamel, J. Chem. Phys. 70, 463 (1979).

43. E. Thiele, M. F. Goodman and J. Stone, Chem. Phys. Lett. 69, 18 (1980); Opt. Eng. 19, 10 (1980).

44. (a) R. V. Ambartzumian, Yu. A. Gorokhov, V. S. Letokhov, G. N. Makarov, A. A. Puretskii and N. P. Furzikov, JETP Lett. 23, 194 (1976); Opt. Commun. 18, 517 (1976); (b) R. V. Ambartzumian, V. S. Letokhov, G. N. Makarov and A. A. Puretskii, Opt. Commun. 25, 69 (1978).

45. A. N. Oraevskii. A. A. Stepanov and V. A. Shcheglov, Sov. Phys. JETP 42, 1012 (1976).

46. T. P. Cotter, unpublished results.

47. L. M. Narducci and J. M. Yuan, Phys. Rev. A 22, 261 (1980).

48. J. Lin, unpublished results.

49. J. R. Stine and D. W. Noid, Chem. Phys. Lett. 77, 287 (1981); Opt. Commun. 37, 187 (1981); 31 161 (1979).

50. M. H. Nayfeh, K. King, G. B. Hillard, I. S. Shahin and A. H. Nayfeh, Phys. Rev. A 26, 1988 (1982).

51. A. M. F. Lau and C. K. Rhodes, Phys. Rev. A 16, 2392 (1977).

52. M. Hutchinson and T. F. George, J. Phys. Chem. 87, 2037 (1983).

53. H. Feshbach, Ann. Phys. 43, 410 (1967).

54. P. R. Brooks, R. F. Curl and T. C. Maguire, Ber. Bunsenges. Phys. Chem. 86, 401 (1982).

55. P. Hering, P. R. Brooks, R. F. Curl, Jr., R. S. Judson and R. S. Lowe, Phys. Rev. Lett. 44, 687 (1980).

56. B. E. Wilcomb and R. E. Burnham, J. Chem. Phys. 74, 6784 (1981).

57. H. P. Grieneisen, H. Xue-Jing and K. L. Kompa, Chem. Phys. Lett. 82, 421 (1981).

58. T. C. Maguire, P. R. Brooks and R. F. Curl, Jr., Phys. Rev. Lett. 50, 1918 (1983).

59. R. E. Smalley, L. Wharton and D. H. Levy, J. Chem. Phys. 66, 2750 (1977), and references therein.

60. T. D. Russell, B. M. DeKoven, J. A. Blazy and D. H. Levy, J. Chem. Phys. 72, 3001(1980).

61. M. Sulkes, J. Tusa and S. A. Rice, J. Chem. Phys. 72, 5733 (1980).

62. D. E. Brinza, B. A. Swartz, C. M. Western and K. C. Janda, J. Chem. Phys. 79, 1541 (1983).

63. W. L. Hase and C. S. Sloane, J. Chem. Phys. 64, 2256 (1976).

64. J. A. Beswick and J. Jortner, J. Chem. Phys. 68, 2277 (1978).

65. B. A. Waite and W. H. Miller, J. Chem. Phys. 73, 3713 (1980).

66. H. Feshbach, A. K. Kerman and P. H. Lemmer, Ann. Phys. (N.Y.) 41, 230 (1967).

67. I. H. Zimmerman and T. F. George, J. Chem. Phys. 4, 315 (1974).

68. R. J. Bieniek, Phys. Rev. A 18, 392 (1978).

69. R. J. Bieniek, J. Phys. B: At. Mol. Phys. 13, 4405 (1980); 14, 1707 (1981).

70. K. S. Lam and T. F. George, Phys. Rev. A, in press.

71. J. C. Polanyi and R. J. Wolf, J. Chem. Phys. 75, 5951 (1981).

72. H.-J. Foth, J. C. Polanyi and H. H. Telle, J. Phys. Chem. 86, 5027 (1982).

73. M. Hutchinson and T. F. George, Phys. Rev. A 28, 490 (1983).

74. K. S. Kochelashvilli, N. V. Karlov, A. N. Orlov, R. P. Petrov, Yu. N. Petrov and A. M. Prokhorov, JETP Lett. 21, 302 (1975).

75. V. I. Goldanskii, V. A. Namiot and R. V. Khokhlov, Sov. Phys. JETP 43, 1226 (1976)

76. N. V. Karlov and A. M. Prokholov, Sov. Phys. Usp. 20, 721 (1977).

77. M. S. Dzhidzhoev, A. I. Osipov, V.Ya. Panchenko, V. T. Platonenko, R. V. Khokhlov and K. V. Shaitan, Sov. Phys. JETP 47, 684 (1978).

78. M. S. Slutsky and T. F. George, Chem. Phys. Lett. 57, 474 (1978); J. Chem. Phys. 70, 1231 (1978).

79. J. Lin, Ph.D. Thesis, University of Rochester (1980).

80. J. Lin and T. F. George, Chem. Phys. Lett. 66, 5 (1979).

81. J. Lin, A. C. Beri, M. Hutchinson, W. C. Murphy and T. F. George, Phys. Lett. 79A, 233 (1980).

82. J. Lin and T. F. George, J. Chem. Phys. 72, 2554 (1980).

83. J. Lin and T. F. George, Surface Sci. 100, 381 (1980); 107, 417 (1981); 115, 569 (1982).

84. J. Lin and T. F. George, J. Phys. Chem. 84, 2957 (1980).

85. J. Lin, X. Y. Huang and T. F. George, Z. Phys. B 48, 355 (1982).

86. J. Lin and T. F. George, J. Chem. Phys. 78, 5197 (1983).

87. J. Lin and T. F. George, Phys. Rev. B 24, 65 (1981); B 28, 76 (1983).

88. Recent reviews are: (a) T. F. George, J. Lin, K. S. Lam and C. Chuang, Opt. Eng. 19, 100 (1980); (b) T. F. George, J. Lin, A. C. Beri and W. C. Murphy, Prog. Surf. Sci. (1984), in press.

89. (a) C. Jedrzejek, K. F. Freed, S. Efrima and H. Metiu, Chem. Phys. Lett. 74, 43 (1980); 79, 227 (1981); Surface Sci. 109, 191 (1981); (b) G. Korzeniewski, E. Wood and H. Metiu, J. Vac. Sci. Tech. 20, 594 (1982); (c) S. Efrima, C. Jedrzejek, K. F. Freed, E. Hood and H. Metiu, J. Chem. Phys. 79, 2436 (1983).

90. D. Lucas and G. E. Ewing, Chem. Phys. 58, 385 (1981).

91. M. P. Casassa, F. G. Celii and K. C. Janda, J. Chem. Phys. 76, 5295 (1982).

92. (a) H. J. Kreuzer and D. N. Lowy, Chem. Phys. Lett. 78, 50 (1981); (b) Z. W. Gortel, H. J. Kreuzer, P. Piercy and R. Teshima, Phys. Rev. B 27, 5066 (1983).

93. B. J. Garrison, D. J. Diestler and S. A. Adelman, J. Chem. Phys. 67, 4317 (1977).

94. A. V. Khmelev, V. V. Apollonov, V. D. Borman, B. I. Nokolaev, A. A. Sazykin, V. I. Troyan, K. N. Firsov and B. A. Frolov, Sov. J. Quantum Electron. 7, 1302 (1977).

95. M. S. Djidjoev, R. V. Khokhlov, A. V. Kiselev, V. I. Lygin, V. A. Namiot, A. I. Osipov, V. I. Panchenko and B. I. Provotorov, in Tunable Lasers and Applications, ed. by A. Mooradian, T. Jaeger and P. Stokseth (Springer, Berlin, 1976), p. 100 ff.

96. N. V. Karlov, R. P. Petrov, Yu. N. Petrov and A. M. Prokholov, JETP Lett. 24, 258 (1976).

97. (a) M. E. Umstead and M. C. Lin, J. Phys. Chem. 82, 2047 (1978); (b) L. D. Talley, D. E. Tevault and M. C. Lin, Chem. Phys. Lett. 66, 584 (1979); (c) M. E. Umstead, L. D. Talley, D. E. Tevault and M. C. Lin, Opt. Eng. 19, 94 (1980); (d) M. E. Umstead, J. W. Fleming and M. C. Lin, IEEE J. Quantum

Electron. QE-16, 1227 (1980); (e) L. D. Talley, W. A. Sanders, D. J. Bogan and M. C. Lin, J. Chem. Phys. 75, 3107 (1981); (f) G. S. Selwyn, G. T. Fujimoto and M. C. Lin, J. Phys. Chem. 86, 760 (1982); (g) G. T. Fujimoto, G. S. Selwyn, J. T. Keiser and M. C. Lin, J. Phys. Chem. 87, 1906 (1983).

98. D. Lichtman and Y. Shapira, CRC Crit. Rev. Solid State Mater. Sci. 8, 93 (1978).

99. J. Heidberg, H. Stein and E. Riehl, Phys. Rev. Lett. 49, 666 (1982).

100. (a) T. J. Chuang, J. Chem. Phys. 72, 6303 (1980); 74, 1453, 1461 (1980); 76, 3828 (1982); J. Vac. Sci. Tech. 18, 638 (1981); 21, 798 (1982); (b) T. J. Chuang and H. Seki, Phys. Rev. Lett. 49, 382 (1982); (c) H. Seki and T. J. Chuang, Solid State Commun. 44, 473 (1982).

101. A recent review is: T. J. Chuang, Surface Sci. Rep. (1983), in press.

102. (a) A. C. Beri and T. F. George, J. Chem. Phys. 78, 4288 (1983); (b) B. Bendow and S. C. Ying, Phys. Rev. B 7, 622 (1973).

103. R. Lefebvre and J. Savolainen, J. Chem. Phys. 60, 2509 (1974); N. M. Witriol, Chem. Phys. Lett. 98, 77 (1983); J. J. Yeh, C. M. Bowden and J. H. Eberly, J. Chem. Phys. 76, 5936 (1982).

104. J. H. Bechtel, J. Appl. Phys. 46, 1585 (1975).

105. M. N. Ozisik, Boundary Value Problems in Heat Conduction (International Textbook, Scranton, 1968); H. S. Carslaw and J. C. Jaeger, Conduction of Heat in Solids, 2nd Ed. (Oxford, London, 1959).

106. J. Lin and T. F. George, J. Appl. Phys. 54, 382 (1983).

107. A. Nitzan and R. J. Silbey, J. Chem. Phys. 60, 4070 (1974).

108. R. F. Willis, W. Ho and E. W. Plummer, Surface Sci. 80, 593 (1979).

109. (a) B. N. J. Persson and R. Ryberg, Solid State Commun. 36, 613 (1980); Phys. Rev. B 24, 6954 (1981); (b) S. Anderson and B. N. J. Persson, Phys. Rev. Lett. 45, 1421 (1980).

110. J. Lin, unpublished results.

111. (a) E. W. Montroll, in Fundamental Problems in Statistical Mechanics, ed. by E. G. D. Cohen (North-Holland, Amsterdam, 1962); (b) E. W. Montroll and K. E. Shuler, Adv. Chem. Phys. 1, 361 (1958): (c) V. M. Kenkre, E. W. Montroll and M. F. Shlesinger, J. Stat. Phys. 9, 45 (1973); (d) A. Blumen and G. Zumofen, J. Chem. Phys. 75, 892 (1982); 76, 3713 (1982).

112. J. M. Thomas and W. J. Thomas, Introduction to the Principles of Heterogeneous Catalysis (Academic, New York, 1967).

113. J. T. Yates, J. J. Zinck, S. Sheard and W. H. Weinberg, J. Chem. Phys. 70, 2266 (1979).

114. W. Kern and V. S. Ban, in Thin Film Processes, ed. by J. L. Vossen and W. Kern (Academic, New York, 1978), p. 257.

115. (a) T. F. Deutsch, D. J. Ehrlich and R. M. Osgood, Jr., Appl. Phys. Lett. 35, 175 (1979); (b) R. Solanki, P. K. Boyer, J. E. Mahan and G. J. Collins, Appl. Phys. Lett. 38, 572 (1981).

116. (a) C. P. Christensen and K. M. Lakin, Appl. Phys. Lett. 32, 254 (1978); (b) D. J. Ehrlich, R. M. Osgood, Jr. and T. F. Deutsch, Appl. Phys. Lett. 39, 957 (1981).

117. C. W. White and P. S. Peercy, Eds., Laser and Electron Beam Processing of Materials (Academic, New York, 1980).

118. R. M. Osgood, Jr. and S. R. J. Brueck, Eds., Laser Diagnostics and Photochemical Processing for Semiconductor Devices (Elsevier, New York, 1983) - Volume 17 of the Materials Research Society Symposium Proceedings.

Figure Captions

Fig. 1. Power law for the average number of photons absorbed per molecule: (A) fluence dependence $\langle N\rangle \propto \phi^q$ and (B) intensity dependence $\langle N\rangle \propto I^q$. Non-linear effects with $q<1$ result from the anharmonicity of the absorption cross section [Eq. (II.16)]. The dots are the experimental data based on the measurement of laser fluence[15(a)] and laser intensity.[15(b)]

Fig. 2. Schematic energy diagram for infrared multiphoton excitation of a polyatomic molecule. The discrete states of the active mode are initially excited and coupled to the quasi-continuum which may be further pumped to reach the true continuum by absorbing enough photons. Note that in the quasi-continuum the energy populations are usually determined by a set of incoherent rate (master) equations.

Fig. 3. Popluation of the photon energy (P_n) vs. number of photons absorbed per molecule (n) in the quasi-continuum region characterized by: (A) thermal distribution [Eq. (II.25)], Poisson distribution in a harmonic model and (C) with the anharmonic corrections.[32]

Fig. 4. Red-shift diagrams of the optimal detunings for infrared excitation of the SF_6 molecule: (A) maximum active (ν_3)-mode excitation ($\bar{n}_1^*$) vs. external detuning (Δ_E') and (B) maximum ν_2-mode excitation ($\bar{n}_2^*$) vs. internal detuning (Δ_I') with a fixed $\Delta_E'/2\pi \approx 2.7\ cm^{-1}$.

Fig. 5. The time-dependent average excitations of the active mode ($\bar{n}_1$), the ν_2 mode ($\bar{n}_2$) and the ν_6 mode ($\bar{n}_3$) for the detunings $(\Delta_E'/2\pi, \Delta_I'/2\pi)$ = (A) (0, 0) exact resonance, (B) (0, 20) far-off internal resonance and (C) (2.71, 1.00). $\Delta_E'/2\pi = 2.71$ is the optimal external detuning for the SF_6 molecule.[12]

Fig. 6. Time evolution of the average excitation of SF_6 subject to one and to two infrared lasers at various scaled [in unit of $(\gamma_1+\gamma_2)$] Rabi frequencies $\Omega_i = (A_i I_{i_o})^{1/2}/(\gamma_1+\gamma_2)$ and scaled detuning $D_i = \Delta_i/(\gamma_1+\gamma_2)$: (A) simultaneous excitation by two lasers with (Ω_1,Ω_2) = (0.5, 1) and single laser excitations

with (B) $(\Omega, D) = (1, 8)$, (C) $(\Omega, D) = (0.5, 1)$ and (D) $(\Omega, D) = (1.5, 2)$. Here the time scale is in the unit of laser pulse duration (τ) with intensity profiles $I_i(t) = I_{i_o} \sin^4(\pi t/\tau)$, $i = 1, 2$.[47]

Fig. 7. Two radiative mechanisms for curve-switching ($j = \frac{1}{2} \leftrightarrow j = \frac{3}{2}$) in an excimer system. Process I: during the collision a laser L1 excites a bound state of the system. Subsequently, a stimulated emission brings the system into a new channel. Process II: while in the initial bound state, the system absorbs a photon from a second laser, L2, and enters a second bound state. As in I, the system is brought into the final channel through an emission stimulated by L1.

Fig. 8. Illustration of possible collisional conversions involving two lasers. The open channels $|\alpha\rangle$ and $|\beta\rangle$ are radiatively coupled to the bound states $|s\rangle$, $|t\rangle$, and $|u\rangle$ by the first laser. These bound states are themselves mutually coupled by the second laser, which induces real as well as virtual transitions (solid and dashed arrows, respectively). Two non-radiative interactions are also included. The spin-orbit interaction couples the open channels $|\alpha\rangle$ and $|\beta\rangle$ and is denoted by the curved arrow in (1); the second, unspecified, interaction couples $|t\rangle$ to a third channel $|\gamma\rangle$ and is depicted in (3).

Fig. 9. Schematic representation of the HeI_2 molecule in the X and B electronic states. The motion of He is in a potential defined with respect to the distance, r, from the He atom to the center of mass of I_2. The other coordinate, R, is the separation of the I atoms. In the absence of radiation there are certain collisional energies, E_i, for which the system undergoes resonance scattering. Here the motion in the I_2 bond is strongly coupled to the motion in the HeI bond. In the excited excimer state, the $I\text{-}I^-$ bond is isoelectronic with the XeI ground state (which is weakly bound), wherein the roles of strong bond and weak bond are switched. After formation of the vibrationally predissociative resonance in the X state, a photon may be absorbed exciting the system into a predissociative excimer state. Subsequently, predissociation occurs: vibrational energy from the $I^-\text{-}He^+$ bond is transferred to the weak $I\text{-}I^-$ bond resulting in bond dissociation.

Fig. 10. Radiative scattering pathways with initial scattering energy E_i. Top: L1 (long arrow) effects a continuum-to-bound transition. The level spacing in the bound state manifold is such that a subsequent transition by L2 (short arrow) can be made to a higher level), with subsequent decay to the initial scattering state but at an increased translational energy E_f. Bottom: the same electronic system but with different isotopic composition. The intermediate level spacing does not permit a significant transition by L2, therefore only elastic scattering is permitted.

Fig. 11. The normalized steady-state excitation as a function of detuning for the harmonic case $\varepsilon^* = 0$ (solid curve) and anharmonic cases with ε^* = critical value $(\varepsilon^{**}) = 5/3$ (dashed curve) and $\varepsilon^* = 6$ (dashed-dotted curve). The bistable transition points are shown by P, Q, R and S. The parameters used are $(\gamma_1, \gamma_2, A) = (1, 10, 2.5)$, with the units of γ_1 in $10^4 s^{-1}$, γ_2, ε^* and Δ in cm^{-1}, I in W/cm^2 and A in 10^4 cm/W/s. Note that 1 cm^{-1} corresponds to $3 \times 10^{10} s^{-1}$ in frequency.[85]

Fig. 12. Schematic diagrams for the heat-bath models: (I) simple case with irreversible energy flow from A to B and (II) modified case for energy flow between A and B while being damped by the common bath C.

Fig. 13. Schematic energy level diagrams for the A, B and C modes, where V_i are the pumping rates between the i-th and the (i+1)-th vibrational levels of the active mode, coupled to the B mode via multiphonon coupling through the factor g_i; γ_m denotes the energy relaxation of the m-th level of the B mode due to its coupling to the C modes which are condensed modes with density of states ρ.[79]

Fig. 14. Energy populations of the A, B and C modes for two-photon multiphonon processes, given by P_A, P_B and P_C, respectively, for (pumping rate, coupling factor, damping rate) = (V, g, γ) = (A) (4,0.1,0.4) selective excitation and (B) (4,1,1) nonselective thermal heating.[84]

Fig. 15. (A) Hydrogenic lattice modes of H chemisorbed on W(100) at saturation coverage with H occupying a C_{2v} point group symmetric bridge site. Motions of the H atoms vertical and lateral to the surface are indicated by the arrows ↑ and →(↗), respectively. (B) Schematic diagram indicating the frequency spectrum

of the H/W(100) system. Note that the IR active ν_1 mode (1048.6 cm^{-1}) is coupled to the ν_2 and ν_3 modes by the fourth-order anharmonic coupling $\lambda' Q_1^2 Q_2 Q_3$.[12]

Fig. 16. Dynamical features of the average excitations of the active mode ($\bar{n}_1$), the ν_2 mode ($\bar{n}_2$) and the ν_3 mode ($\bar{n}_3$) for the heterogeneous system H/W with detunings ($\Delta_E'/2\pi, \Delta_I'/2\pi$) = (A) (0,0) exact resonance and (B) (10,80). Here we have used the following parameters: laser intensity $I = 10^8$ W/cm^2, anharmonic coupling constant $\lambda = 5\ cm^{-1}$ and initial temperature $T_0 = 300$ K.

Fig. 17. The distribution functions of four-photon excitations ($\langle n(t)\rangle = 4$), for a Poisson population (--), diffusion model population (for $\alpha = 1$) with S=1 (-·-) and S=6 (····), Boltzmann population with S=1 (-···-) and S=6 (—), and quantal population with $S = \alpha = 1$ (-····-).

Fig. 18. The desorption probabilities of $n^* = 5$ [defined by Eq.(IV.88)] associated with the distribution functions shown in Fig. 17.[82]

Fig. 19. Time-dependent excitations $\langle n_{A,B}(t)\rangle$ of the active modes for the harmonic case, i.e., $\varepsilon^* = 0$ with $(V,\gamma,\Delta_A,\Delta_B) = (10,1,4,8)$ and D' = (A) 0, (B) 2, (C) D* and (D) 10. $D^* = (\Delta_A+\Delta_B)/2 = 6$ is the transition value where $N_- = 0$.[86]

Fig. 20. Time evolution of the reduced selectivity [Eq.(IV.96)] for the non-interacting [curves (A) - (B)] and interacting isotopic system [curves (B') - (G')]. The parameters used are: $V = 10$, $\gamma_1^{A,B} = \gamma_2^{A,B} = 4$, $\varepsilon_A^* = \varepsilon_B^* = \varepsilon^*$ and $(D',\varepsilon^*,\Delta_A,\Delta_B)$ = (A)(0,ε**,5,10), (B) (0,ε**,5,-5), (C) (0,0,5,10), (D) (0,ε**,5,0), (E) (0,0,5,-5); and $(\varepsilon^*,\Delta_A,\Delta_B) = (\varepsilon^{**},5,10)$ with D' = (B') 2, (C') 4, (D') 6, (F') D* and (G') 10. $\varepsilon^{**} = 1.28$ is the critical anharmonicity as defined in Fig. 11, and $D^* = (\Delta_A+\Delta_B)/2$ is the coupling strength at the transition point defined by Eq.(III.95) for $N_- = 0$.

Fig. 21. Total steady-state excitation profiles in $(N_+, \omega_{A,B}, D')$-space for $\epsilon^* = 0$, $\gamma_2^{A,B} = 0$, $V = 10$ and $(\omega_B - \omega_A, \gamma_1^A, \gamma_1^B) = $ (A) (15,5,5), (B) (15,7,3), (C) (5,3,7) and (D) (5,3,7), where $N_+ = X + Y$ is the total steady-state excitation, $X \equiv \langle n_A \rangle_{s.s}$ and $Y = \langle n_B \rangle_{s.s.}$ given by the numerical solutions of Eq.(IV.89).[86]

Fig. 22. Schematic diagrams of adspecies-surface systems and the associated energy leve's, where A, B and M represent the adspecies (adatom or admolecule), C represents the substrate (or bath modes), and the laser radiation is indicated by the wiggly lines. Several types of desorption channels are illustrated: (I) direct desorption via active-mode excitation, (II) direct desorption via the quasi-continuum, (III) indirect desorption via tunneling, (IV) indirect desorption via substrate heating, (V) phonon-assisted desorption and (VI) indirect desorption via dynamics.

Fig. 23. Flow chart of the methodology of LSSP, indicating both classical and quantum treatments of the absorption cross section. By solving the master equation in energy space and in lattice-site space, we are able to investigate the energy population, desorption and migration, which are essential components of heterogeneous rate processes.

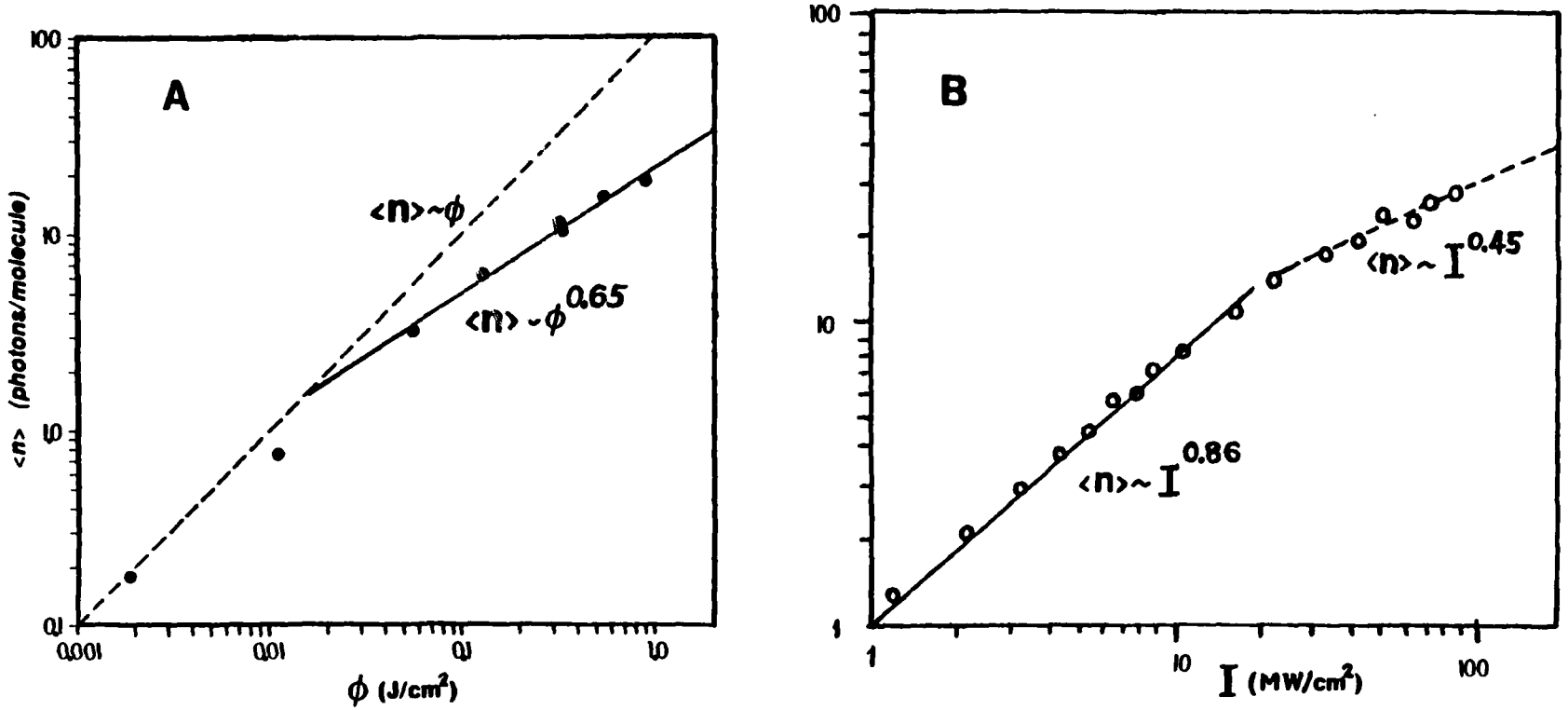

Fig. 1 (A) & (B) / Lin et al

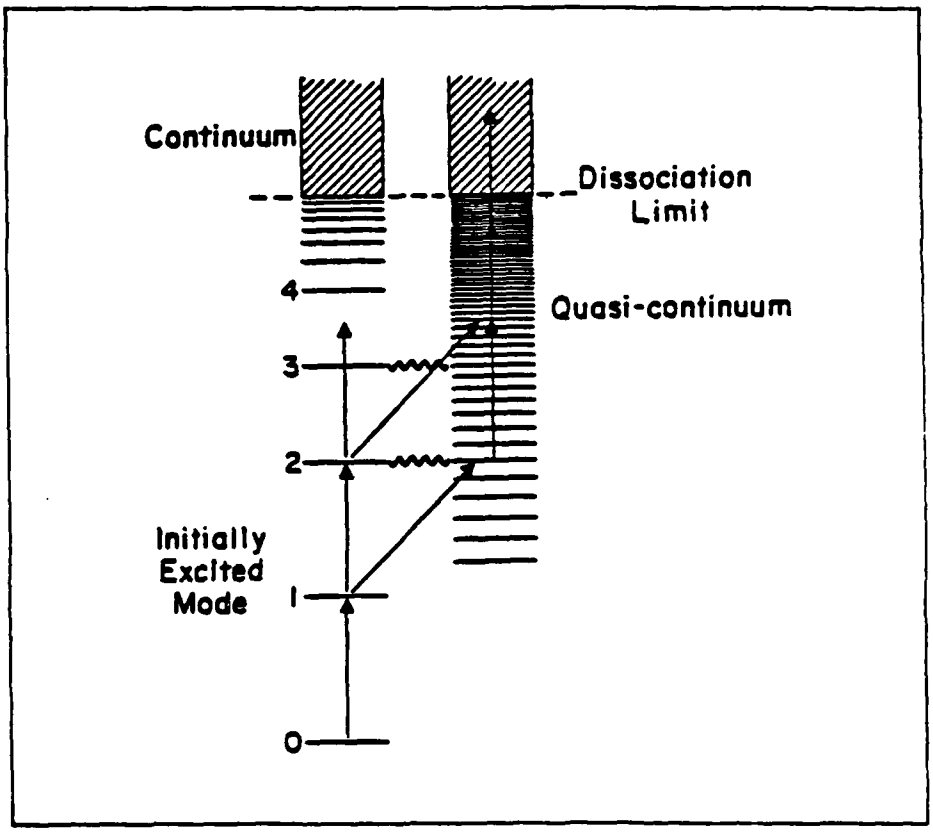

Fig. 2 / Lin et al

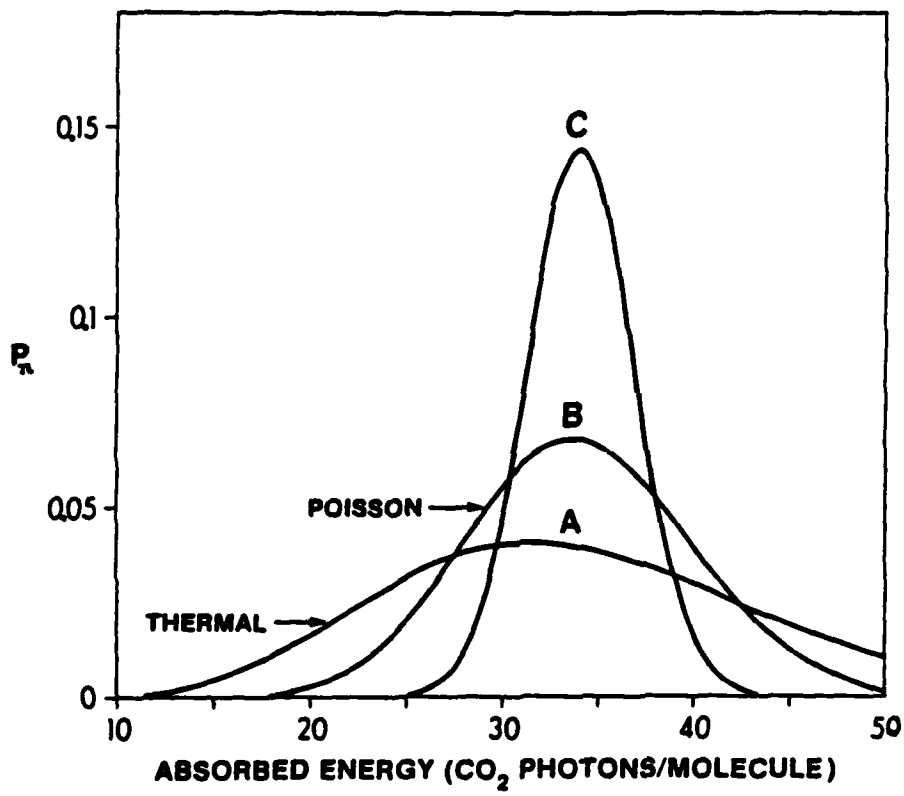

Fig. 3 / Lin et al

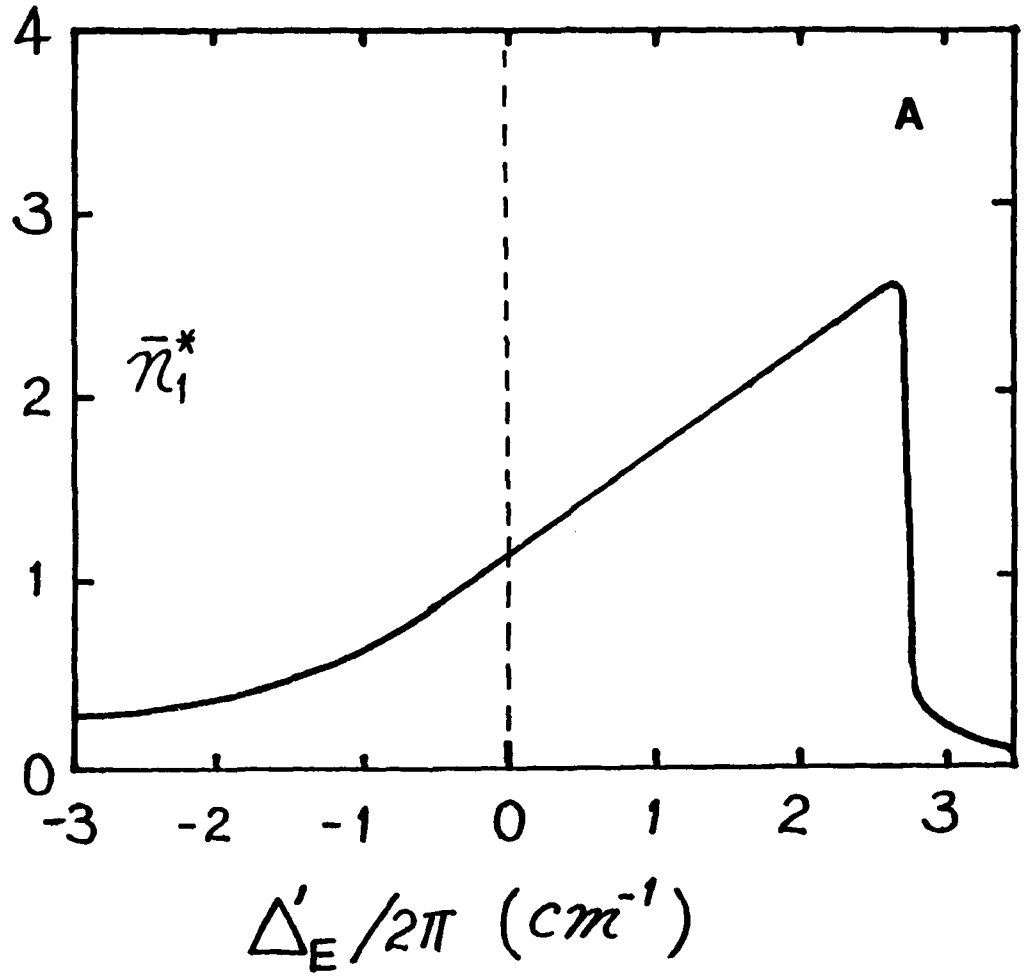

Fig. 4 (A) / Lim et al

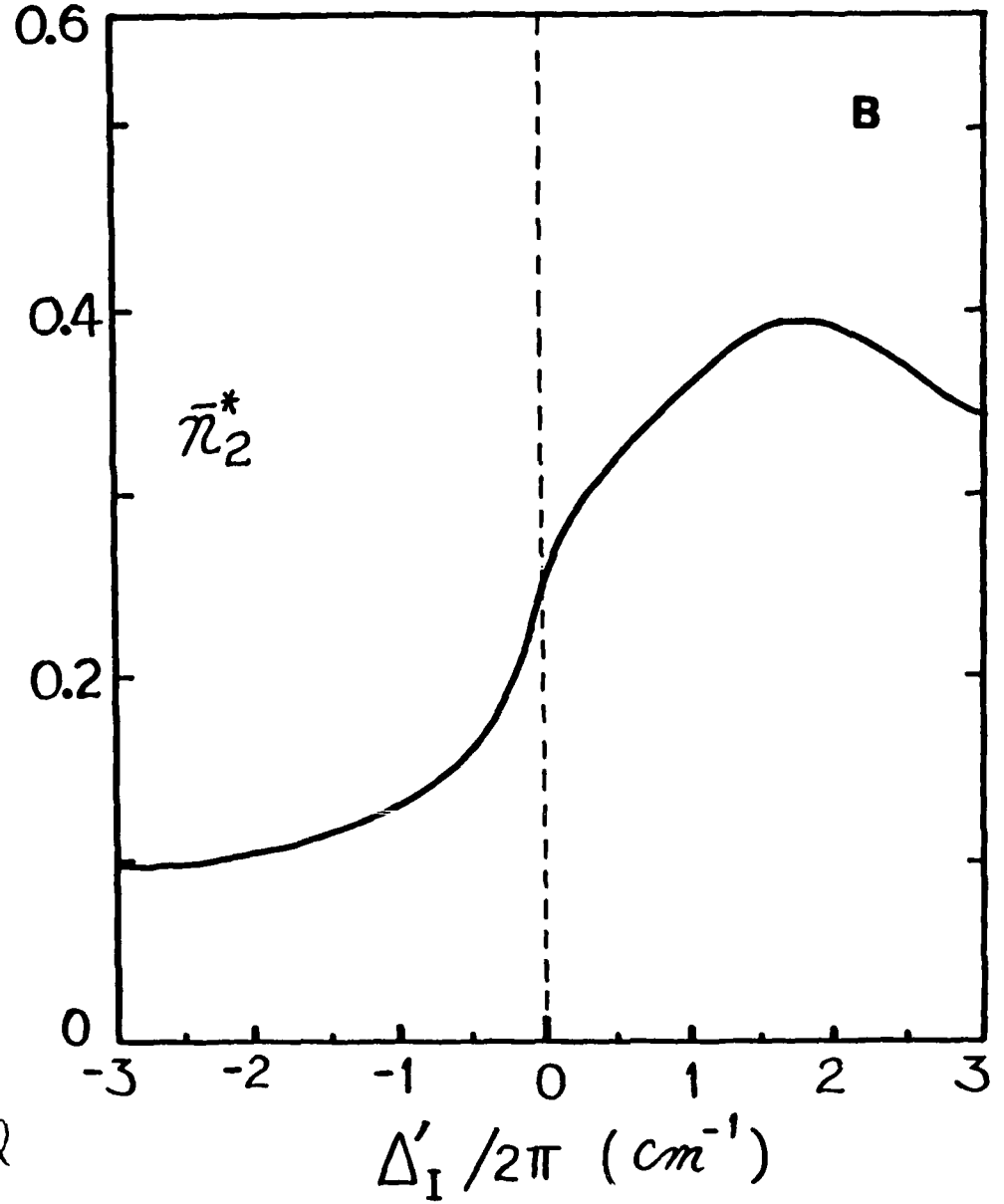

Fig. 4(B)/Lm et al

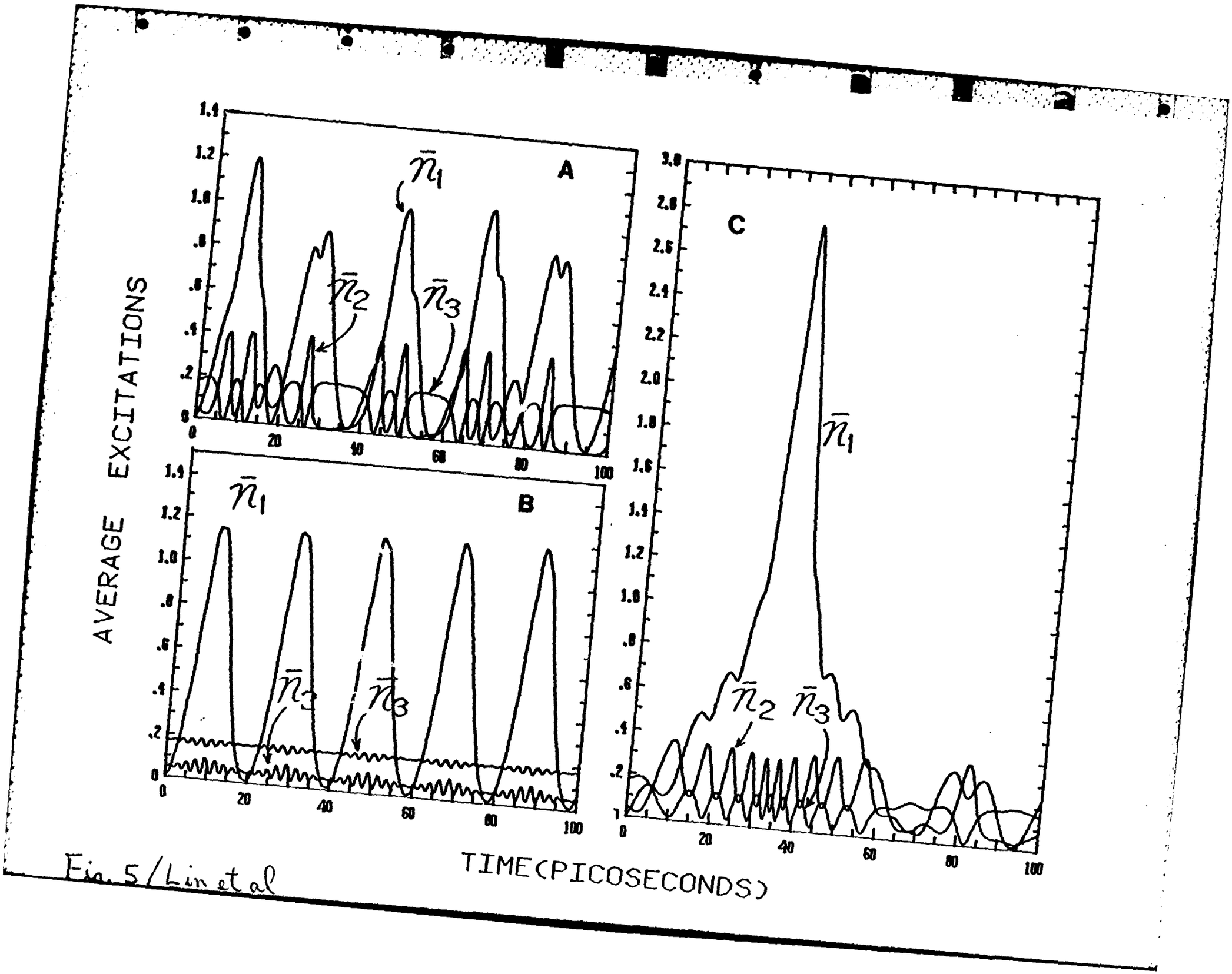

Fig. 5/Lin et al

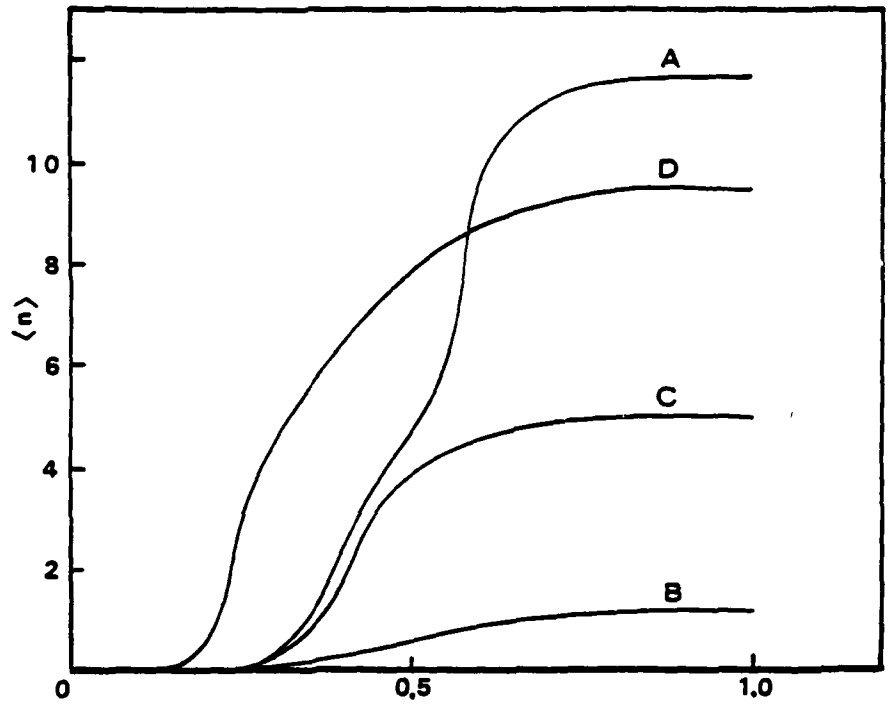

Fig 6 / Lin et al

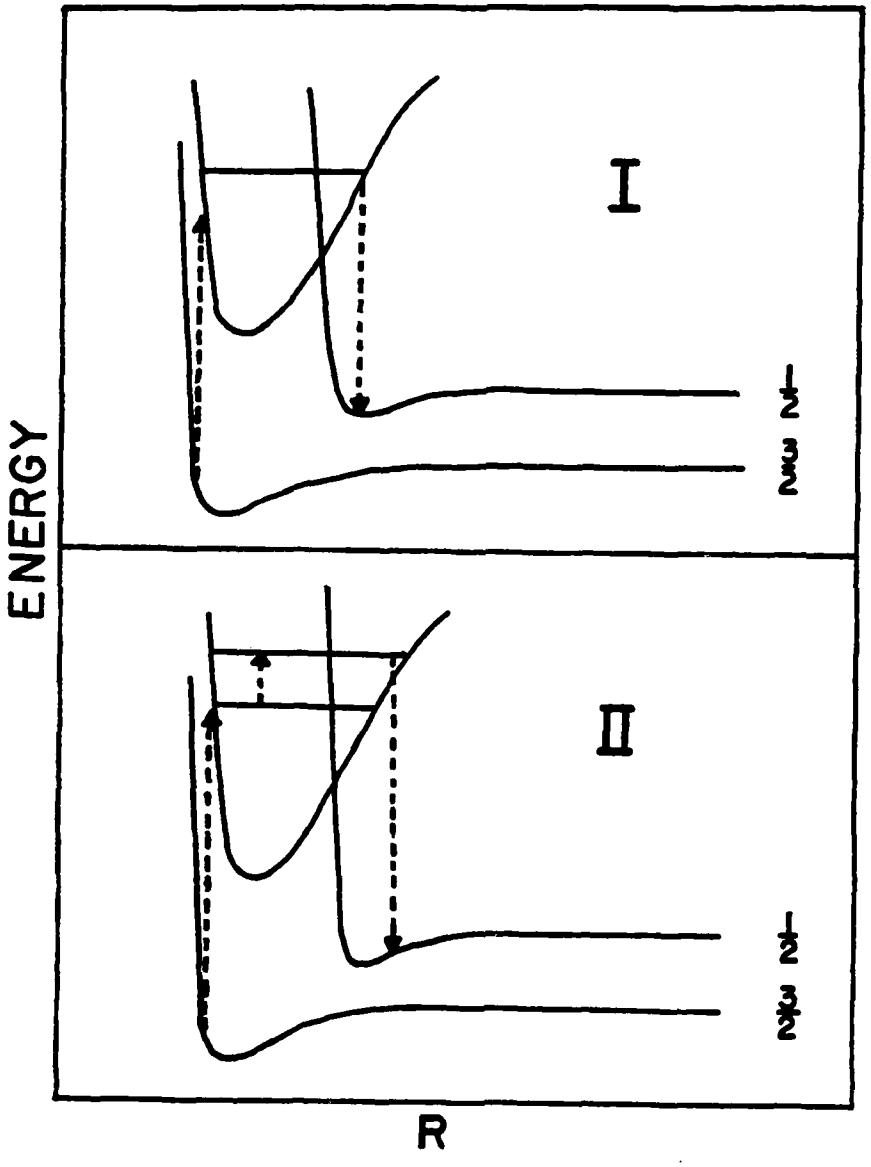

Fig. 7 / Lun et al

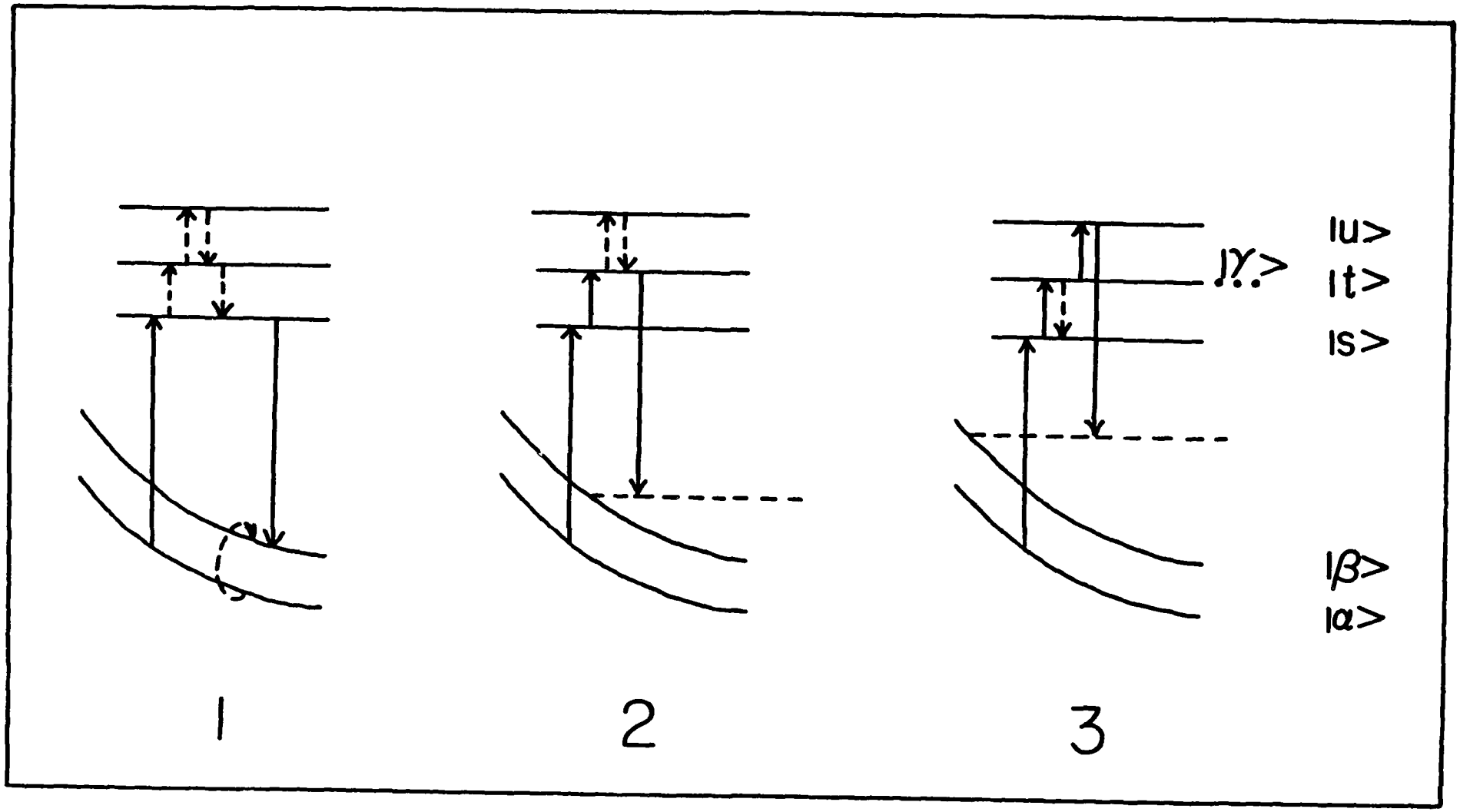

Fig. 8 / Lin et al

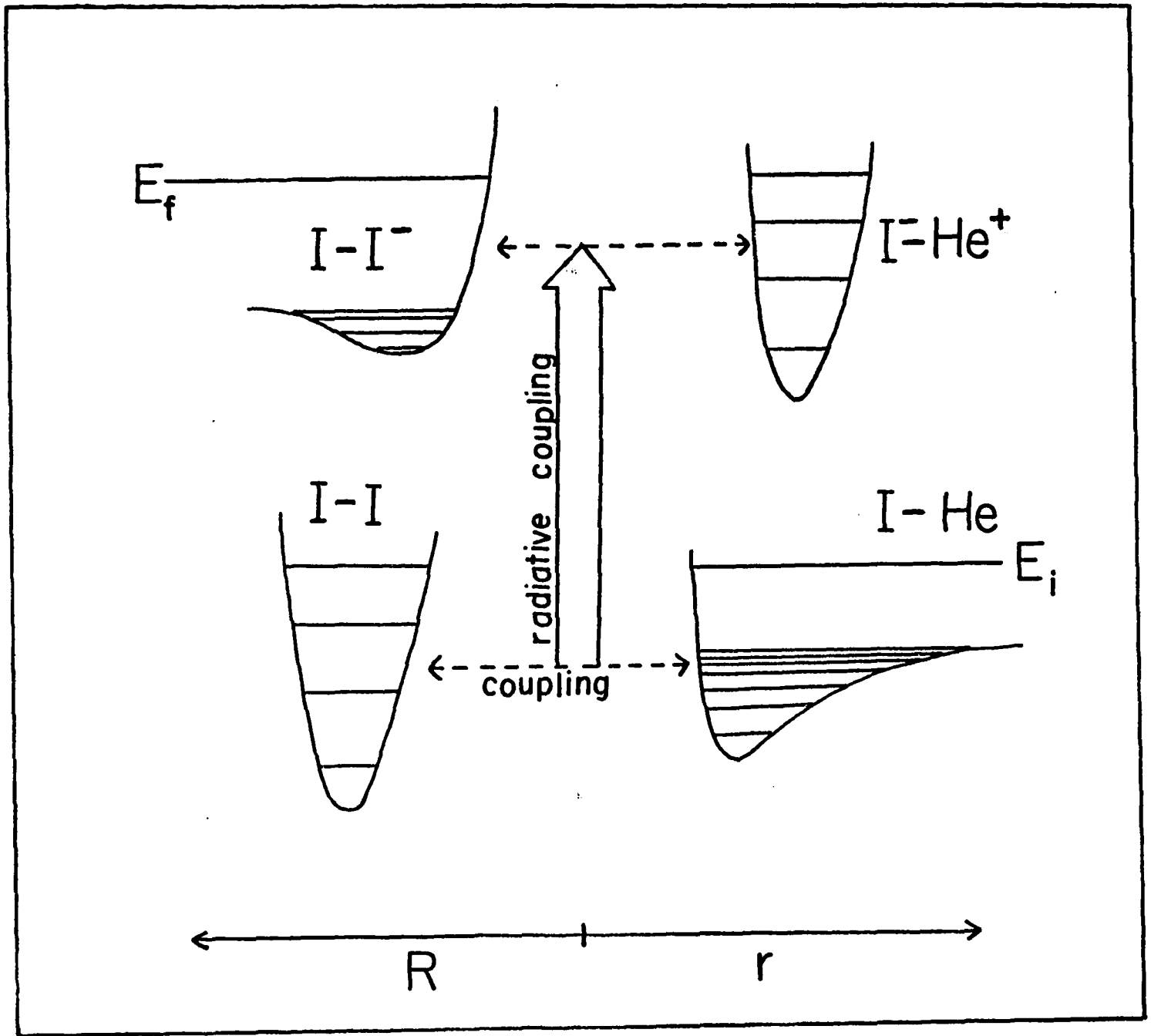

Fig. 9 / Lin et al

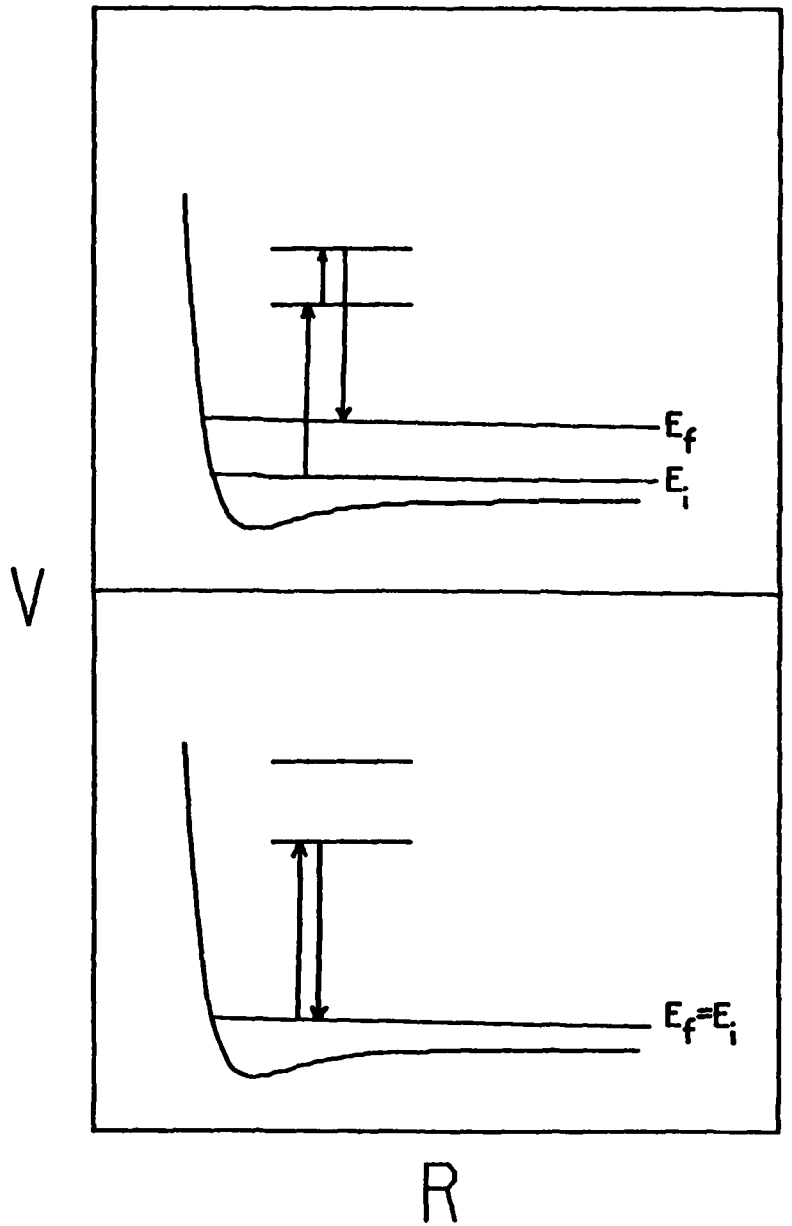

Fig. 10/ Lam et al

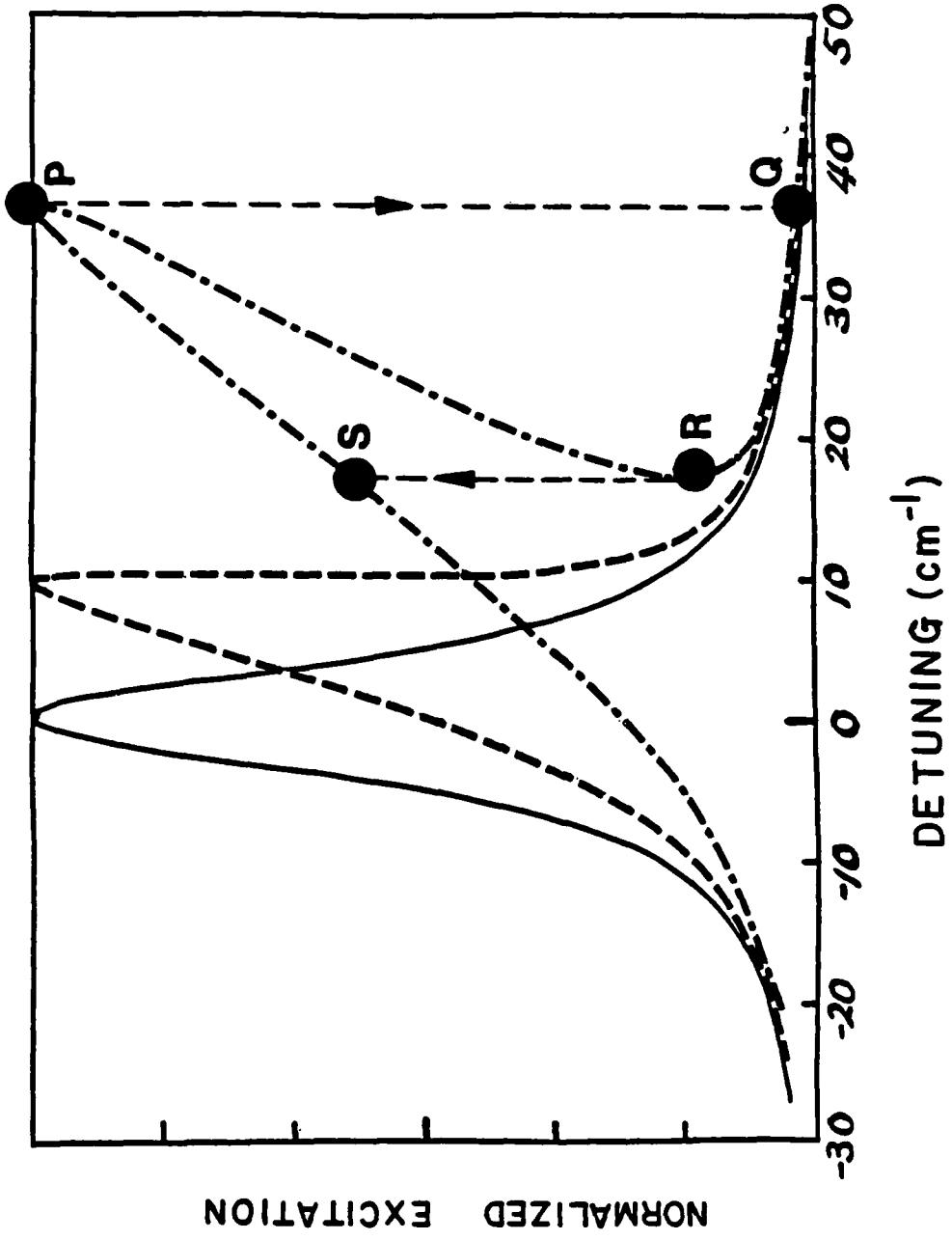

Fig. 11 / Lin et al.

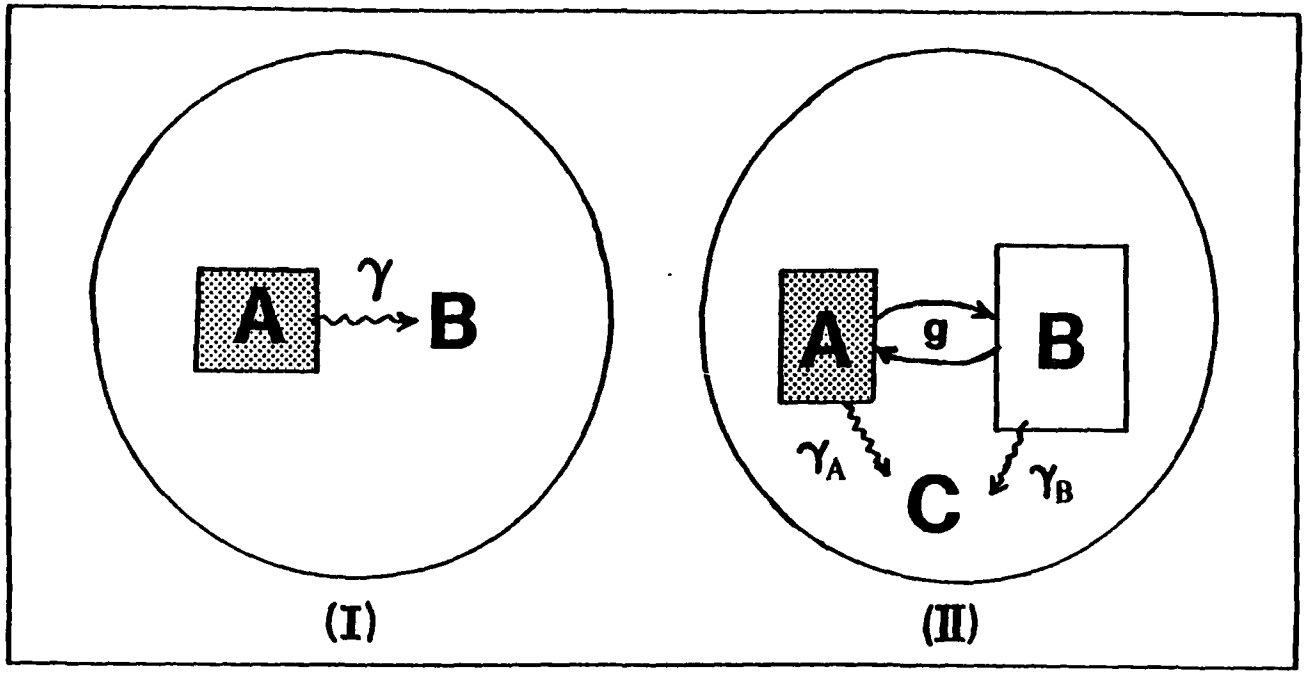

Fig. 12 / Lin et al.

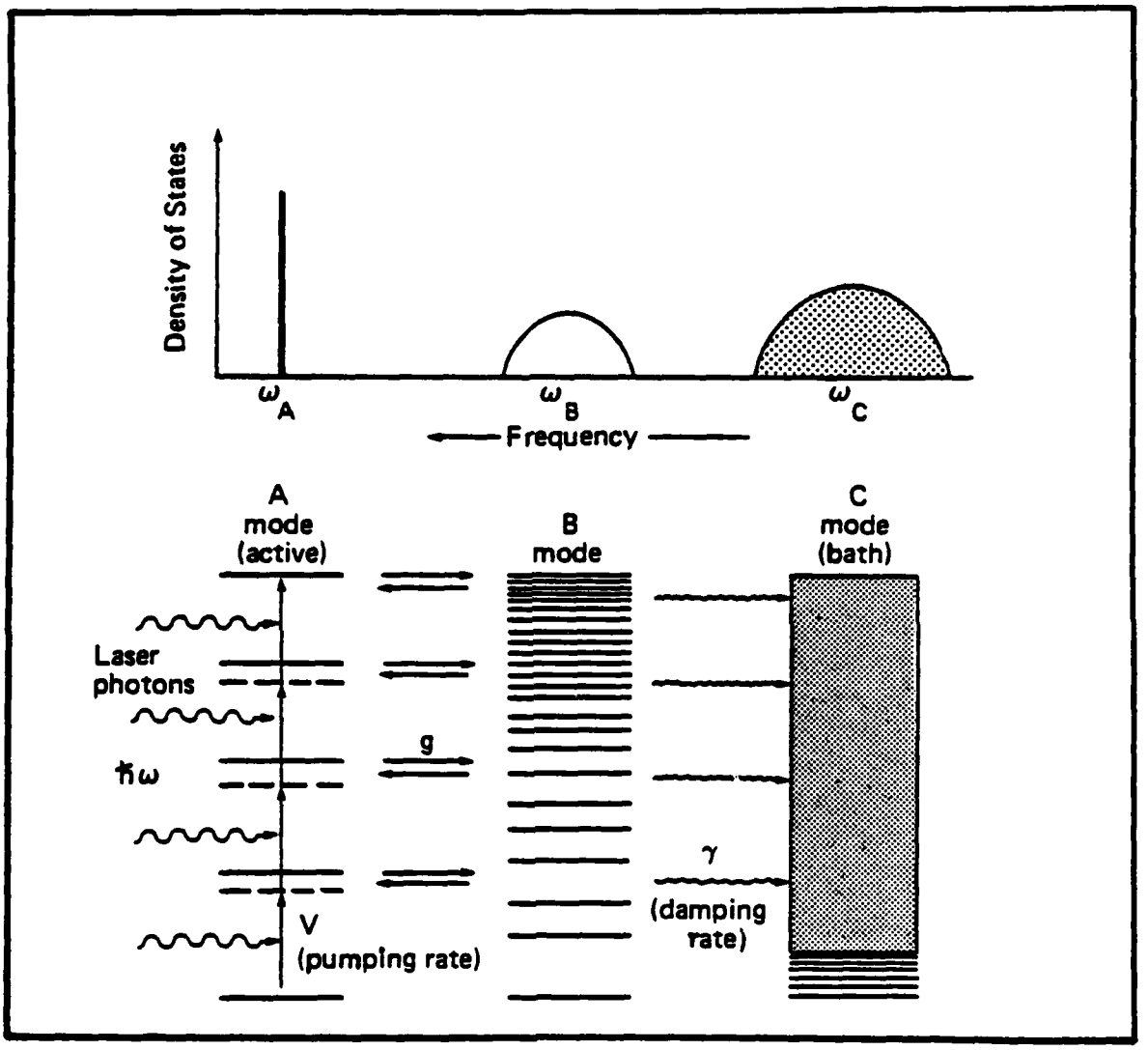

Fig. 13 / Lin et al.

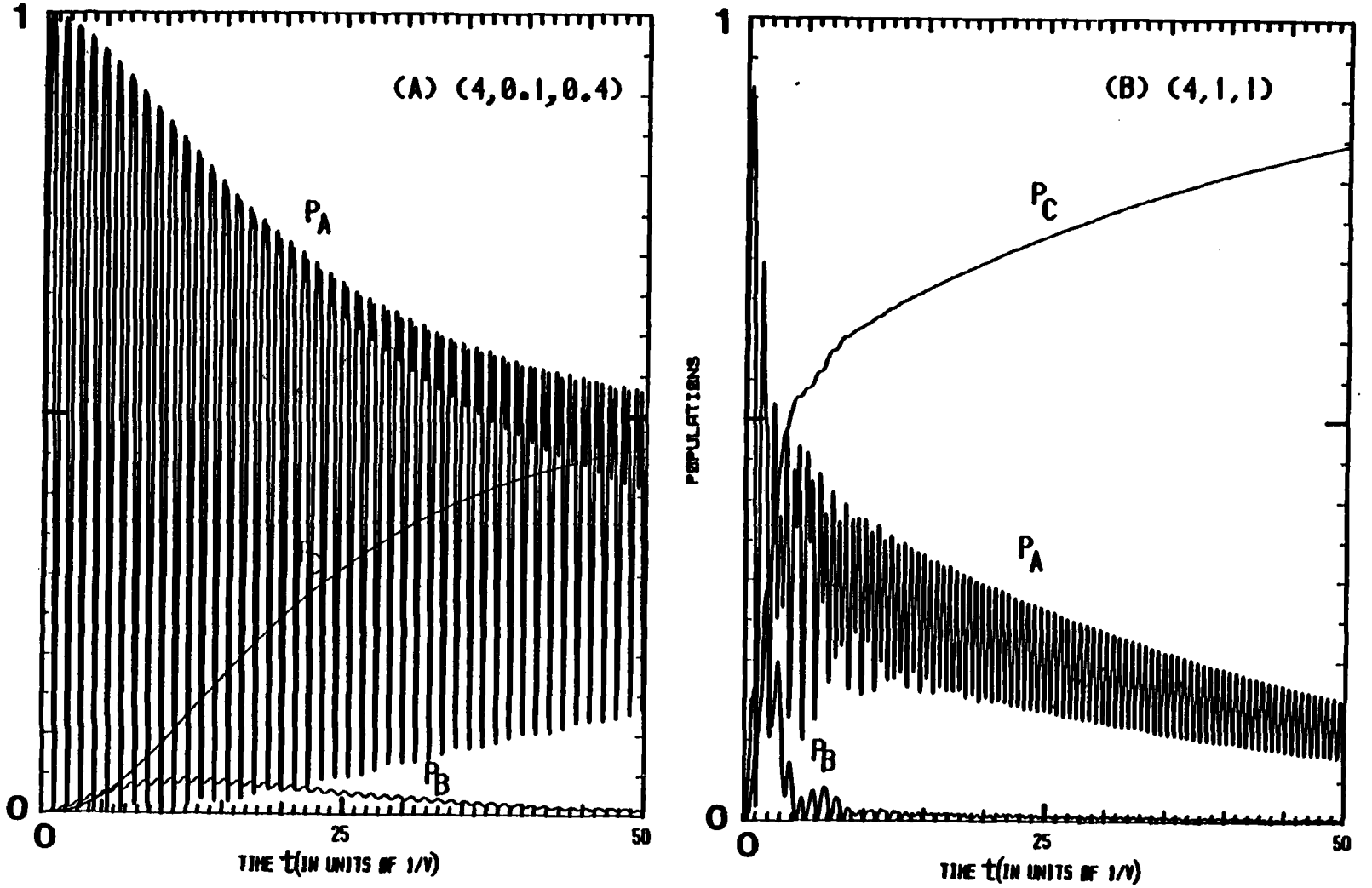

Fig. 14 / Lin et al.

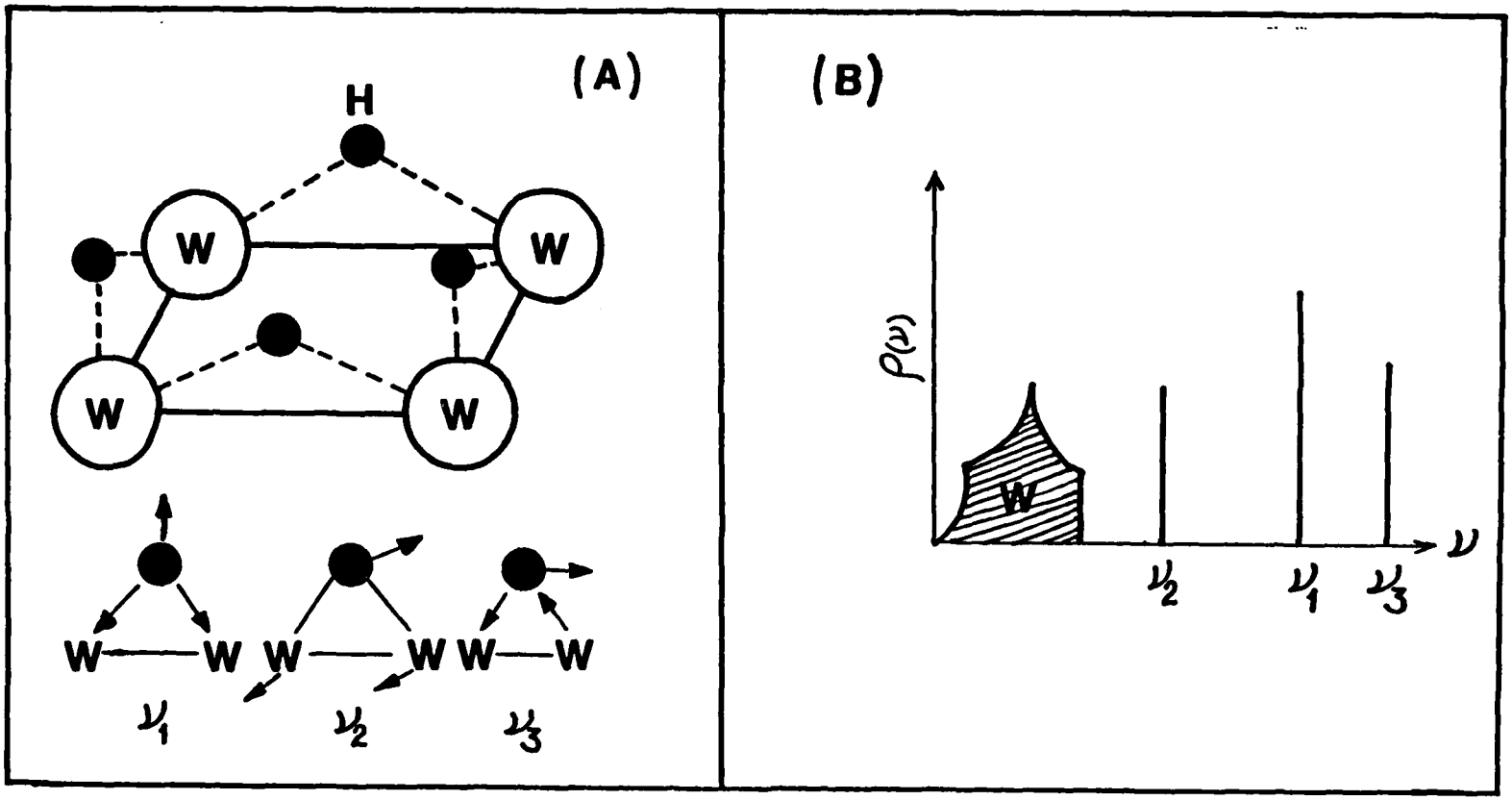

Fig 15 / Lin et.al.

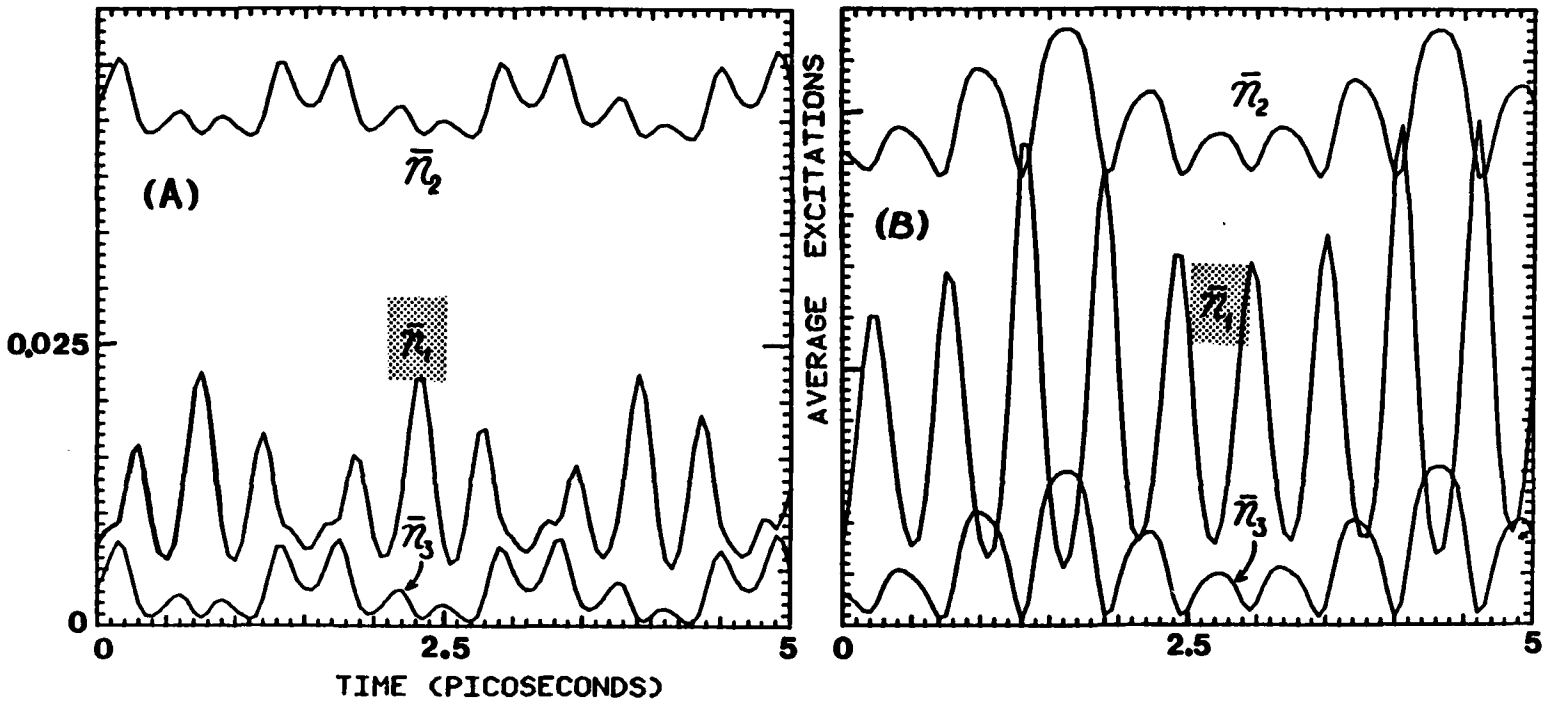

Fig. 16 / Lin et al.

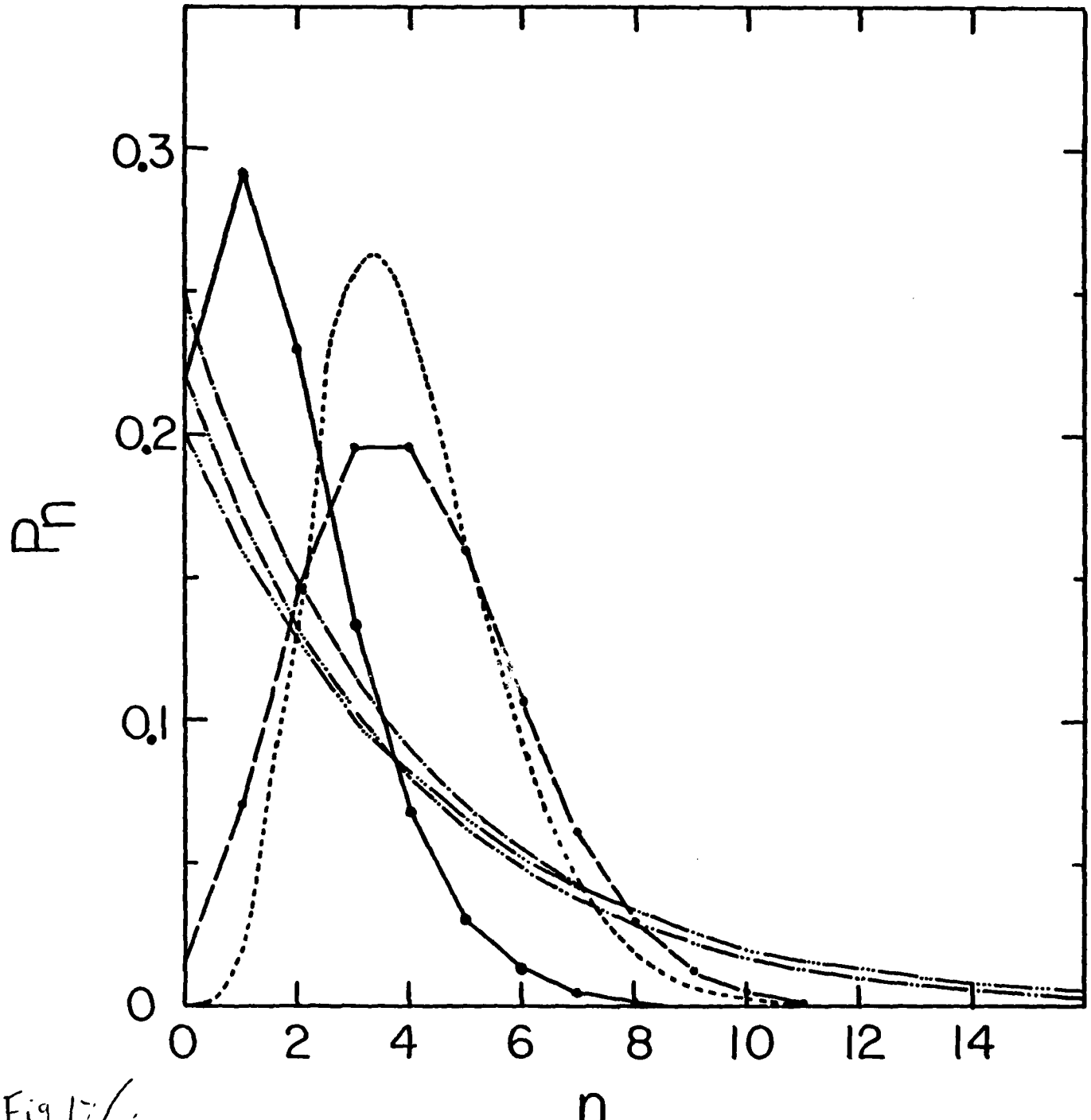

Fig 17/ in set

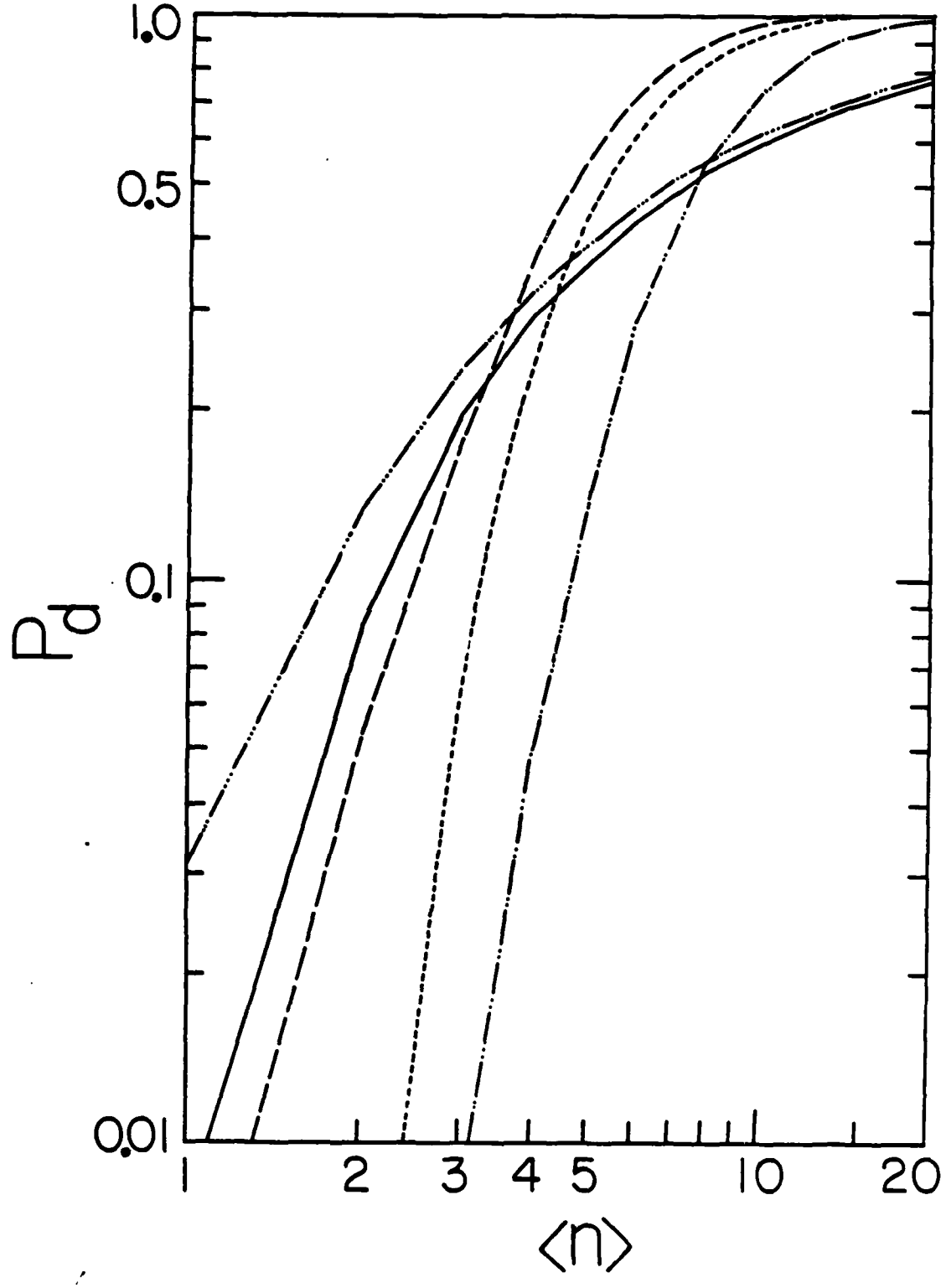

Fig 18 / Kinstaf

Fig. 19 / Lin et al

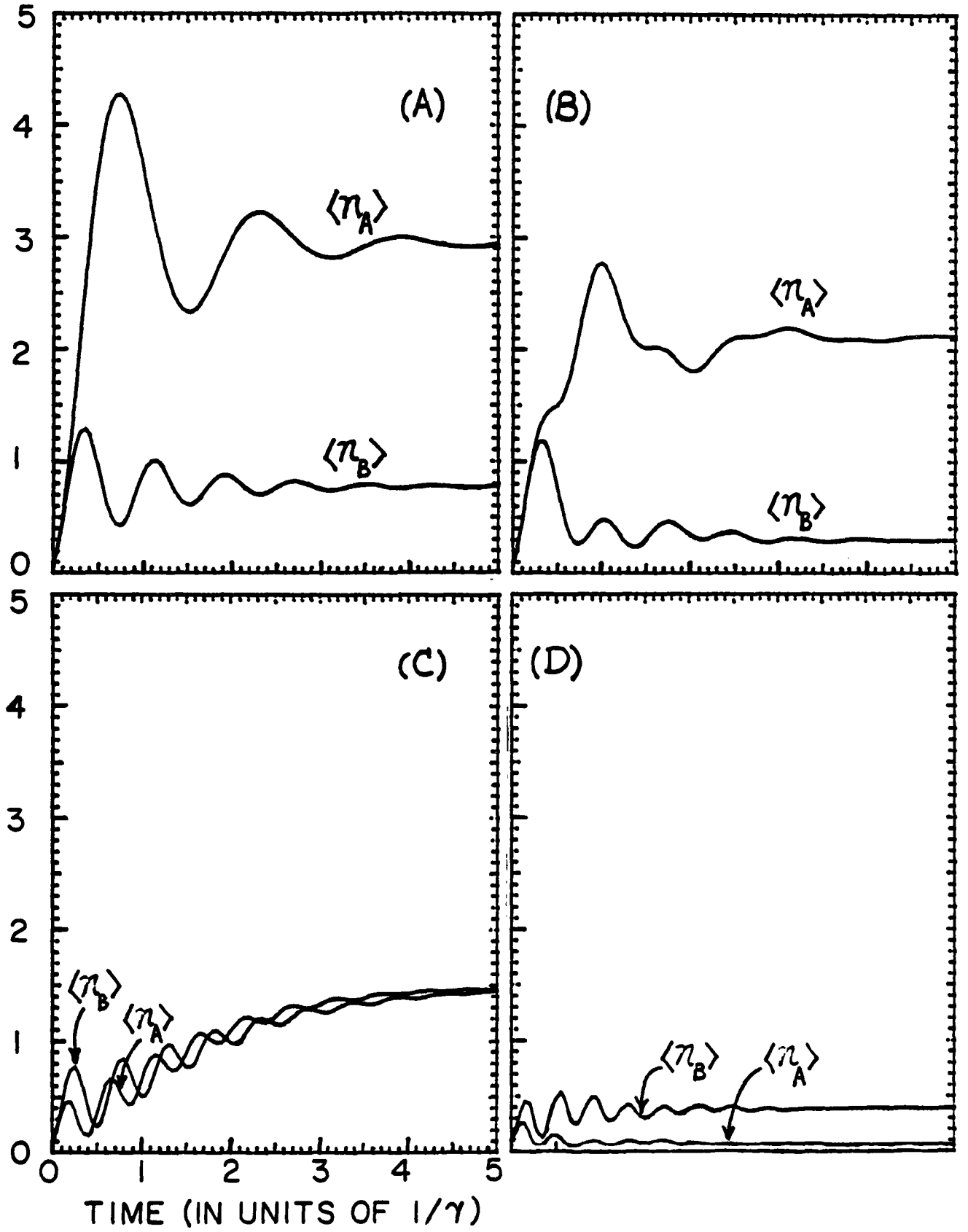

Fig. 20 / Lin et al

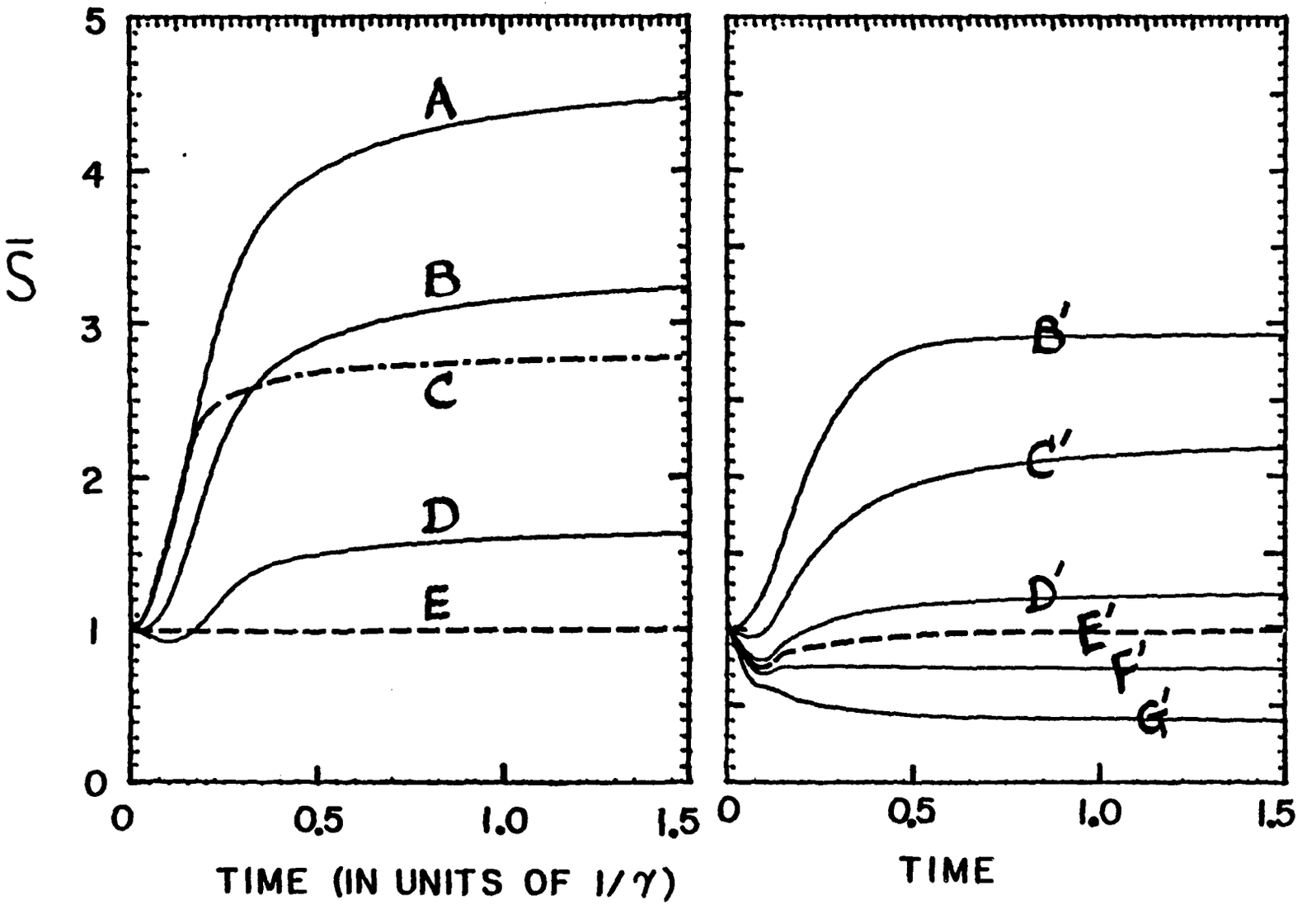

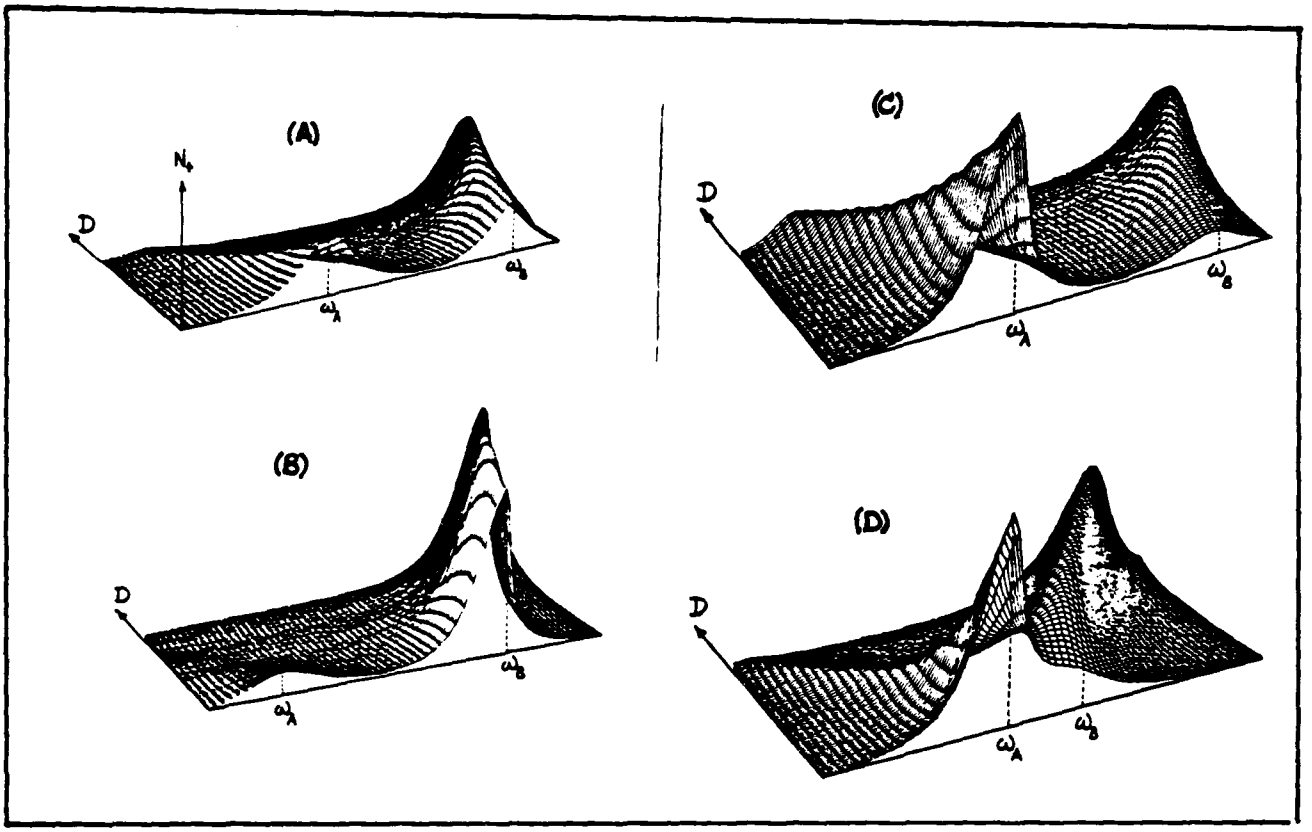

Fig. 21 / Lin et al

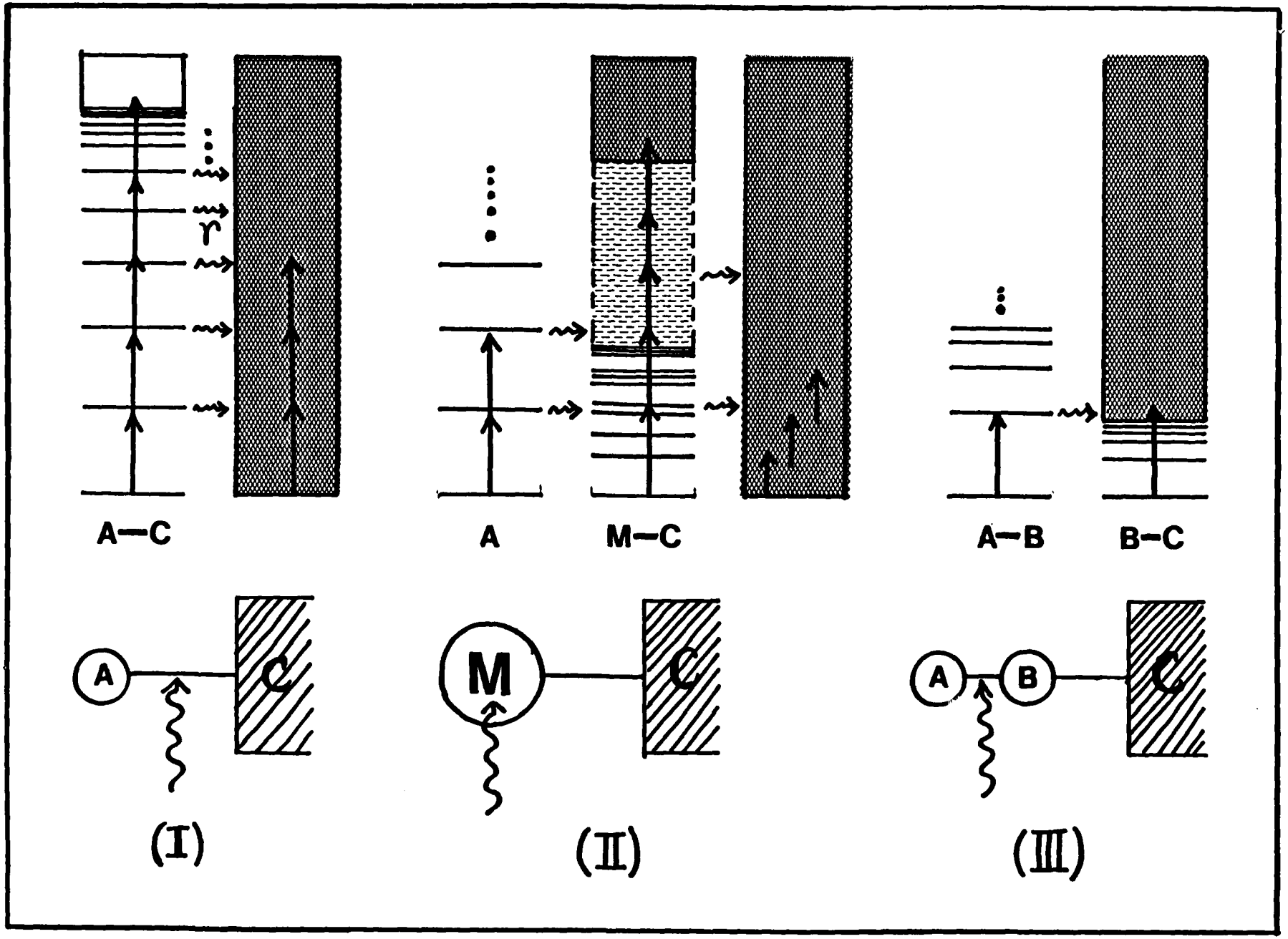

Fig. 22 (I)-(III)

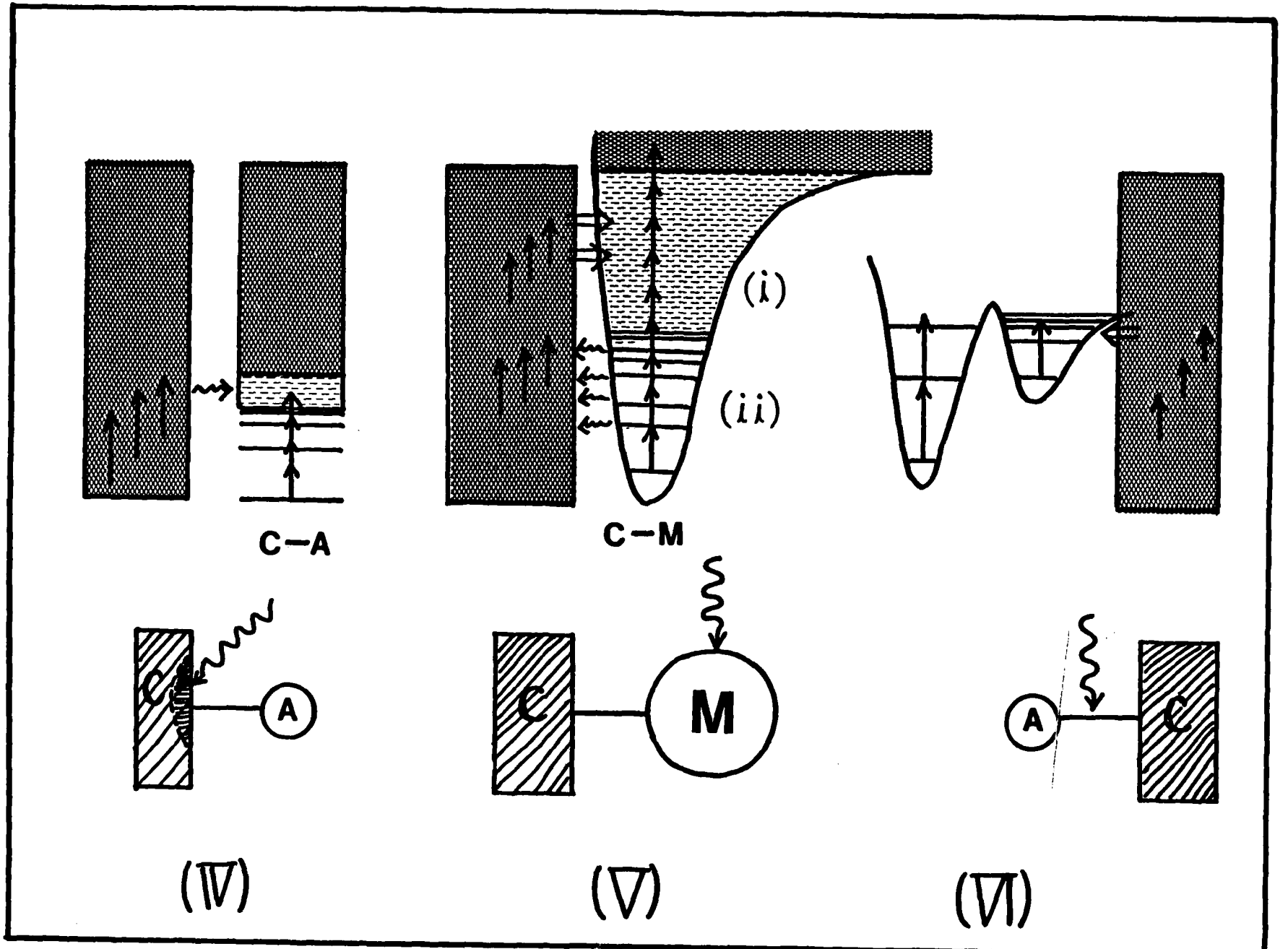

Fig. 22 (Ⅳ)–(Ⅵ)

472:GAN:716-4
94/GEN

TECHNICAL REPORT DISTRIBUTION LIST, GEN

	No. Copies
Office of Naval Research Attn: Code 413 800 North Quincy Street Arlington, Virginia 22217	2
ONR Pasadena Detachment Attn: Dr. R. J. Marcus 1030 East Green Street Pasadena, California 91106	1
Commander, Naval Air Systems Command Attn: Code 310C (H. Rosenwasser) Department of the Navy Washington, D.C. 20360	1
Defense Technical Information Center Building 5, Cameron Station Alexandria, Virginia 22314	12
Dr. Fred Saalfeld Chemistry Division, Code 6100 Naval Research Laboratory Washington, D.C. 20375	1
U.S. Army Research Office Attn: CRD-AA-IP P. O. Box 12211 Research Triangle Park, N.C. 27709	1
Mr. Vincent Schaper DTNSRDC Code 2803 Annapolis, Maryland 21402	1
Naval Ocean Systems Center Attn: Dr. S. Yamamoto Marine Sciences Division San Diego, California 91232	1
Dr. David L. Nelson Chemistry Program Office of Naval Research 800 North Quincy Street Arlington, Virginia 22217	1
Naval Ocean Systems Center Attn: Mr. Joe McCartney San Diego, California 92152	1
Naval Weapons Center Attn: Dr. A. B. Amster, Chemistry Division China Lake, California 93555	1
Naval Civil Engineering Laboratory Attn: Dr. R. W. Drisko Port Hueneme, California 93401	1
Dean William Tolles Naval Postgraduate School Monterey, California 93940	1
Scientific Advisor Commandant of the Marine Corps (Code RD-1) Washington, D.C. 20380	1
Naval Ship Research and Development Center Attn: Dr. G. Bosmajian, Applied Chemistry Division Annapolis, Maryland 21401	1
Mr. John Boyle Materials Branch Naval Ship Engineering Center Philadelphia, Pennsylvania 19112	1
Mr. A. M. Anzalone Administrative Librarian PLASTEC/ARRADCOM Bldg 3401 Dover, New Jersey 07801	1

TECHNICAL REPORT DISTRIBUTION LIST, 056

	No. Copies
Dr. G. A. Somorjai Department of Chemistry University of California Berkeley, California 94720	1
Dr. J. Murday Naval Research Laboratory Surface Chemistry Division (6170) 455 Overlook Avenue, S.W. Washington, D.C. 20375	1
Dr. J. B. Hudson Materials Division Rensselaer Polytechnic Institute Troy, New York 12181	1
Dr. Theodore E. Madey Surface Chemistry Section Department of Commerce National Bureau of Standards Washington, D.C. 20234	1
Dr. J. M. White Department of Chemistry University of Texas Austin, Texas 78712	1
Dr. Keith H. Johnson Department of Metallurgy and Materials Science Massachusetts Institute of Technology Cambridge, Massachusetts 02139	1
Dr. J. E. Demuth IBM Corporation Thomas J. Watson Research Center P. O. Box 218 Yorktown Heights, New York 10598	1
Dr. C. P. Flynn Department of Physics University of Illinois Urbana, Illinois 61801	1
Dr. W. Kohn Department of Physics University of California (San Diego) La Jolla, California 92037	1
Dr. R. L. Park Director, Center of Materials Research University of Maryland College Park, Maryland 20742	1
Dr. W. T. Peria Electrical Engineering Department University of Minnesota Minneapolis, Minnesota 55455	1
Dr. Chia-wei Woo Department of Physics Northwestern University Evanston, Illinois 60201	1
Dr. Robert M. Hexter Department of Chemistry University of Minnesota Minneapolis, Minnesota 55455	1
Dr. R. P. Van Duyne Chemistry Department Northwestern University Evanston, Illinois 60201	1
Dr. S. Sibener Department of Chemistry James Franck Institute 5640 Ellis Avenue Chicago, Illinois 60637	1
Dr. M. G. Lagally Department of Metallurgical and Mining Engineering University of Wisconsin Madison, Wisconsin 53706	1

TECHNICAL REPORT DISTRIBUTION LIST, 056

	No. Copies
Dr. Robert Gomer Department of Chemistry James Franck Institute 5640 Ellis Avenue Chicago, Illinois 60637	1
Dr. R. G. Wallis Department of Physics University of California, Irvine Irvine, California 92664	1
Dr. D. Ramaker Chemistry Department George Washington University Washington, D.C. 20052	1
Dr. P. Hansma Physics Department University of California, Santa Barbara Santa Barbara, California 93106	1
Dr. J. C. Hemminger Chemistry Department University of California, Irvine Irvine, California 92717	1
Dr. Martin Fleischmann Department of Chemistry Southampton University Southampton SO9 5NH Hampshire, England	1
Dr. G. Rubloff IBM Thomas J. Watson Research Center P. O. Box 218 Yorktown Heights, New York 10598	1
Dr. J. A. Gardner Department of Physics Oregon State University Corvallis, Oregon 97331	1
Dr. G. D. Stein Mechanical Engineering Department Northwestern University Evanston, Illinois 60201	1
Dr. K. G. Spears Chemistry Department Northwestern University Evanston, Illinois 60201	1
Dr. R. W. Plummer University of Pennsylvania Department of Physics Philadelphia, Pennsylvania 19104	1
Dr. E. Yeager Department of Chemistry Case Western Reserve University Cleveland, Ohio 41106	1
Professor D. Hercules University of Pittsburgh Chemistry Department Pittsburgh, Pennsylvania 15260	1
Professor N. Winograd The Pennsylvania State University Department of Chemistry University Park, Pennsylvania 16802	1
Professor T. F. George The University of Rochester Chemistry Department Rochester, New York 14627	1
Professor Dudley R. Herschbach Harvard College Office for Research Contracts 1350 Massachusetts Avenue Cambridge, Massachusetts 02138	1
Professor Horia Metiu University of California, Santa Barbara Chemistry Department Santa Barbara, California 93106	1
Professor A. Steckl Rensselaer Polytechnic Institute Department of Electrical and Systems Engineering Integrated Circuits Laboratories Troy, New York 12181	1

TECHNICAL REPORT DISTRIBUTION LIST, 056

	No. Copies	No. Copies
Dr. John T. Yates Department of Chemistry University of Pittsburgh Pittsburgh, Pennsylvania 15260	1	
Professor G. H. Morrison Department of Chemistry Cornell University Ithaca, New York 14853	1	
Captain Lee Myers AFOSR/NC Bolling AFB Washington, D.C. 20332	1	
Dr. David Squire Army Research Office P. O. Box 12211 Research Triangle Park, NC 27709	1	
Professor Ronald Hoffman Department of Chemistry Cornell University Ithaca, New York 14853	1	

END

FILMED